P. Vasarmidis

Assessment of the influence of permeable pile groins on nearshore hydraulics

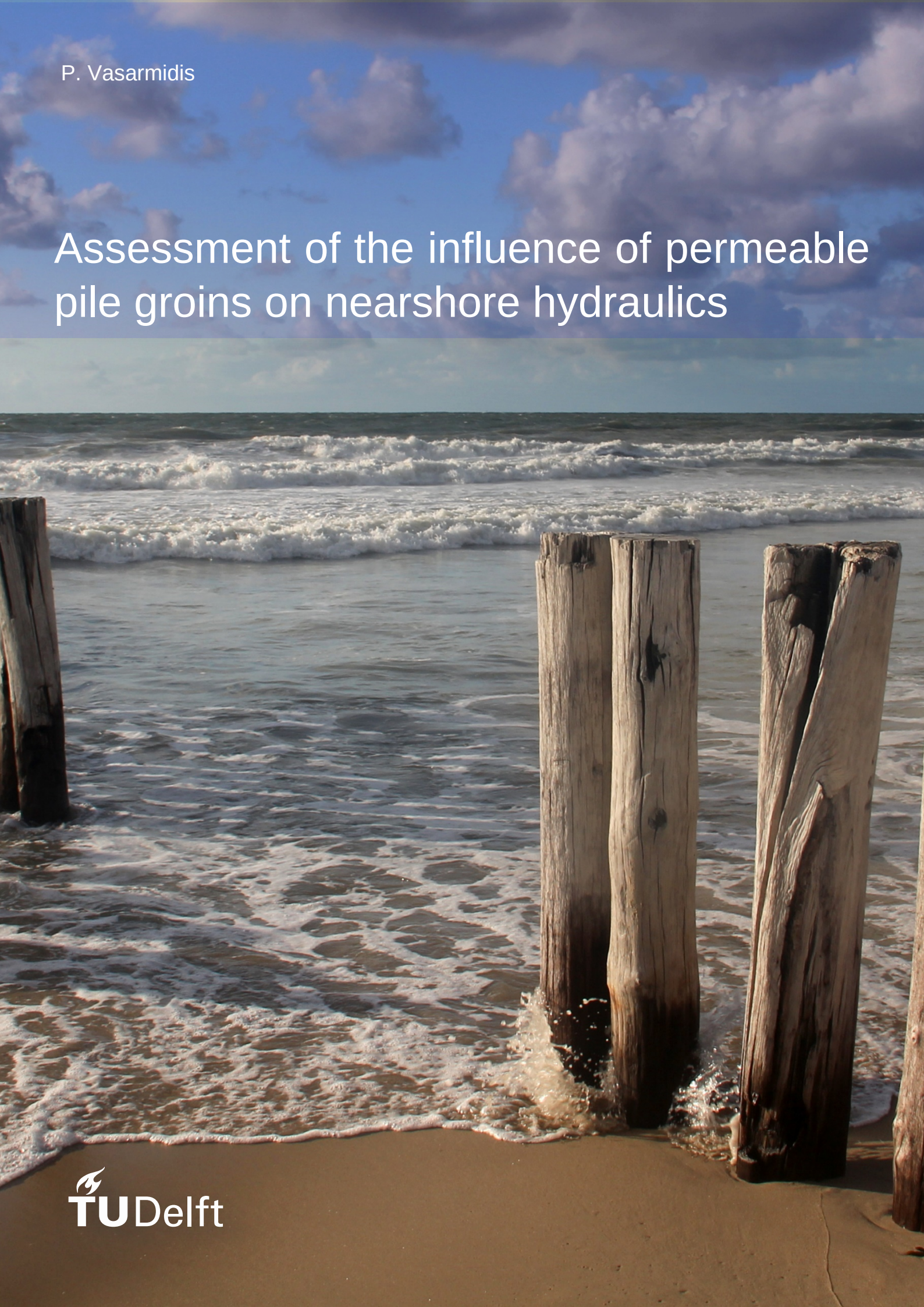

TU Delft

Cover photo: A permeable pile groin at Domburg coast, The Netherlands - Photo by els f, www.panoramio.com

Assessment of the influence of permeable pile groins on nearshore hydraulics

By

Panagiotis Vasarmidis

in partial fulfilment of the requirements for the degree of

Master of Science

in Civil Engineering, Track – Hydraulic Engineering

at the Delft University of Technology,

to be defended publicly on 9th August, 2016 at 9:30 AM

Supervisor:	Marcel Stive	
Thesis committee:	Prof. dr. ir. M.J.F. Stive	TU Delft
	Dr. ir. M. Zijlema	TU Delft
	Dr. Y.E. Qinghua	TU Delft
	MSc. R. Zhang	TU Delft

TU Delft

Preface

The present thesis is the outcome of research done in TUDelft, in order to obtain my Master Degree in Civil Engineering at Delft University of Technology, with a specialization in Coastal Engineering. The objective of this report is to assess the influence of permeable pile groins on nearshore hydraulics at Domburg coast by means of process-based model (SWASH). Experimental results from Hulsbergen's report have been used in order to validate the SWASH model and evaluate its capabilities.

Panagiotis Vasarmidis

09/08/2016

Acknowledgments

I would like to express my gratitude to those who supported me during the process of my graduation.

First of all, I would like to thank my assessment committee; Marcel Stive, Marcel Zijlema, Qinghua Ye and Rong Zhang who supported me throughout all the stages of this project. I am thankful for their aspiring guidance, invaluable constructive criticism and friendly advice during the project work. Thank you for all your time and patience.

Further my special thank is directed to Myrsini Michalaki, I appreciate all the hours you gave to me to evaluate my report and my research. Also, I would like to thank Mike Papadimitriou and Nick Stekas for their valuable help with Linux scripting. A special thanks is expressed to Nikolaos Diplarakos and Anastasios Smyrnis for sharing their knowledge. Last but not least, I would like to thank my family and friends for their support and encouragement through the whole process of attaining the Master Degree in Hydraulic Engineering, in TU Delft.

Panagiotis Vasarmidis

09/08/2016

Summary

One of the most economically and ecologically important issues related to coastal engineering is the preservation of the coastal areas. The mean to do so, is the good understanding of the sediment transport mechanisms that are involved in the transformation of coasts. In order to protect these valuable areas, man-made structures have been developed, such as permeable pile groins which are among the oldest, but also to the most interesting coastal structures.

They constitute of wooden piles driven into the seabed perpendicular to the shore and thus they allow both water and sediment to pass through them, acting as a hydraulic roughness on the longshore current leading to a reduced littoral current velocity in their vicinity. However, although permeable pile groins have been constructed along many world's coastlines through the years, the research done on how they affect the coastal system is still limited. The aim of this study is to bridge the existing knowledge gap and provide a clearer view on the factors that influence the nearshore hydraulics at Domburg coast.

The evaluation of permeable pile groins is going to be done by means of a process-based model in SWASH. The SWASH model will be used for the examination of several hydraulic conditions, and will be afterwards validated using the results from the experiments that Hulsbergen carried out. The validation of the model is done in several steps, in order to make the understanding of the influence of each parameter easier. First, only the wave induced current is examined, followed by the tide induced current. The combination of wave and tide induced current follows and last but not least two (2) different types of permeable piles groins are implemented. By this method, not only the influence of permeable pile groins is examined, but also the capability of SWASH itself to capture the real phenomena and give accurate results.

The results of the present study revealed that SWASH model is very capable of capturing the real behavior of the current, since high correlation with the experimental results can be observed for all the test-cases examined. The results also showed a clear retardation of the current due to the presence of the pile groins which in turn leads to a reduction in the capacity of the current to transport sediment.

Contents

List of figures

List of tables

List of symbols

b	distance between two piles	m
c	wave celerity	m/s
c_g	wave group velocity	m/s
c_f	bottom friction coefficient	-
c_0	phase velocity at deep water	m/s
C	Chezy coefficient	$m^{1/2}/s$
C_D	drag coefficient	-
C_M	inertia coefficient	-
C_S	Smagorinsky coefficient	-
D	diameter of the piles	m
E_w	wave energy per unit surface area	J/m^2
f	Darcy resistance coefficient	-
f	frequency	Hz
F	force	N
F_D	drag force	N
F_I	inertia force	N
Fr	Froude number	-
g	gravitational acceleration	m/s^2
H	wave height	m
H_b	wave height at breaking	m
H_0	wave height at deep water	m
H_s	Significant wave height	m
h	water depth	m
h_b	water depth at breaking position	m
I	slope of the energy head	-
K	number of layers	-
K_{sh}	shoaling factor	-
k	wave number	1/m
k	Von Karman constant	-
k_r	roughness height	m
l_m	Prandtl mixing length	m

l_S	Smagorinsky length scale	m
l_x	domain length in x-direction	m
l_y	domain length in y-direction	m
L	wave length	m
n	Manning number	$s/m^{1/3}$
n	ratio c_g to c	-
P	permeability expressed in percent	-
p	pressure	Pa
p_h	hydrostatic pressure	Pa
p_{nh}	non-hydrostatic pressure	Pa
p_{tide}	tidal pressure	Pa
R	hydraulic radius	m
Re	Reynold's number	-
S	radiation stress	N/m
t	time	s
T	wave period	s
$tan\, a$	beach slope	-
U	wave power per unit wave crest width	J/ms
u	flow velocity in x-direction	m/s
u_τ	shear velocity	m/s
v	flow velocity in y-direction	m/s
V	longshore current speed	m/s
x	co-ordinate axis perpendicular to coastline	m
y	co-ordinate axis parallel to coastline	m
α	breaking onset parameter	-
β	breaking offset parameter	-
γ	breaker index	-
Δ	filter length (grid size)	m
Δx	grid size in x-direction	m
Δy	grid size in y-direction	m
ζ	surface elevation	m
$\overline{\eta}$	wave induced water level setup	m
θ	wave angle	°

ν_t	eddy viscosity	m^2/s
ρ	density of water	kg/m^3
τ_b	bed shear stress	Pa
φ_0	wave crest angle relative to the depth contours	°

1. Introduction

1.1 Problem definition

The transport of sediment in coastal areas has been and will continue to be one of the most interesting fields of coastal engineering. The coastal areas form a unique ecosystem that has to be preserved at any cost. The coasts in the Netherlands and specific the southwest Zeeland coast have large public and economic importance, and the understanding of the sediment transport along them is of great interest.

In order to protect these valuable areas man-made structures have been developed. One of them is permeable pile groins which belong worldwide to the oldest, but also to the most interesting coastal structures. A permeable pile groin system is composed of one or more rows of piles driven into the seabed which are perpendicular to shore (Poff, 2004). The permeability of a groin is defined by the ratio of the open area to the total area. In the case of a permeable pile groin this operation is achieved by placing the piles with a determinate distance to one another (Figure 1.1).

Figure 1.1: Permeable pile groin at Domburg coast (Photo by jwarmelink, www.panoramio.com)

Permeable pile groins permit both water and sediment to pass through them. Because of this function, they act as a hydraulic roughness on the longshore current leading to a reduced littoral current velocity in the pile-groin field. In sequence, this leads to a decrease of the capacity of the current to transport sediment and a raising of the underwater profile in the groin vicinity. The shoreline shifts seaward parallel to the initial shoreline until a balance is reached (Bakker, 1984), producing a more uniform coastline (Figure 1.2) in contrast with the typical saw-tooth pattern of the impermeable groins (Figure 1.3). Furthermore, permeable pile groins may diminish the downdrift erosion which is one of the most important disadvantages of their impermeable counterparts.

Figure 1.2: Uniform shoreline of the Domburg coast (nl.wikipedia)

Figure 1.3: Saw-tooth shoreline of the North Carolina coast (Program for the Study of Developed Shorelines)

The most important advantages of permeable groins as provided by the field observations (Bakker, 1984) are:

- Decrease of the longshore current velocity
- Seaward shift of the shoreline
- Continuous growth of the underwater profile
- Seaward shift of the outer shoal leading higher waves to break further offshore
- Flexible construction
- Uniform shoreline
- Low cost construction

These effects can be noticed at Figure 1.4.

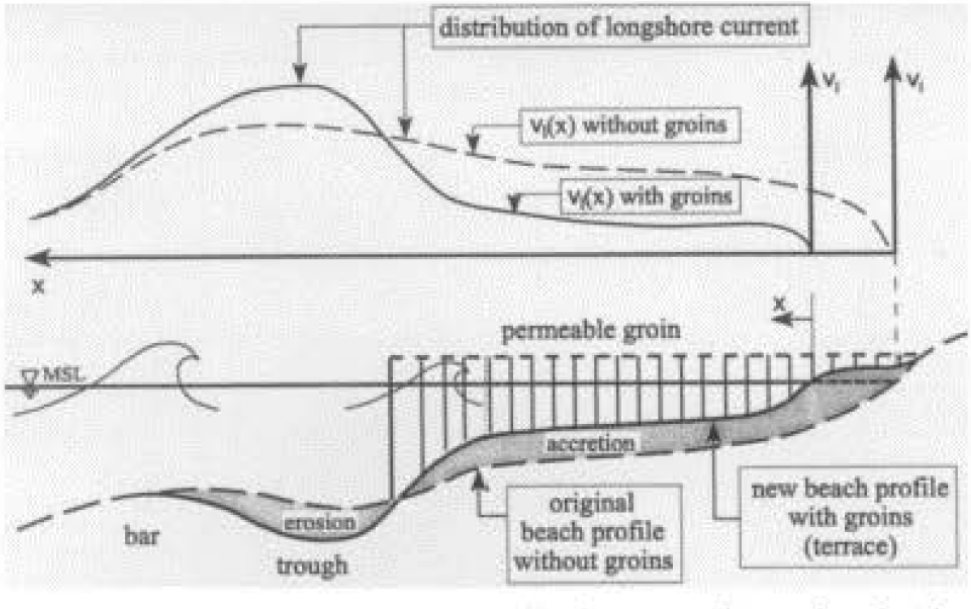

Figure 1.4: Longshore current velocity distribution and beach profile along a coastline with and without pile groins (Trampenau, 2004)

As a consequence of these positive effects, pile groins have been widely used at the southwest Zeeland coast in the Netherlands, where the tidal range reaches 4m, to retard the longshore current and reduce the longshore sediment transport capacity, in order to protect the coast from erosion. The stretch of Walcheren coast, has suffered erosion mainly due to the main strong tidal currents of 1 m/s occurring at the 10 m water depth offshore superposed by wave induced longshore current in the same direction. The pile row groins usually stand 2.5 m higher than the mean water level (Van Lynden, 2007). Because of the high crest level of the groins, they are prone to severely wave attack leading to high maintenance cost. Despite the fact that the permeable groins have been constructed for several years along many world's coastlines, there is limited research or study on their effects on the coastal system. This study aims to contribute to bridge the knowledge gap. A more detailed study of this type of constructions will provide the opportunity for better understanding of the dominant factors that influence the nearshore hydraulics at Domburg coast.

1.2 Research question

The main objective of this Master Thesis Project is to assess the influence of permeable pile groins on nearshore hydraulics at Domburg coast by means of numerical model (SWASH).

However, several sub-questions have to be answered at first, in order to successfully derive the primary objective of this study.

- To what extent is SWASH capable of modelling alongshore wave induced currents?
- To what extent is SWASH capable of modelling alongshore tide induced currents?
- How does the longshore wave induced current respond to a permeable pile groin?
- How does the tidal current respond to a permeable pile groin?
- Does the structure produce rip-currents and how much is their magnitude?
- Does the structure affect the wave conditions and in what way?
- Are there circulation cells downdrift of the groins?
- How do the different permeable pile groin schemes affect the nearshore current?

1.3 Research method

In order to address all the aforementioned steps towards answering the research question, a SWASH model is created. The way of approaching the solution is divided in four steps. The results of each one of them are compared to the results obtained from Hulsbergen's experiment and thus the validation of the SWASH model is examined. Following, the four steps followed are summarized:

1. Wave transformation and wave induced alongshore current: In this case only waves are present. The influence of different model input parameters is examined, such as the number of vertical layers, bottom friction model, turbulence model and discretization scheme. The results of Hulsbergen's experiment are used in order to validate and calibrate our model.

2. Tide induced current: The second part considers only tide. The implementation of the tide in the SWASH source code is according to the master thesis of Floris de Wit (2016). The results of Hulsbergen's experiment for this hydraulic condition are used in order to validate and calibrate the model.

3. Wave + Tide induced current: In the third part of the present thesis, the hydraulic condition, where the tidal currents and waves are combined, is examined. This is the

most crucial hydraulic condition that erodes the Domburg coast. This situation is also described in Hulsbergen's report making the validation of SWASH model feasible.

4. **Wave + Tide induced current + Permeable pile groins:** The final stage towards answering the research question is to examine how the permeable pile groins effect the longshore current under the combination of wave and tide induced current. Two different pile groin schemes are going to be examined, both of which are going to be validated after comparison with the experiment.

1.4 Outline

The present thesis constitutes of an introductory chapter (Chapter 1), that gives a description of the tasks that have been carried out, and two other parts, which include the literature study and the implementation of it in a specific case study respectively. A final part describes the conclusions of the study as well as recommendations for future studies.

The first section consists of two chapters: Chapter 2 gives the theoretical background regarding groins, waves, tide etc. as well as a description of the software used, SWASH, its capabilities and limitations. Chapter 3 includes a description of Hulsbergen's report, which is the source of the data to validate the results of the present thesis.

The second section is about the case studies examined in the present thesis. Chapter 4 presents the analyses, meaning model set up, results and conclusions, conducted for the case where only wave induced current is present. Chapter 5 includes the same information but for the case where only tide is present. The combination of wave and tide induced current is given in Chapter 6. Chapter 7 presents the most important part of the study, which is the implementation of permeable pile groins for different hydraulic conditions.

Finally comes the third part of the thesis that includes the conclusions and recommendations for future studies (Chapter 8). Following appendixes A and B are presented which include additional figures for wave induced current and additional figures for longshore current profiles inside permeable pile groin systems respectively.

2. Background Information

2.1 Introduction

At first, general information about groins is given in Section 2.2. Section 2.3, Section 2.4 and Section 2.5 describe coastal processes related to tide and waves and how these processes interact with the permeable pile groins (Section 2.6). Furthermore, this chapter illustrates some basic concepts related to bottom friction in Section 2.7 and to turbulent mixing in Section 2.8. Finally, in Section 2.9, the main characteristics of the SWASH model, which will be used in the present master thesis, are presented.

2.2 Groins

Groins structures have been very popular all over the world among the years. They have initially been successfully used for the protection of river banks. However, due to the fact that coastal erosion developed into one of the most serious problems of coastal engineering, groins transferred to coastal protection (Trampenau, 2004). The main function of a groin system is to interrupt water flow and limit the movement of sediment. Subsequently, accretion takes place in the groin field and the shoreline shifts seaward.

The mostly used type of groin worldwide is the classical impermeable groin. Impermeable groins block entirely longshore sediment transport. Since they act as a barrier to the longshore flow of sediment, they induce accretion along the updrift coast and erosion along the downdrift coast. Due to this important drawback, careful research and study should be done before their installation along a coast.

On the other hand, permeable pile groins, due to their permeability, do not lead to erosion along their downdrift coast. The permeability of a groin is defined by the ratio of the open area to the total cross-sectional area. In the case of a permeable pile groin this operation is achieved by placing the piles with a determinate distance to one another (Figure 2.1).

$$P = \frac{b}{D + b} \tag{2.1}$$

with:

P permeability expressed in percent,
D diameter of the piles,
b distance between two piles.

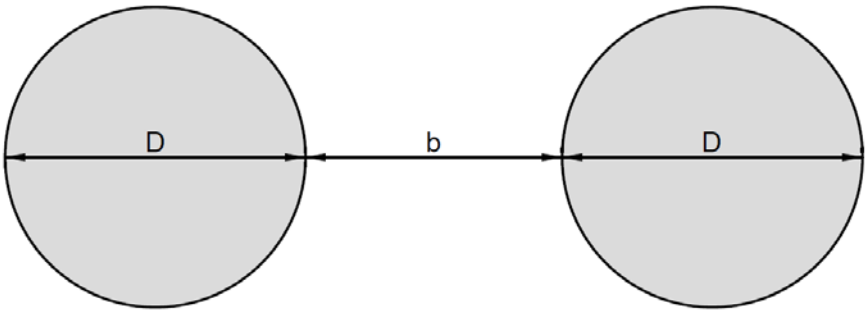

Figure 2.1 Permeability of pile groin

The permeability of a groin defines the resistance of the groin on the longshore flow. Low permeability means a high resistance to the flow, whereas high permeability leads to a low resistance. Many studies have been done in order to determine the optimum permeability of pile groins with respect to their hydraulic functioning. Jager and Weiss (1986/1990) proposed an increase in groin spacing at the outer limits of the groin field in order to reduce the downdrift erosion. This is also the design that has been followed in the case of pile groins at Domburg coast.

The most popular type of permeable pile groins is the timber piles which are widespread at the coasts of Baltic Sea and also at Domburg cost. One disadvantage of this type of piles is that they are exposed to damage by marine borers, which leads to high maintenance costs. However, use of concrete piles can overcome the borer problem.

2.3 Tide and tidal currents

Isaac Newton (1642-1727) was the first to determine that the origin of the tide is the gravitational pull of the moon and the sun on the water in the oceans. Tide is the periodic rise and fall in the level of the water in oceans and seas. The most typical timescale of tidal variation is that of the semi-diurnal (twice a day) and diurnal tides (once a day). The difference between the high and low tide is called tidal range. This vertical rise and fall leads to a flow that is called tidal current.

Since the movement of the tides is deflected by Coriolis and blocked by land masses, rotary movements are formed in oceans basins which are counter-clockwise in the Northern hemisphere and clockwise in the Southern hemisphere (Bosboom and Stive, 2013). These rotary movements are called amphidromic systems and the centers of these rotations are called amphidromic points.

In the Figure 2.2, the propagation of the tide in the North Sea can be observed. At the southwest Zeeland coast in the Netherlands, the tidal range can reach 4m. As a consequence, pile groins have been widely used to protect the coast from erosion. The stretch of Walcheren coast, has suffered erosion mainly due to the strong tidal currents of 1 m/s occurring at 10 m water depth offshore enhanced by wave induced longshore current in the same direction.

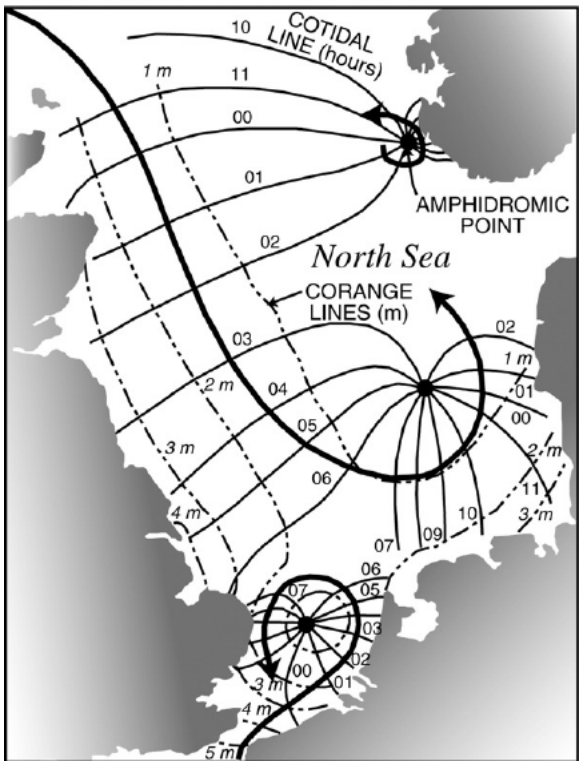

Figure 2.2 Propagation of the tide in the North Sea

2.4 Waves and wave related currents

As waves approach a coast, they are affected by the presence of the seabed through processes such as refraction, shoaling, bottom friction and wave breaking. In addition, if the waves come in touch with a coastal structure like a breakwater, they will be transformed by diffraction.

The wave energy E and the wave power U can be described as (Bosboom and Stive, 2013):

$$E_w = \frac{1}{8} pgH^2 \tag{2.2}$$

$$U = Ec_g = Enc \tag{2.3}$$

with:

H	wave height
c_g	wave group velocity
c	wave celerity
n	ratio c_g to c

Shoaling

Assuming that the dissipation of the wave energy during the propagation of the wave between two arbitrary locations in a coastal area is approximately zero then the wave power remains constant:

$$U = E_1 n_1 c_1 = E_2 n_2 c_2 \Rightarrow \frac{H_2}{H_1} = \sqrt{\frac{c_1}{c_2}\frac{n_1}{n_2}} \tag{2.4}$$

If the location 1 is in deep water and the location 2 is in the intermediate water with depth h then the equation 2.4 yields:

$$\frac{H}{H_0} = \sqrt{\frac{1}{\left(1 + \frac{2kh}{\sinh(2kh)}\right)\tanh(kh)}} = K_{sh} \tag{2.5}$$

The parameter K_{sh} is called the shoaling factor and connects the change of the wave height with the change of the wave length and the depth.

Refraction

When a wave approaches depth contours at an angle, it tends to become parallel to the contours (Figure 2.3). The fact that the crest in deeper parts travels faster than in the shallower parts, leads to this phenomenon which is called refraction and can be described by the Snell's law:

$$\frac{sin\varphi_2}{c_2} = \frac{sin\varphi_1}{c_1} \tag{2.6}$$

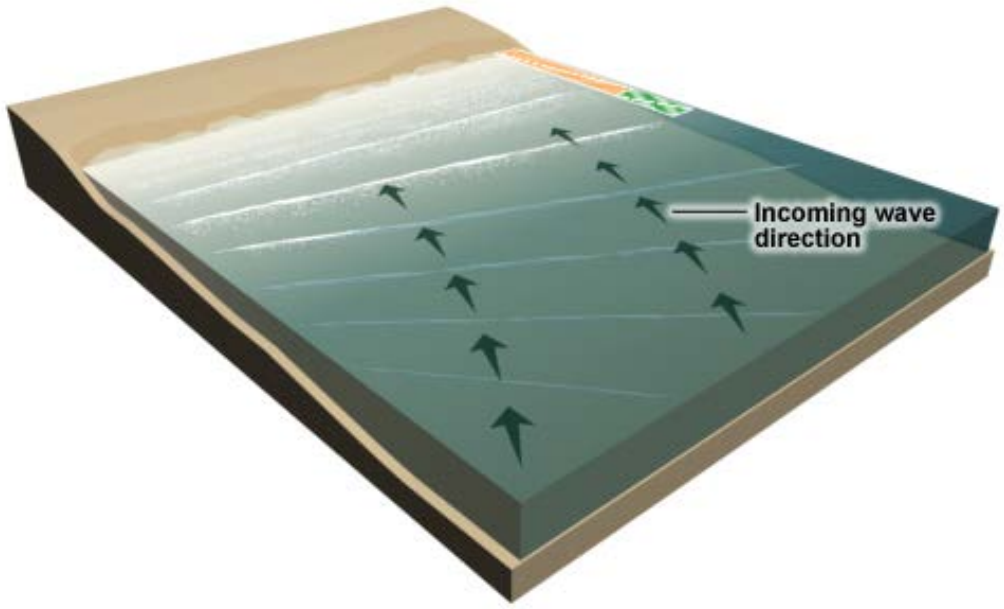

Figure 2.3 Obliquely incident waves propagating on uniform depth contours (COMET)

Diffraction

Diffraction is taking place when there are coastal structures such as breakwaters and groins. Diffraction is the phenomenon by which the waves propagate into the lee zone (shadow zone) behind the coastal structures by transfer of energy along the wave crests (Bosboom and Stive, 2013). In Figure 2.4 it can be observed that a part of the wave is blocked by the structure and the other part bends around the breakwater and penetrates into the shadow zone.

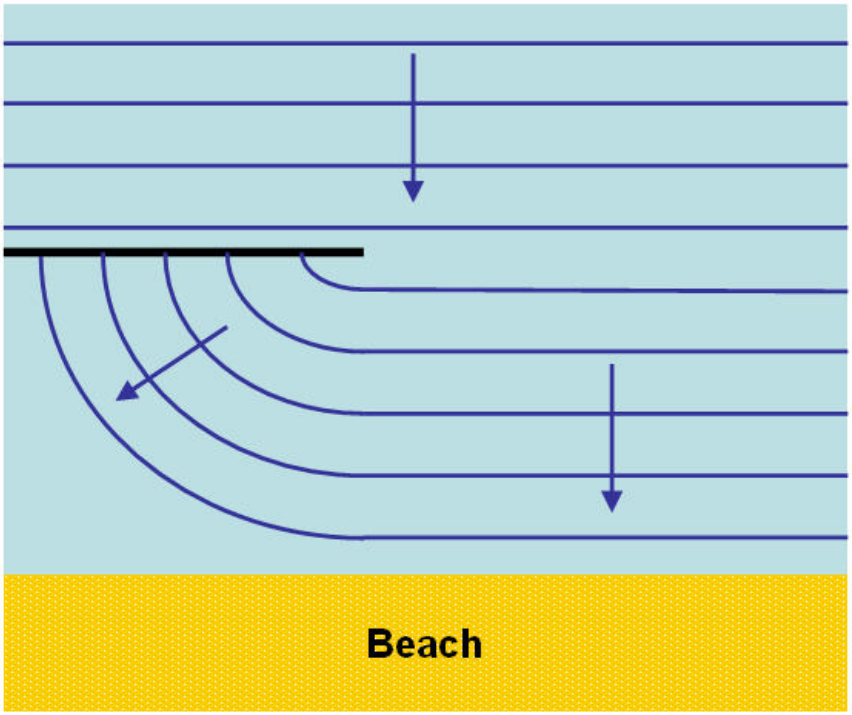

Figure 2.4 Diffraction of a wave train by a breakwater (cronodon.com)

Wave breaking

As it is already mentioned, shoaling increases the wave height until infinity. However, a wave becomes unstable and breaks when the particle velocity is becoming higher than the velocity of the wave crest (Bosboom and Stive, 2013). The basic equation that defines the limiting wave steepness was expressed by Miche (1944):

$$\gamma = \left[\frac{H}{L}\right]_{max} = 0.142\tanh(kh) \tag{2.7}$$

with:

γ	breaker index
H	wave height
L	wave length

Radiation Stress-Wave-induced forces

Radiation stress was defined by Longuet-Higgins and Stewart (1964) as the excess momentum flux which is carried by the waves. The radiation stress can be translated as the additional forcing due to the presence of the waves which means that varying radiation stresses lead to changes in the mean water level (set-up, set-down) and to the mean flow (wave induced longshore current).

The radiation stress components for waves travelling in a direction θ relative to the positive x-direction are given by:

$$S_{xx} = \left(n - \frac{1}{2} + ncos^2\theta\right)E \tag{2.8}$$

$$S_{yy} = \left(n - \frac{1}{2} + nsin^2\theta\right)E \tag{2.9}$$

$$S_{xy} = S_{yx} = ncos\theta sin\theta E \tag{2.10}$$

As it is already mentioned, the wave forces exist due to the wave-induced horizontal changes in momentum flux. The net force in the x-direction and y-direction are given by:

$$F_x = -\left(\frac{\partial S_{xx}}{\partial x} + \frac{\partial S_{xy}}{\partial y}\right) \tag{2.11}$$

$$F_y = -\left(\frac{\partial S_{yy}}{\partial y} + \frac{\partial S_{yx}}{\partial x}\right) \tag{2.12}$$

For an alongshore uniform coast the equations 2.11 and 2.12 yield to:

$$F_x = -\frac{\partial S_{xx}}{\partial x} \tag{2.13}$$

$$F_y = -\frac{\partial S_{yx}}{\partial x} \tag{2.14}$$

Wave set-up and set-down

The wave set-up and set-down are very important phenomena in the coastal hydrodynamics. The change in the mean water level due to the break of the waves leads to a slope and a pressure gradient to balance the onshore component of the radiation stress. The equilibrium between the radiation stress gradient and pressure term due to the water level slope gives (Bosboom and Stive, 2013):

$$F_x = -\frac{dS_{xx}}{dx} = \rho g h \frac{d\overline{\eta}}{dx} = \rho g (h_0 + \overline{\eta}) \frac{d\overline{\eta}}{dx} \tag{2.15}$$

with:

x	co-ordinate axis pointing from land to sea
h_0	still-water depth at point x
$\overline{\eta}$	wave induced water level setup at point x

It is worth mentioning that in the shoaling zone the term dS_{xx}/dx is positive leading to an offshore wave force. Therefore the factor $d\overline{\eta}/dx$ (water level gradient) is negative which means that the water surface becomes lower (set-down) in the shoaling zone. On the other hand, in the surf zone the term dS_{xx}/dx is negative yielding an onshore wave force. Therefore the factor $d\overline{\eta}/dx$ (water level gradient) is positive which means that the water surface becomes higher (set-up) in the surf zone (Figure 2.5).

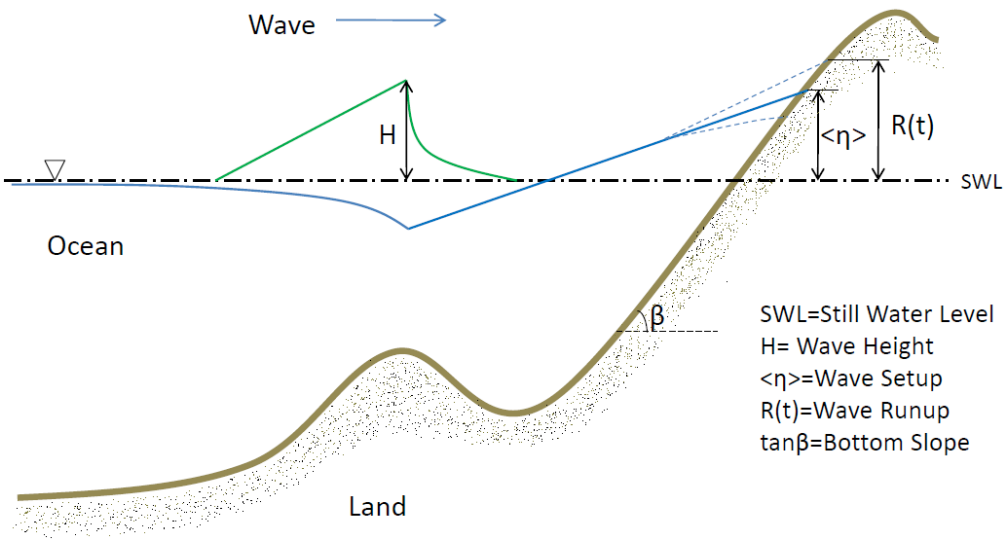

Figure 2.5 Set-down and set-up (barrowgeoblog.blogspot.nl)

Alongshore current

The longshore current plays a dominant role in the nearshore zone since it affects to a great extent the sediment transport. The longshore current is created by the transfer of momentum from the wave motion to the mean flow and it is running parallel to the shoreline (Figure 2.6). In particular, the shore-parallel component of the radiation stress (Eq. 2.14) is the factor that generates the longshore current. It is noteworthy that apart from wave–induced current, also tide and wind can generate an alongshore current (Section 2.3).

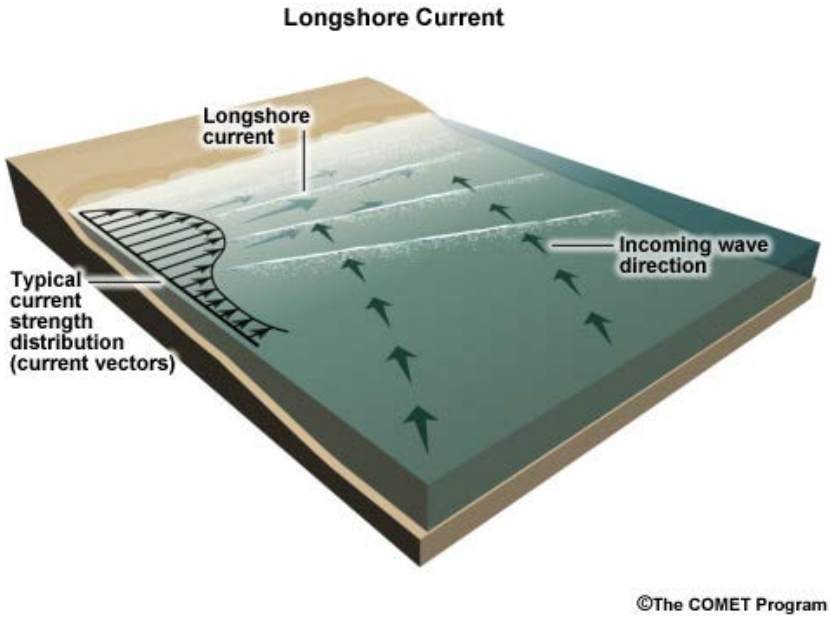

Figure 2.6 Longshore current (COMET)

A simple analytical solution for the wave-induced longshore current can be derived, under the assumptions of longshore homogeneity in bathymetry and wave height, constant beach slope,

no lateral dispersion and a simple breaking model ($\gamma_b = H_b/h_b = constant$). According to Bosboom and Stive (2013), under these assumptions, the longshore current in the surf zone is given by:

$$V(x) = \frac{5}{16}\pi \frac{H_b}{c_f} g \frac{sin\varphi_0}{c_0} \frac{h}{h_b} tana \tag{2.16}$$

with:

V	longshore current speed
c_f	bottom friction coefficient
$\tan a$	beach slope
φ_0	wave crest angle relative to the depth contours
H_b	wave height at the break point
h_b	water depth at the break point
c_0	phase velocity at deep water

According to Eq. 2.16, the longshore current velocity in the surf zone is proportional to the depth (h) with a maximum at the break point. Furthermore, because the fact that the radiation shear stress S_{yx} is constant seaward of the breaker line, the longshore current velocity reduces immediately to zero offshore of the break point. As it is already mentioned, the effect of the lateral dispersion of momentum by turbulence has not been taken into account at the Eq. 2.16. Including lateral dispersion leads to smooth out the velocity profile (Figure 2.7).

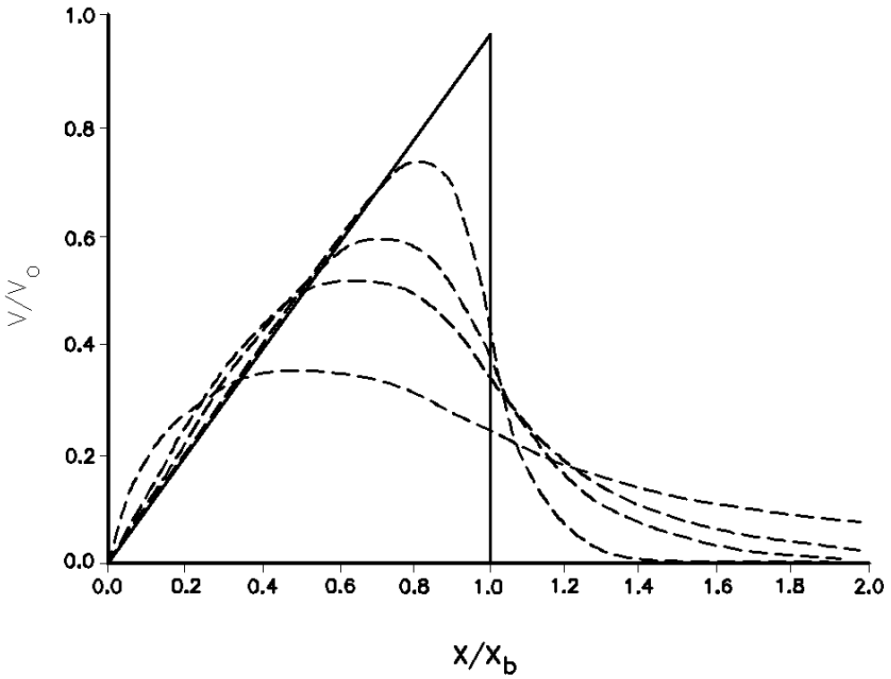

Figure 2.7 Longshore velocity distribution (solid line=no lateral dispersion, dashed line=with lateral dispersion) CEM

The main goal of the permeable pile groins is to act as a hydraulic roughness on the longshore current in order to retard it in their vicinity. In this way, they decrease the capacity of the current to transport sediment. Having said this, the understanding and estimation of the longshore current is of major importance.

2.5 Rip currents

Rip currents are strong, narrow currents that flow seaward from the surf zone (Bosboom and Stive, 2013). They can be generated by longshore variations in wave setup. The longshore gradient in wave setup creates a flow that travels from the position of highest waves and setup toward the position of the lowest waves and setup. In this way, at certain intervals along the shoreline, the longshore current will form a rip current (Figure 2.8).

Moreover, rip currents can be generated when longshore currents meet an obstacle, for instance a permeable pile groin. According to Hulsbergen (1973), seaward current of 0.3 m/s at the tip of the permeable pile groin can be generated. However, permeable groins with relatively high permeability over their entire length can diminish rip currents and circulation cells (Trampenau, 2000).

Rip currents are important for the coastal area because of the fact that they can transport large amounts of sediment offshore, out of the coastal system and thus they act as an erosion mechanism. Furthermore, considerable scours have been observed along the tip of permeable pile groins due to rip currents which can affect the stability of the piles. In addition, apart from erosion, rip currents are dangerous for human life due to their large magnitude of velocity. Finally, rip currents can block the longshore current to a great extent making the permeable pile groins to act as impermeable.

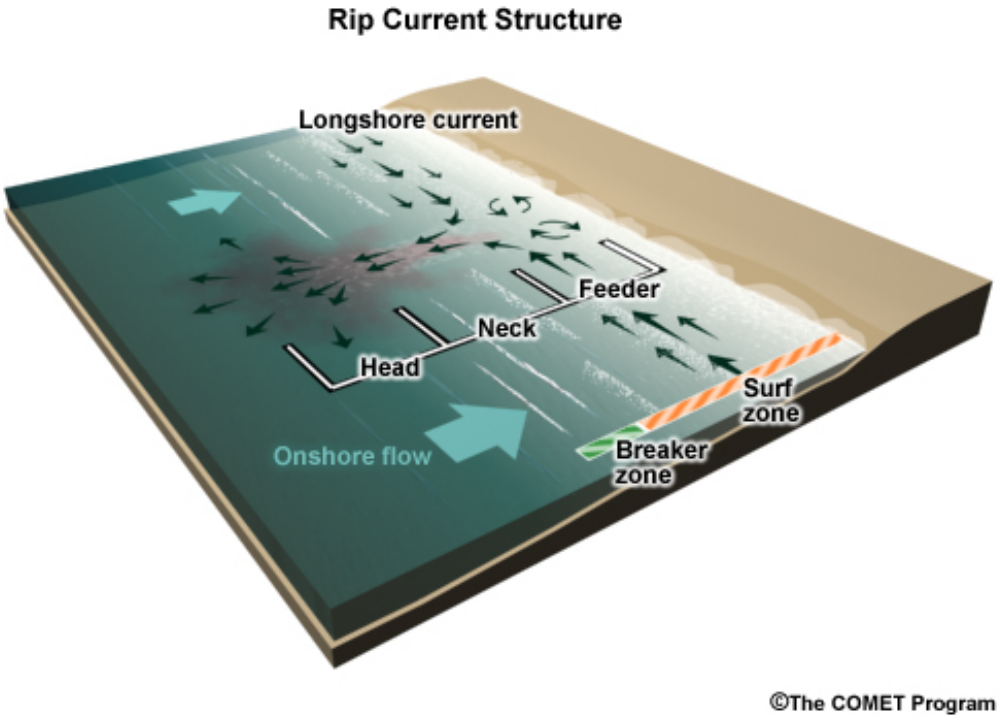

Figure 2.8 Rip current pattern (COMET)

2.6 Interaction of piles with flow and waves

The Morison equation (Morison, 1950) can be used to quantify the total force on pile in oscillatory flow. Morison (1950) found a relation between the force on a vertical pile as a function of the velocity and the acceleration of water particles in a wave. The part of the force that is caused by the flow velocity is the drag force (F_D) and the part that is caused by the acceleration of the water particles is the inertia force (F_I).

The total force is given by:

$$F = F_D + F_I = \frac{1}{2}\rho C_D D h u|u| + \frac{1}{4}\rho C_M \pi h D^2 \frac{\partial u}{\partial t} \quad (2.17)$$

$$u = \omega a \frac{\cosh(k(d+z))}{\sinh(kd)} \sin(\omega t) \quad (2.18)$$

$$\frac{\partial u}{\partial t} = \omega^2 a \frac{\cosh(k(d+z))}{\sinh(kd)} \cos(\omega t) \quad (2.19)$$

with:

F	total force
F_D	drag force
F_I	inertia force
C_D	drag coefficient
C_M	inertia coefficient
ρ	density of the fluid
D	diameter of the pile
h	length of the pile immersed in the water
u	horizontal velocity of the water particles
$\frac{\partial u}{\partial t}$	horizontal acceleration of the water

As it can be observed, the drag coefficient (C_D) is very important in order to predict and estimate the damping effect of the piles. In this master thesis, a value of $C_D = 1.5$ is used according to RIZA (2003) for stem of trees.

On the other hand, previous studies have proved that the permeable pile groins as their impermeable counterparts do not affect the waves in a direct way. However, there are indirect mechanisms such as the seaward shift of the shoreline due to sedimentation and the development of a terrace in the groin field as well as the steeper beach slope at the groin tip that cause the higher water waves to break further seaward (Trampenau, 2000). This function plays a very important role during severe storm conditions as it increases the energy dissipation.

2.7 Bottom friction

Bottom friction is a dominant force in the hydrodynamic balance of coastal areas due to the limited water depth in contrast with the deep water where friction is negligible. This is a consequence of the fact that bottom friction is a surface force which increases as the water depth decreases. In addition, bottom friction is proportional to the square of the current

velocity (Eq. 2.20), making it a very important factor. In the following paragraphs, the different friction concepts that are examined in the present master thesis, are presented.

Dimensionless friction coefficient

The bed shear stress is related to the flow velocity through a dimensionless bed resistance coefficient (bed friction coefficient).

$$c_f = \frac{\tau_b}{\rho u|u|} \tag{2.20}$$

with:

c_f	dimensionless friction coefficient
τ_b	bed shear stress
ρ	density of the water
u	flow velocity

Chezy formula

$$u = C\sqrt{RI} \tag{2.21}$$

with:

u	flow velocity
C	Chezy coefficient
R	hydraulic radius
I	slope of the energy head

The Chezy coefficient C in not dimensionless ($m^{1/2}/s$) and represents a smoothness coefficient which means that a large value of C leads to a low roughness (Schiereck updated by Verhagen, 2012). The Chezy coefficient can be related to the equivalent roughness k_r according to Nikuradse-Colebrook (Eq. 2.22) and to the dimensionless friction coefficient c_f (Eq. 2.23).

$$C = \frac{\sqrt{g}}{k}\ln\frac{12R}{k_r} = 18\log\frac{12R}{k_r} \tag{2.22}$$

$$C = \sqrt{\frac{g}{c_f}} \tag{2.23}$$

Manning formula

$$u = \frac{1}{n}R^{2/3}\sqrt{I} \tag{2.24}$$

with:

u	flow velocity
n	Manning number
R	hydraulic radius
I	slope of the energy head

The manning number is also not dimensionless ($s/m^{1/3}$) and represents a roughness coefficient. The manning number can be related to the dimensionless friction coefficient c_f, see Equation (2.25).

$$n = R^{1/6}\sqrt{\frac{c_f}{g}} \tag{2.25}$$

Colebrook-White formula

The Colebrook-White equation is suitable for pipe flow and can be written as:

$$\frac{1}{\sqrt{f}} = -2\log_{10}\left(\frac{k}{14.83R} + \frac{2.52}{Re\sqrt{f}}\right) \tag{2.26}$$

with:

f	Darcy resistance coefficient
k	roughness coefficient
R	hydraulic radius
Re	Reynold's number

Logarithmic wall law

The logarithmic wall law was first expressed by Theodore von Kármán (1930) and states that the average velocity of a turbulent flow at a certain point is proportional to the logarithm of the distance from that point to the wall. The logarithmic law of the wall can be written as:

$$u = \frac{u_\tau}{k}\ln\frac{y}{y_0} \tag{2.27}$$

with:

u	flow velocity
u_τ	shear velocity
k	Von Karman constant
y_0	distance from the boundary at which the velocity goes to zero

It is worth mentioning that the Equation (2.27) is only applicable to parts of the flow that are close to the bed (wall).

2.8 Turbulent mixing

The theoretical estimation and prediction of turbulence continues to be a fundamental problem of the hydrodynamics. The major difficulty derives from the random nature of turbulence phenomena. A turbulence model is defined as a set of equations which determine the turbulent transport terms in the mean flow equations and as a consequence close the system of equations. In the following paragraphs, different turbulent mixing models both for horizontal and vertical direction will be examined.

2.8.1 Horizontal mixing

Constant horizontal eddy viscosity

Constant horizontal eddy viscosity may be used for the whole flow field of large water bodies. This concept is highly important for depth average calculations where only horizontal transport is considered. Moreover, it can give reliable results for problems of limited vertical resolution.

Prandtl mixing length

Prandtl in 1925 suggested the first proper turbulence model which is capable to describe the distribution of the eddy viscosity. This is known as the Prandtl mixing length hypothesis which states that the eddy viscosity v_t is proportional to the local mean velocity gradient and to the mixing lengthl_m (Eq. 2.28).

$$v_t = {l_m}^2 \left|\frac{dU}{dy}\right| \tag{2.28}$$

with:

v_t	eddy viscosity
l_m	mixing length
$\frac{dU}{dy}$	velocity gradient

The Prandtl mixing length model is suitable for simple shear-layer dominated or pressure-driven flows where experimental correlations for the mixing length exist. Other advantages are that it is easy to implement and does not need large computational times. On the other hand, Prandtl mixing length hypothesis is unsuitable for complex flows in which the turbulent length scale varies. Having said this, it is incapable for flows that include separation or circulation.

Smagorinsky model

Smagorinsky model is the simplest model and has been proven to perform reasonably well. It is a Large Eddy Simulation (LES) which assumes that the energy production and dissipation of the small scales are in equilibrium. The Smagorinsky model could be summarized as:

$$v_t = {l_S}^2 |\bar{S}| \tag{2.29}$$

$$|\bar{S}| = \sqrt{\bar{S}_{ij}\bar{S}_{ij}} \tag{2.30}$$

$$\overline{S_{ij}} = \frac{1}{2}\left(\frac{\partial \overline{u_i}}{\partial x_j} + \frac{\partial \overline{u_j}}{\partial x_i}\right) \tag{2.31}$$

$$l_S = (C_S \Delta) \tag{2.32}$$

with:

v_t	eddy viscosity
l_S	Smagorinsky length scale
C_S	Smagorinsky coefficient
Δ	filter length (grid size)
$\overline{u_i}$	averaged velocity in x_i direction
$\overline{u_j}$	averaged velocity in x_j direction

The Smagorinsky constant usually has the value between 0.1 and 0.2 and has to be determined as an input. As a consequence, this is a drawback due to the fact that this single constant is incapable to represent with accuracy different turbulent flows.

2.8.2 Vertical mixing

k-ε model

The k-epsilon turbulence model is a two equation model which can describe turbulence by means of two transport equations (PDEs). The first equation is provided for the turbulent

kinetic energy k and the second one for the energy dissipation ε. According to Launder and Spalding (1974), the standard k-ε turbulence model is described at Equations 2.33 and 2.34.

For turbulent kinetic energy k

$$\frac{\partial(\rho k)}{\partial t}+\frac{\partial(\rho k u_i)}{\partial x_i}=\frac{\partial}{\partial x_j}\left[\frac{\mu_t}{\sigma_k}\frac{\partial k}{\partial x_j}\right]+2\mu_t E_{ij}E_{ij}-\rho\varepsilon \tag{2.33}$$

For energy dissipation ε

$$\frac{\partial(\rho\varepsilon)}{\partial t}+\frac{\partial(p\varepsilon u_i)}{\partial x_i}=\frac{\partial}{\partial x_j}\left[\frac{\mu_t}{\sigma_\varepsilon}\frac{\partial \varepsilon}{\partial x_j}\right]+C_{1\varepsilon}\frac{\varepsilon}{k}2\mu_t E_{ij}E_{ij}-C_{2\varepsilon}\rho\frac{\varepsilon^2}{k} \tag{2.34}$$

The eddy viscosity

$$\mu_t=\frac{\rho C_\mu k^2}{\varepsilon} \tag{2.35}$$

The closure coefficients are given by (Rodi, 1980):

$$C_{1\varepsilon}=1.44, C_{2\varepsilon}=1.92, C_\mu=0.09, \sigma_k=1.0, \sigma_\varepsilon=1.3$$

Within the vegetation canopy, it is assumed that all energy of the mean flow is converted to turbulent energy due to the plant drag. Considering vegetation effects, the k-ε equations in the conservative form are given by Equations 2.36 and 2.37 as suggested by Gangfeng Ma (2013).

$$\frac{\partial(Dk)}{\partial t}+\nabla\cdot(Duk)=\nabla\cdot\left[D\left(v+\frac{v_t}{\sigma_k}\right)\nabla k\right]+D(P_s+C_{fk}P_v-\varepsilon) \tag{2.36}$$

$$\frac{\partial(D\varepsilon)}{\partial t}+\nabla\cdot(Du\varepsilon)=\nabla\cdot\left[D\left(v+\frac{v_t}{\sigma_\varepsilon}\right)\nabla\varepsilon\right]+\frac{\varepsilon}{k}D(C_{1\varepsilon}(P_s+C_{f\varepsilon}P_v)-C_{2\varepsilon}\varepsilon) \tag{2.37}$$

The values of the two empirical constants $C_{fk}=0.07$ and $C_{f\varepsilon}=0.16$ are selected as suggested by Shimizu and Tsujimoto (1994)

2.9 SWASH model

2.9.1 General information

SWASH (Simulating Waves till Shore) is a non-hydrostatic open source code model based on the work of Stelling and Zijlema (2003), Stelling and Duinmeijer (2003), Zijlema and Stelling (2005, 2008) and Smit et al. (2013). The main utility of the SWASH is to provide an efficient and robust model that allows a wide range of time and space scales of surface waves and shallow water flows in complex environments to be applied. It has no limitations and can capture flow phenomena with spatial scales from centimeters to kilometers and temporal scales from seconds to hours (The SWASH team, 2016).

SWASH is not a Boussinesq-type wave model. SWASH in contrast with Boussinesq-type wave models, improves its frequency dispersion by increasing the vertical layers. On the other hand, Boussinesq-type wave models increase the order of derivatives of dependent variables to ameliorate their frequency dispersion. In addition, the effects of wave-wave and wave-current interaction in shallow water are automatically included. Therefore, SWASH does not need to

calculate the radiation stresses and subsequently to solve a wave-averaged hydrodynamic model separately.

2.9.2 Governing equations

SWASH is a numerical model for simulating non-hydrostatic, free-surface, rotational flow and transport phenomena in one, two or three dimensions. According to the manual, the governing equations are the nonlinear shallow water equations including non-hydrostatic pressure and some transport equations (The SWASH team, 2016).

The depth-averaged, non-hydrostatic, free-surface flow in a two dimensional horizontal domain can be described by the nonlinear shallow water equations. Furthermore, the nonlinear shallow water equations can be derived from the incompressible Navier-Stokes equations. Consequently, for the depth-averaged case, the momentum equations (Eq. 2.38, Eq. 2.39) and the continuity equation (Eq. 2.40) are given by:

$$\frac{\partial u}{\partial t}+u\frac{\partial u}{\partial x}+v\frac{\partial u}{\partial y}+g\frac{\partial \zeta}{\partial x}+\frac{1}{h}\int_{-d}^{\zeta}\frac{\partial q}{\partial x}dz+c_f\frac{u\sqrt{u^2+v^2}}{h}=\frac{1}{h}\left(\frac{\partial h\tau_{xx}}{\partial x}+\frac{\partial h\tau_{xy}}{\partial y}\right) \quad (2.38)$$

$$\frac{\partial v}{\partial t}+u\frac{\partial v}{\partial x}+v\frac{\partial v}{\partial y}+g\frac{\partial \zeta}{\partial y}+\frac{1}{h}\int_{-d}^{\zeta}\frac{\partial q}{\partial y}dz+c_f\frac{v\sqrt{u^2+v^2}}{h}=\frac{1}{h}\left(\frac{\partial h\tau_{yx}}{\partial x}+\frac{\partial h\tau_{yy}}{\partial y}\right) \quad (2.39)$$

$$\frac{\partial \zeta}{\partial t}+\frac{\partial hu}{\partial x}+\frac{\partial hv}{\partial y}=0 \quad (2.40)$$

with:

t	time
u, v	depth-averaged flow velocities in x- and y- directions
ζ	surface elevation
d	still water depth
h	water depth
q	non-hydrostatic pressure normalized by the density
g	gravitational acceleration
c_f	bottom friction coefficient
$\tau_{xx,}\tau_{xy,}$	horizontal turbulent stress terms

2.9.3 Applicability of SWASH

According to the manual, SWASH accounts for the following physical phenomena:

- wave propagation, frequency dispersion, shoaling, refraction and diffraction,
- nonlinear wave-wave interactions (including surf beat and triads),
- wave breaking,
- wave run-up and run-down,
- moving shoreline,
- bottom friction,
- partial reflection and transmission,
- wave interaction with structures,
- wave-current interaction,
- wave-induced currents,

- vertical turbulent mixing,
- subgrid turbulence,
- wave damping induced by aquatic vegetation,
- rapidly varied flow,
- tidal waves,
- tidal currents,
- bores and flood waves,
- wind driven flows,
- space varying wind and atmospheric pressure,
- density driven flows,
- transport of suspended load for (non)cohesive sediment,
- turbidity flows and
- transport of tracer.

As it can be observed, SWASH is applicable for many phenomena which are associated with the present Master Thesis (underlined phenomena). As a result, SWASH is the perfect tool to assess the influence of permeable pile groins on nearshore hydraulics.

3. Data for calibration and validation

3.1 Introduction

In this chapter, the experiment of Hulsbergen, which is used to validate and evaluate the results from the SWASH model, is presented. Despite the age of the experiment (1973), Hulsbergen's report gives us the opportunity to validate our model in every step due to the large amount of measurements.

3.2 Hulsbergen (1973)

In order to study the influence of permeable pile groins on nearshore hydraulics, Hulsbergen used permeable groins on laboratory scale. The hydraulic conditions that were examined in the laboratory were based on the wave and tide conditions of the Domburg coast. These conditions were reduced to laboratory scale by using Froude scaling. Specifically, the length scale factor was $n_l = 40$ and thus the velocity scale factor was $n_v = \sqrt{n_l} = \sqrt{40}$.

The coastal profile of the prototype is presented in Figure 3.1. The bed profile is schematized for the first 140 m with a slope of 1:35. Seawards, the bed has a profile gradient of 1:20 and at depth of 10 m is connected to a horizontal bottom. By using the length scale factor, the bathymetry of the laboratory model is determined as indicated in Figure 3.2.

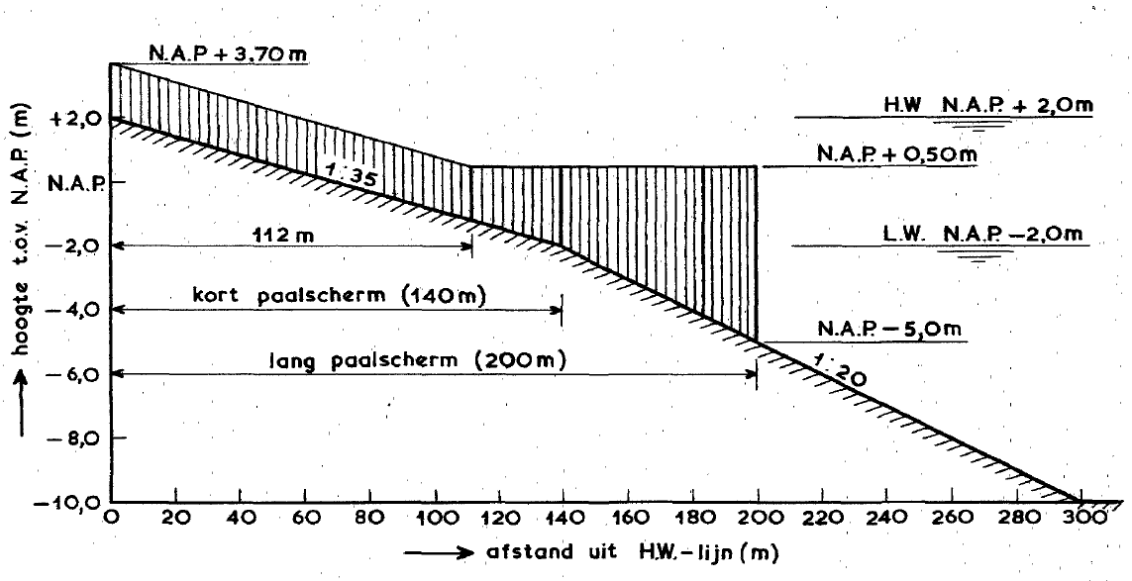

Figure 3.1 Bed profile of the prototype

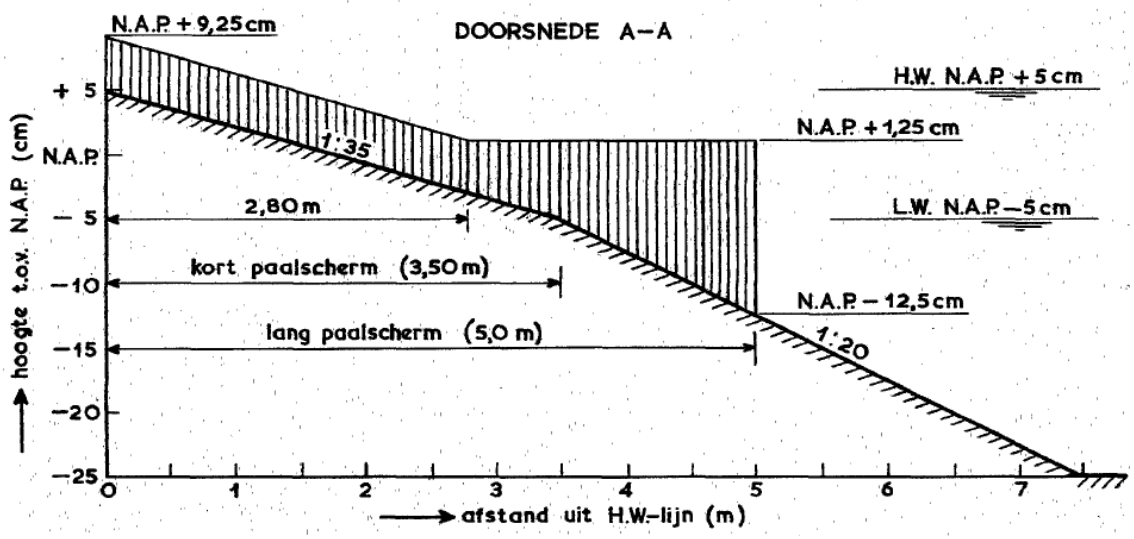

Figure 3.2 Bed profile of the scale model

The dimensions of the basin are showed in Figure 3.3. Regular waves were generated at the top of the basin by a wave maker. The basin had a size of 35.35 m in longshore direction and 12.10 m in cross-shore direction. In the experiments, the groins were represented by wooden piles with a diameter of 0.625 cm. In addition, Hulsbergen examined different groin fields (Figure 3.4) for different hydraulic conditions (Table 3.1). It is worth mentioning that the angle between the piles and the coastline was 90° for all cases and the space of the double-pile screens was 8.75 cm (3.5 m at prototype).

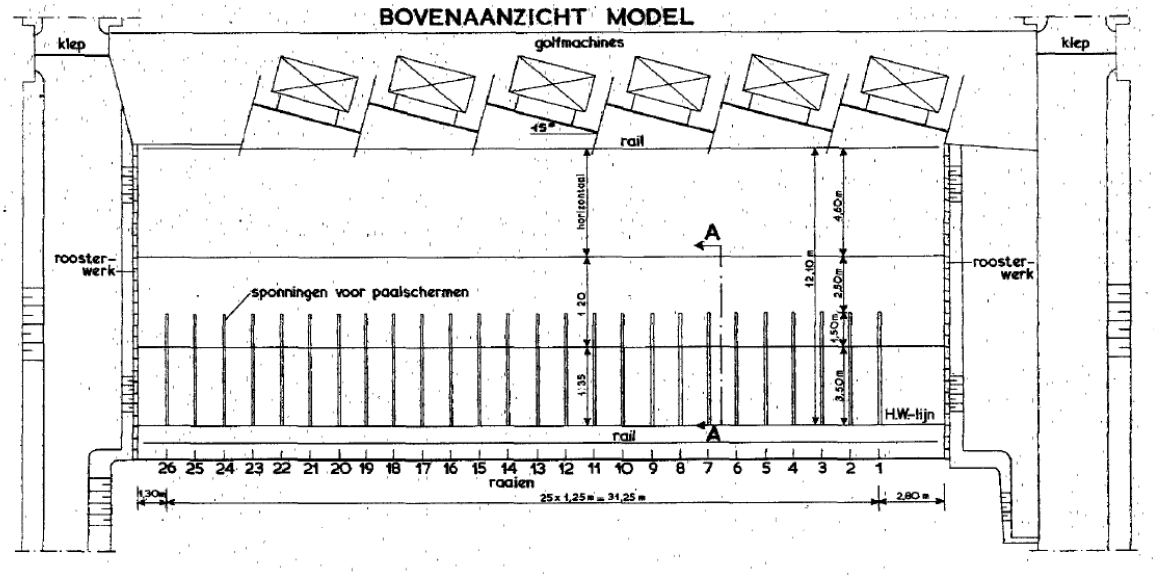

Figure 3.3 Set-up of the basin

Hydraulic condition	water level	flow (l/s)	wave period (s)	wave height (cm)	wave angle	flow direction
1	H.W.	450	no waves			
2	H.W.	450	no waves			
3	H.W.	450	1,04	3,0	15°	
4	H.W.	450	1,04	3,0	15°	
5	H.W.	0	1,04	3,0	15°	
6	L.W.	250	no waves			

Table 3.1 Hydraulic conditions

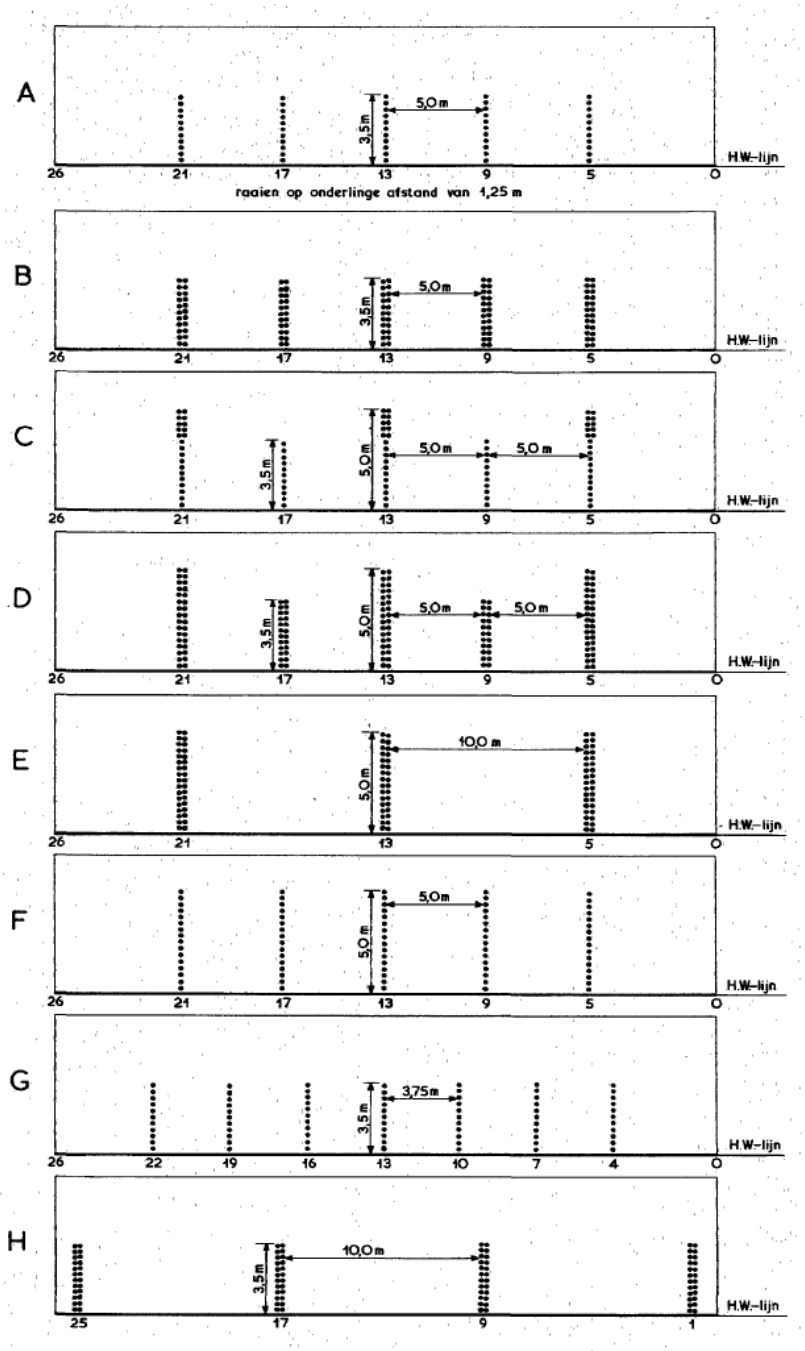

Figure 3.4 Pile groins schematizations

As it can be observed from Figure 3.4, the groin schemes of B and E are closer to the real schematization of the groin at Domburg coast. According to Bakker (1983-1996), groins consisting of two rows of piles were more effective than single row groins with longshore spacing of half the longshore spacing between the double-row groins. Furthermore, Hulsbergen examined how these two forms of groins perform under the hydraulic condition 4 (waves and tide in the same direction) which is the severest situation as it leads to the strongest currents. Finally, Table 3.2 provides the cases that are considered in the present Master Thesis.

Hydraulic condition	water level	tidal current (m/s)	wave period (s)	wave height (m)	wave angle	flow direction	without groin	groin form
1	H.W.	1,0	no waves			←	✓	
4	H.W.	1,0	6,5	1,2	15°	← ← - - -	✓	✓ B,E
5	H.W.	0,0	6,5	1,2	15°	← - - -	✓	

Table 3.2 Cases under consideration in the present Master Thesis

4. Wave transformation and wave induced alongshore current

4.1 Introduction

This chapter considers the case in which only waves (hydraulic condition 5) are present. The results of Hulsbergen's experiment are used in order to validate and calibrate our model. Different model settings concerning the number of vertical layers, bottom friction models, turbulence models and discretization schemes are examined.

At first, in Section 4.2 the general set-up for all test-cases is described. Afterwards, the results for the wave transformation and the wave induced alongshore current are presented in Section 4.3. These results are compared with those of Hulsbergen's report and finally conclusions on this analysis are discussed in Section 4.4.

4.2 Model setup

Domain and bathymetry

The domain of the basin that is used has a size of $l_x = 570\ m$ in cross-shore direction and $l_y = 1500\ m$ in longshore direction. The grid resolution in all the numerical test-cases is set to $\Delta_x \times \Delta_y = 0.5\ m \times 2.0\ m$. According to the SWASH manual (The SWASH team, 2016), for low waves ($H/d \ll 1$) it is sufficient to take 50 grid cells per wave length. However, for relatively high waves, it is better to take at least 100 grid cells per wave length. In the present case, the imposed waves have a wave height of 1.2 m at the deepest part ($d = 12$) and a period of 6.5s. Consequently, the wave length is about 66 m and $H/d = 0.1$. Therefore, the waves are not too low but also not too high either. Finally, a grid size of 0.5 m in the wave propagation direction is used not only for safety reasons, but also for a more effective implementation of the piles (Chapter 7). Having said this, the total number of grid cells for the computational domain would be 1140×750.

The bottom profile of the model is according to Hulsbergen's report (Figure 3.1) and is presented in Figure 4.1. Moreover, the bathymetry of the under consideration basin can be observed in Figure 4.2. It is worth mentioning that after 300 m from the coastline the bed profile is connected to a horizontal bottom.

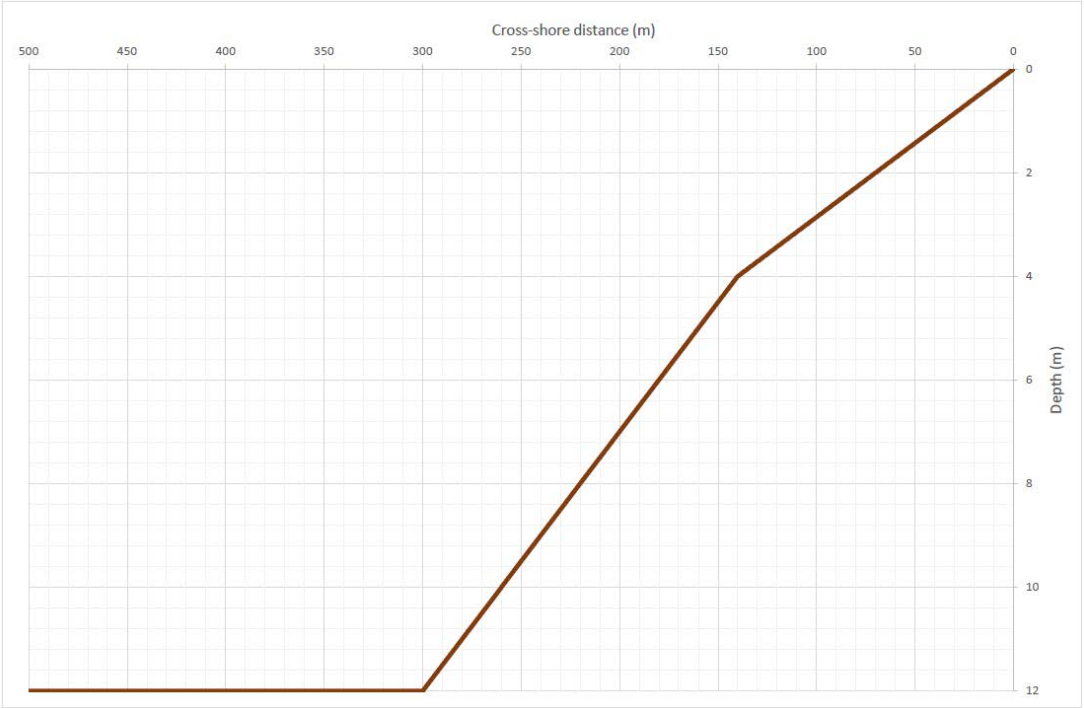

Figure 4.1 Bottom profile

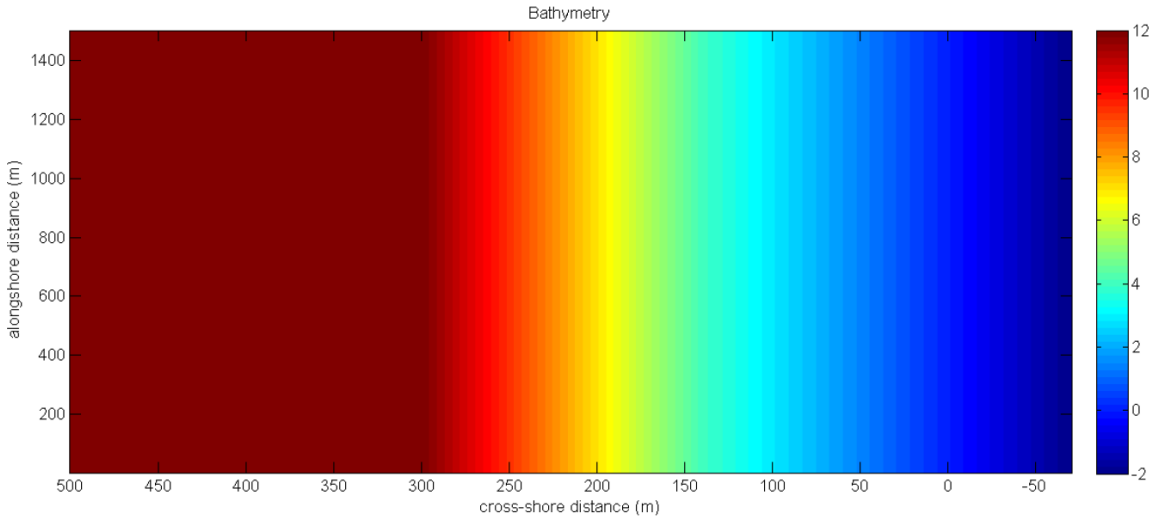

Figure 4.2 Bathymetry of the under consideration coastal area

Boundary conditions

The waves are entering the domain from the offshore boundary (west) with an angle of θ=15° with respect to the cross-shore axis. The waves, which are imposed in the model, are defined as regular waves with a wave height of 1.2 m and a period of 6.5 s. Thus, the boundary condition of the western boundary is weakly reflective.

As far as the eastern boundary is concerned, there is no need for a boundary condition due to the fact that the bed profile is above the mean sea level. More precisely, in order to make sure that the boundary is dry all the time, 70 m of land with a slope of 1:35 is chosen (2 m above

water surface). This is a good option since, as it will be witnessed, in all test-cases the eastern boundary remains dry during the whole simulation. However, at this point, it is noteworthy that because of this option, ILUD-preconditioner is not applicable in our model as it leads to instabilities and crashes in our simulations.

The lateral boundaries, southern and northern are prescribed as repeating boundaries. This means that information leaving at one end of the domain enters at the opposite end. In this way, the current and the wave field is periodic in the longshore direction and the required model length in this direction is reduced. Finally, both the initial water level and velocity components are set to zero.

Numerical settings

Two different discretization types for the advective terms of the momentum equations are examined. These two types are presented in Table 4.1.

Advective terms	Type 1	Type 2
Horizontal advective terms in u/v-momentum equation	BDF	MUSCL
Vertical advective terms in u/v-momentum equation	FIRST	MUSCL
Horizontal advective terms in w-momentum equation	BDF	BDF
Vertical advective terms in w-momentum equation	FIRST	FIRST

Table 4.1 Discretization of advective terms

The first type represents the default settings of SWASH, while the second one differs in the discretization schemes that are used in u/v- momentum equation. High resolution schemes for conservation equations are constructed using some form of TVD (Total Variation Diminishing) limiter in order to avoid the generation of wiggles due to shocks, discontinuities or changes in the solution domain (Hirsch, 1990). One of them is the MUSCL (Monotone Upstream-centered Scheme for Conservation Laws) which is mentioned by Van Leer (1979). However, this will not lead to remarkable differences in the results as it will presented in more detail in the following chapters.

In addition, the Keller-box scheme is applied for the vertical pressure gradient as it provides an accurate short wave propagation. The classical central differencing scheme is not examined in the present master thesis as it is more suitable for stratified flows (The SWASH team, 2016).

Last but not least, the time integration is explicit, which means that a time step restriction is applied based on a Courant number associated with the long wave speed. Due to the fact that the examined model contains wave-wave interactions, a maximum Courant number of 0.5 is applied and a minimum of 0.2.

Number of layers

SWASH model, as already mentioned, improves its frequency dispersion by simply increasing the number of vertical layers. As far as the wave transformation is concerned, the numbers of layers is determined by the linear frequency dispersion. Specifically, according to SWASH manual the higher the value of dimensionless depth kd, the more vertical layers needed. The wave number k is given by:

$$k = \frac{2\pi}{L} \tag{4.1}$$

with:

L wave length

Table 4.2 indicates the range of dimensionless depth kd as function of the number of layers K in SWASH. This range is determined by requiring an error of 1% in the normalized wave celerity. However, it has been observed that for many applications, the use of one vertical layer where the error is 3% gives sufficiently accurate results.

The number of layers K	range	error
1	$kd \leq 0.5$	1%
1	$kd \leq 2.9$	3%
2	$kd \leq 7.7$	1%
3	$kd \leq 16.4$	1%

Table 4.2 Range of dimensionless depth as function of number of layers (The SWASH team, 2016)

In the present situation, at the wave-boundary the wave length is approximately $L = 66\ m$, the water depth is $d = 12\ m$ and therefore the dimensionless depth is $kd = 1.14$. According to the SWASH manual for this value of dimensionless depth, one or two layers are sufficient for typical wave simulations. In the present master thesis though, different number of vertical layers are applied in order to assess the influence of this parameter on the longshore current.

Bottom friction and turbulent mixing

In SWASH both the horizontal and vertical eddy viscosities can be specified. In all tests of the present master thesis, Smagorinsky model is applied for the horizontal eddy viscosity. According to the SWASH manual, in case of lateral mixing of momentum, for instance around the piles of permeable groins which is examined in Chapter 7, it is recommended to apply the Smagorinsky subgrid model. As far as the vertical mixing is concerned, the standard k-ε model, with k the turbulent kinetic energy per unit mass and ε the dissipation of turbulent kinetic energy per unit mass, is employed in all non-depth-averaged calculations.

Additionally, two different bottom friction models are considered, Manning and Logarithmic wall law. Previous numerical experiments have proved that Manning friction model provides a good representation of wave dynamics in the surf zone. However, this model cannot yield accurate results when cases with zero depth-averaged velocity are examined. As a consequence, in the tests with more than one vertical layer, the logarithmic wall law is investigated in order to achieve more accurate representation of the vertical structure of the velocity. It is noteworthy that logarithmic wall law should be combined with the standard k-ε model in the multi-layered mode.

Wave breaking

SWASH is capable to account for energy dissipation due to wave breaking. However, in the case of relatively coarse resolution in the vertical (1-3 layers), the amount of this energy dissipation is underestimated due to the inaccuracy with which the particle velocities near surface are approximated. In these situations, the BREAK command can be used to control wave breaking. The basic idea behind BREAK command is that when local surface steepness exceeds value α then the non-hydrostatic pressure in corresponding grid points is neglected and remains so until local surface steepness reduces below value β. This command in combination with a proper momentum conservation can estimate with relative accuracy the energy dissipation due to wave breaking. Furthermore, skewness and asymmetry of the waves are taken into account

as well. Having said this, in test case 3 and 4 where coarse vertical resolution is used, the BREAK command has been applied. On the other hand, by taking a sufficient number of vertical layers the face velocity at the breaking front will be computed accurately enough and thus, this option should not be activated. For the purpose of this study and in order to keep a balance between the number of vertical layers and the computational time, 8 layers have been applied. From Appendix A, it can be clearly observed that there is a slight influence in the resulting current profile when 10 layers are applied instead of 8. Hence, 8 layers are considered sufficient.

Finally, all test-cases that are investigated in the present chapter and their model settings are summarized in Table 4.3. In addition, Figure 4.3 visualizes the general set-up of the SWASH model for waves only hydraulic condition.

Test-case	Number of layers	Bottom friction	Discretization	Break command	Vertical mixing
1	8	Loglaw	type 2	×	✓
2	8	Manning	type 1	×	✓
3	1	Manning	type 1	✓	×
4	1	Manning	type 2	✓	×

Table 4.3 Model set-up for different test-cases for waves only hydraulic condition

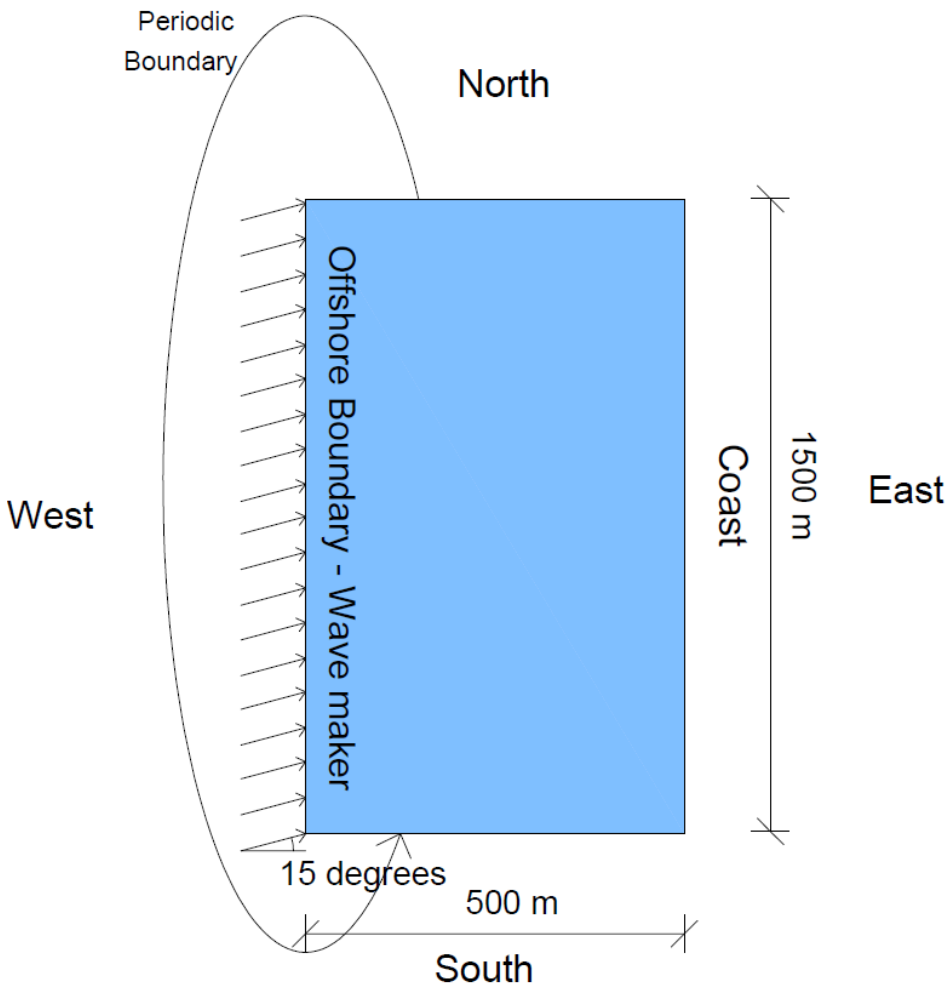

Figure 4.3 General set-up of the SWASH model for waves only hydraulic condition

4.3 Model results

In the present chapter all the results from the different analyses considered are presented. To begin with, the transformation of the waves is examined. In Figure 4.4, the behavior of the significant wave height (H_s) for all the test-cases along the cross-shore is evaluated in respect with the observed breaking position.

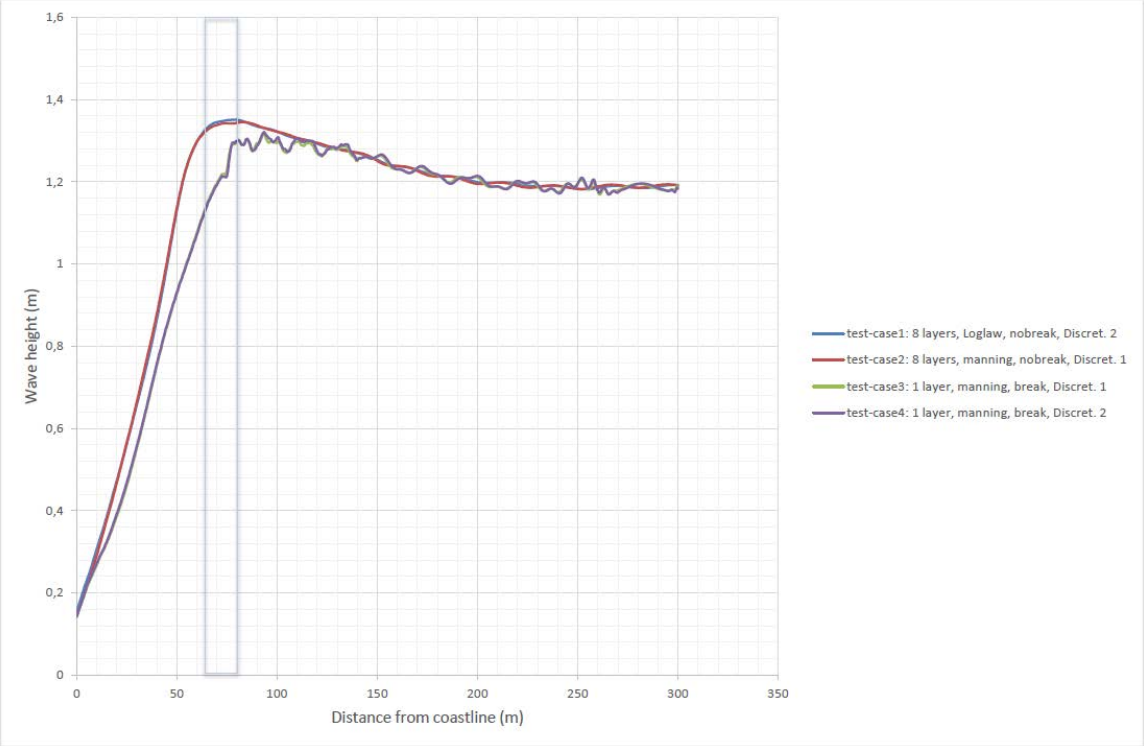

Figure 4.4 Significant wave height for different test-cases

According to Hulsbergen's report, the wave breaking position is located between 65 m and 80 m from the coastline. This area is marked in the figure above. It is clearly observed that the wave breaking positions of the SWASH model simulations are very close to this marked area. In more detail, in test-case 3 and test-case 4, in which 1 vertical layer has been applied, the waves break at a distance of 75 m from the coastline. On the other hand, the waves of the high vertical resolution (8 layers) break closer to the shore at a distance of 60 m from the coastline. The reason behind this difference is the BREAK command which can estimate with relative accuracy the energy dissipation due to wave breaking in cases of relatively coarse resolution in the vertical direction (1-3 layers).

In addition, the usage of coarse resolution in the vertical direction leads to oscillations in the wave height as wave propagates from the offshore boundary to the shoreline. These oscillations are diminished or even eliminated when more vertical layers are applied. As it can be clarified from Figure 4.4, when 8 layers are applied, the wave height transformation follows a steadier pattern. It is worth mentioning that as it will be witnessed in Chapter 6, these oscillations will be affected by the presence of the tidal stream, which in turn will affect the current velocities.

Following, the results that came out for the wave induced current, meaning the velocity with respect to the distance from the coastline, are presented in Figures 4.5 to 4.8. In all the cases the resulting curve is compared to the 3 curves coming from the observations from Hulsbergen's experiment, where the yellow line represents the average values of the velocity whereas the green and orange ones represent the maximum and minimum ones respectively.

In Figures 4.5 and 4.6, the results for test-case 1 and test-case 2 are presented. In both model simulations, eight (8) layers have been induced while their difference lies on the different bottom friction model and the different discretization type that have been used. The two different bottom friction models that are considered are Manning and Logarithmic wall law. The logarithmic wall law is investigated in order to achieve more accurate representation of the vertical structure of the velocity (test-case 1).

From the two figures, it can be observed that the logarithmic wall law (Figure 4.5) leads to higher values for the bottom friction for a roughness height of 0.01 which is equivalent to the use of Manning coefficient of 0.019 $m^{-1/3}s$ (Figure 4.6). This conclusion is derived from the fact that for test case 1 the maximum velocities near the breaking position are lower. As far as the comparison with Hulsbergen's report is concerned, the values of the velocities in both test cases are close to the average values of the experiment. However, as it can be observed the curves from the model simulation experience their maximum value closer to the coastline. This is a consequence of the fact that the modeled waves break more onshore in respect to the observed ones for the cases 1, 2.

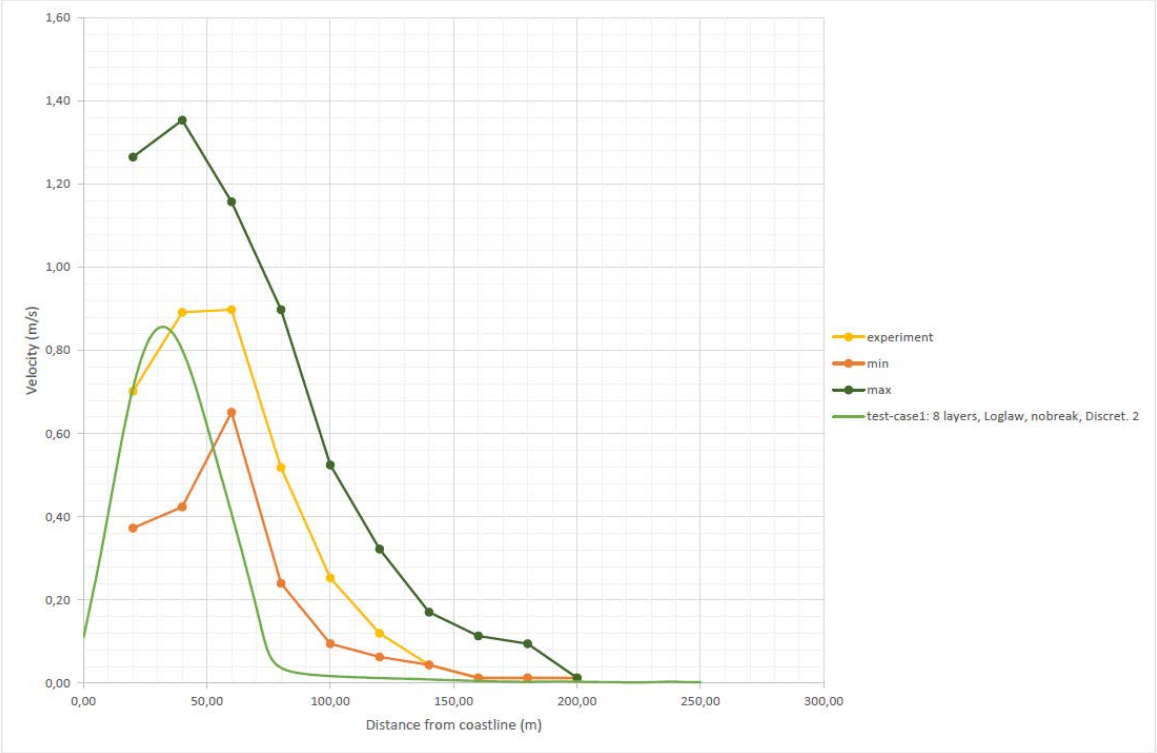

Figure 4.5 Wave induced current for test-case 1

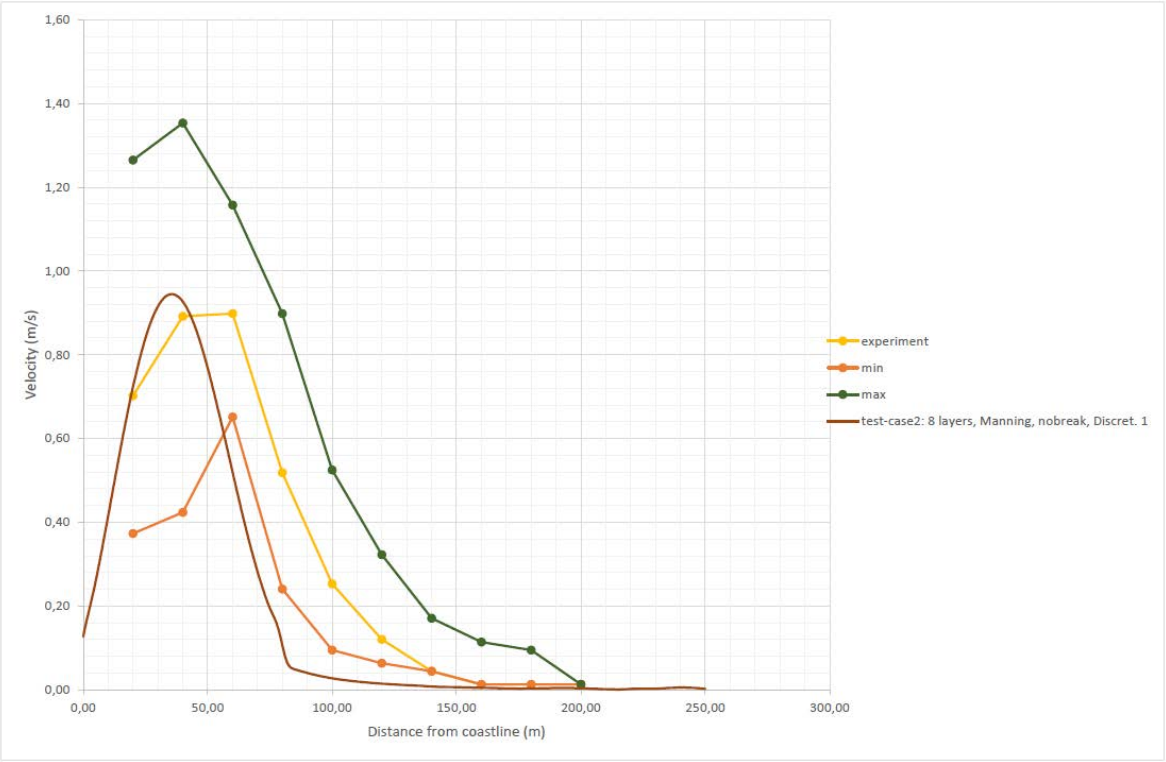

Figure 4.6 Wave induced current for test-case 2

In Figures 4.7 and 4.8, the results for test-case 3 and test-case 4 are presented. The common characteristic of the two simulations is that one (1) layer is applied. However, different discretization schemes are used for the advective terms of momentum equations (Table 4.1). The first type represents the default settings of SWASH, while in the second one, the MUSCL limiter is implemented in order to avoid the generation of wiggles due to shocks, discontinuities or changes in the solution domain (Hirsch, 1990). As it can be witnessed from the figures below, the difference between the two types of discretization is not so pronounced and will be diminished when tide is also present (Chapter 6). The simulation where the MUSC limiter is applied (test case 4) gives higher maximum values for the current velocities than in the case in which the default discretization type is induced.

When comparing these two test cases to Hulsbergen's report, high correlation between the curve of average experimental values and the modeled ones is observed. More precisely, test case 3 with the default discretization type, coincides to a great extent with the experimental values in the whole domain, both in shape and magnitudes. This agreement is achieved by means of the BREAK command, which has the advantage of capturing the exact location of the breaking position.

Additionally, in Table 4.4 the correlations between the modeled curves and the experimental one are presented. The correlation represents the linear relationship between the curves. It can be clearly observed that the curves of test-case 3 (0.93 correlation) and test-case 4 (0.93 correlation) follow the pattern of the experimental curve to a great extent.

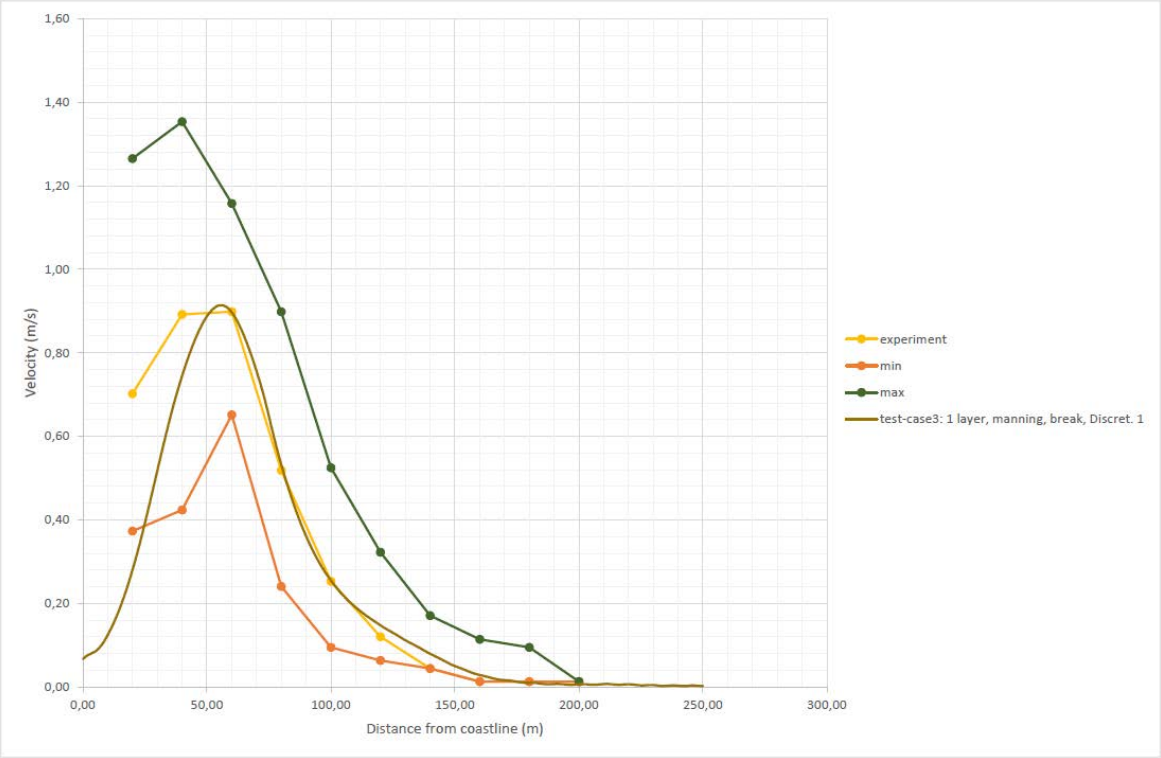

Figure 4.7 Wave induced current for test-case 3

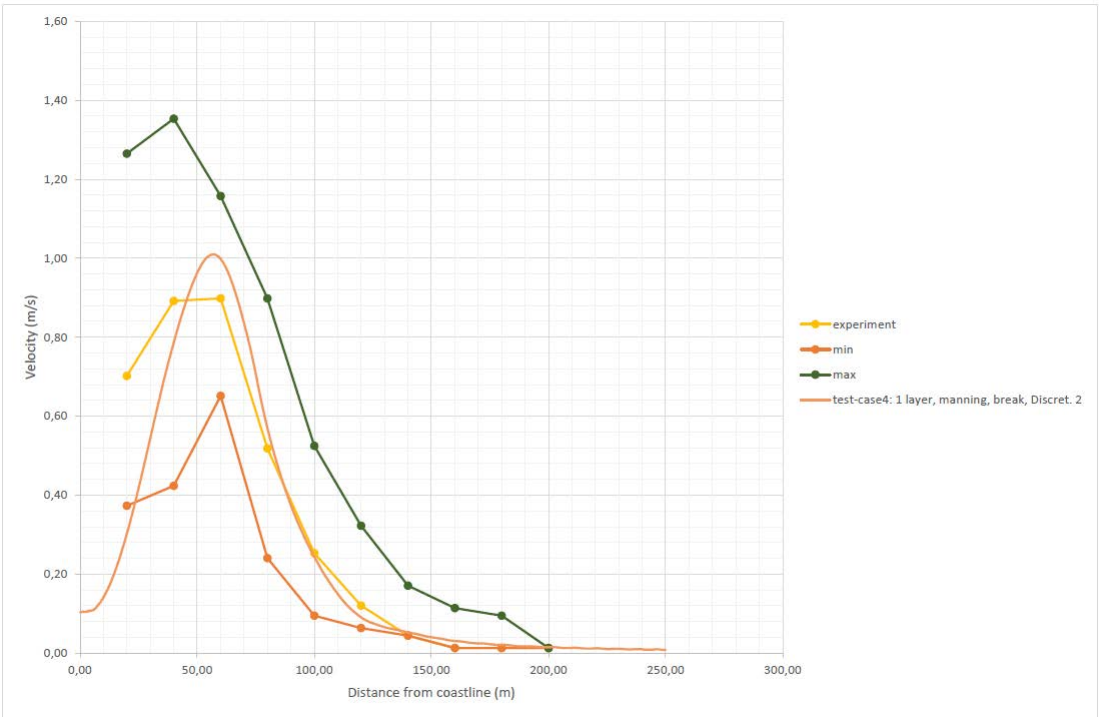

Figure 4.8 Wave induced current for test-case 4

test-case	correlation
1	0.85
2	0.89
3	0.93
4	0.93

Table 4.4 Correlation coefficient between the modeled curves and the experimental one

Finally, in Figure 4.9, the flow pattern of the wave induced current is visualized.

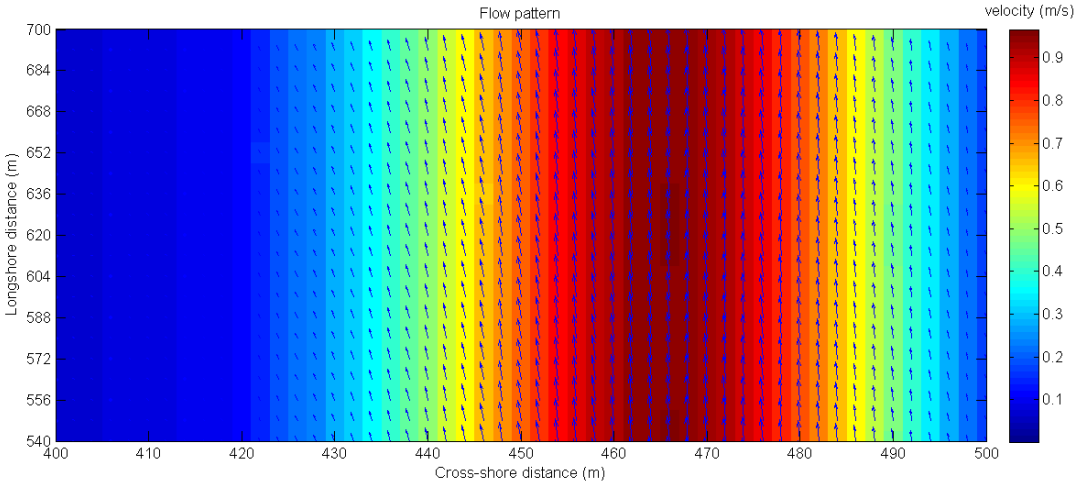

Figure 4.9 Flow pattern obtained from SWASH for the wave induced current

4.4 Conclusions

In Figure 4.10, all the results for the wave induced current are presented in comparison with the experimental results from Hulsbergen.

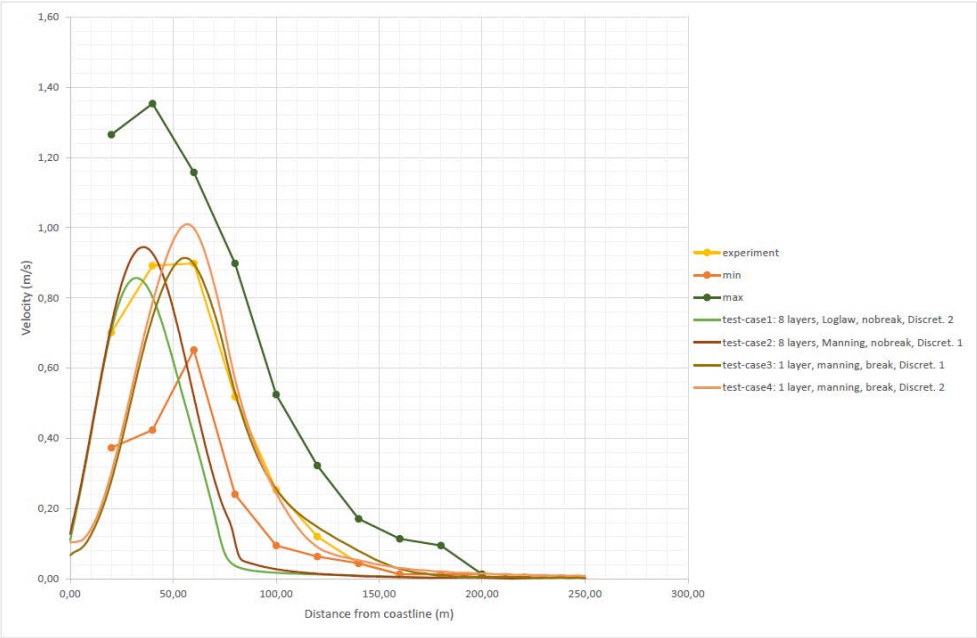

Figure 4.10 All examined test-cases for the wave induced current

The main conclusions of this chapter are summarized below:

- The SWASH model can capture with great accuracy the break position of the waves by means of the BREAK command. However, in cases (test-case1 and test-case 2) in which high vertical resolution (eight layers) has been applied, the waves break closer to the shoreline. These results can be improved by applying the BREAK command with the appropriate α and β values. Nevertheless, for the purpose of the present study and taking into account the high computational time of the analyses due to the large domain, the calibration of α and β values in respect with the number of layers was not examined. As a consequence this forms a strong recommendation for further research on this command that can be more efficiently realized using a smaller domain.

- When eight layers are applied, the wave height transformation follows a steadier pattern in contrast with the simulation with one layer in which oscillations are present. This can be explained by the fact that the ratio of wave height over the water depth is a bit higher than 10%, which is relatively big.

- SWASH model is capable to estimate the wave induced current with relative accuracy as it can be witnessed by the correlation of the experimental and the modeled values. In more detail the test case 3 with the default discretization type and one vertical layer coincides to a great extent with the experimental values in the whole domain, both in shape (0.93 correlation) and magnitudes making SWASH model a perfect tool for such an estimation.

5. Tidal current

5.1 Introduction

This chapter considers the case in which only tide (hydraulic condition 1) is present. The results of Hulsbergen's experiment for this hydraulic condition are used in order to validate and calibrate our model. In addition, the implementation of the tide in the SWASH source code is according to the master thesis of Floris de Wit (2016).

At first, in Section 5.2 the implementation of the tide is considered. Afterwards, the general set-up of the model and its results for the tide induced alongshore current are presented in Section 5.3 and Section 5.4 respectively. These results are compared with those of Hulsbergen's report and finally conclusions on this analysis are discussed in Section 5.5.

5.2 Implementation of the tide

As it is already mentioned, the source code for the implementation of tide in SWASH was developed by Floris de Wit in the framework of a master thesis project with topic "Tide-induced currents in a phase-resolving wave model". This source code is used in the present master thesis.

In previous studies, the tide was included by applying a time averaged alongshore water level gradient in the y-momentum equation. As it is noted in Section 4.2, the lateral boundaries, southern and northern are prescribed as repeating boundaries. This means that the forcing and the bathymetry should be uniform in that direction in order for the continuity to be satisfied. However, a time averaged alongshore water level gradient leads to a water level difference between the two boundaries and thus violates the continuity restriction.

Moreover, another way to model the tide induced alongshore current is by adding a velocity field as lateral boundary condition. Nevertheless, due to the repeating lateral boundaries, any information leaving at one end of the domain enters at the opposite end and as a consequence the velocity field will be added many times in the under consideration flow.

Finally, a new term is added in the alongshore momentum balance. This term represents the pressure gradient induced by the time averaged alongshore water level gradient but without the presence of the water level gradient (Floris de Wit, 2016). Having said this, the pressure term in the alongshore momentum balance (Eq. 5.1) yields to Equation 5.2.

$$\frac{1}{\rho}\frac{\partial(p_h + p_{nh})}{dy} \tag{5.1}$$

$$\frac{1}{\rho}\frac{\partial(p_h + p_{nh})}{dy} + \frac{1}{\rho}\frac{\overline{\partial p_{tide}}}{dy} \tag{5.2}$$

As reported by Floris de Wit, the pseudo alongshore water level gradient can be applied by indicating the time averaged alongshore water level gradient in the input commands of SWASH.

5.3 Model set-up

The domain and bathymetry used in the present chapter is chosen to remain the same as in Section 4.2. This choice provides the possibility of not only comparing the results coming from the implementation of the tide with the ones derived from the waves, but also to combine both wave and tide conditions in the following chapters.

As far as the initial conditions are concerned, an initial flow field based on the expected tidal current velocity which is 1 m/s in the deep portion of the coastal profile ($d = 12\ m$) is applied. The reason behind this option is that the pseudo alongshore water level gradient demands large spin-up times in order to reach the expected tide induced current velocity. Thus, reduced spin-up times are achieved by the initial flow field.

Last but not least, two (2) vertical layers are used in all the cases that are examined in the present chapter, since this resolution can provide accurate results for the tidal current part.

5.4 Model results

According to Hulsbergen's report, the velocity of the tidal current in all cases is 1.0 m/s in the deep portion of the coastal profile. For this reason, different cases with different pseudo alongshore water level gradient are examined in order to achieve this velocity.

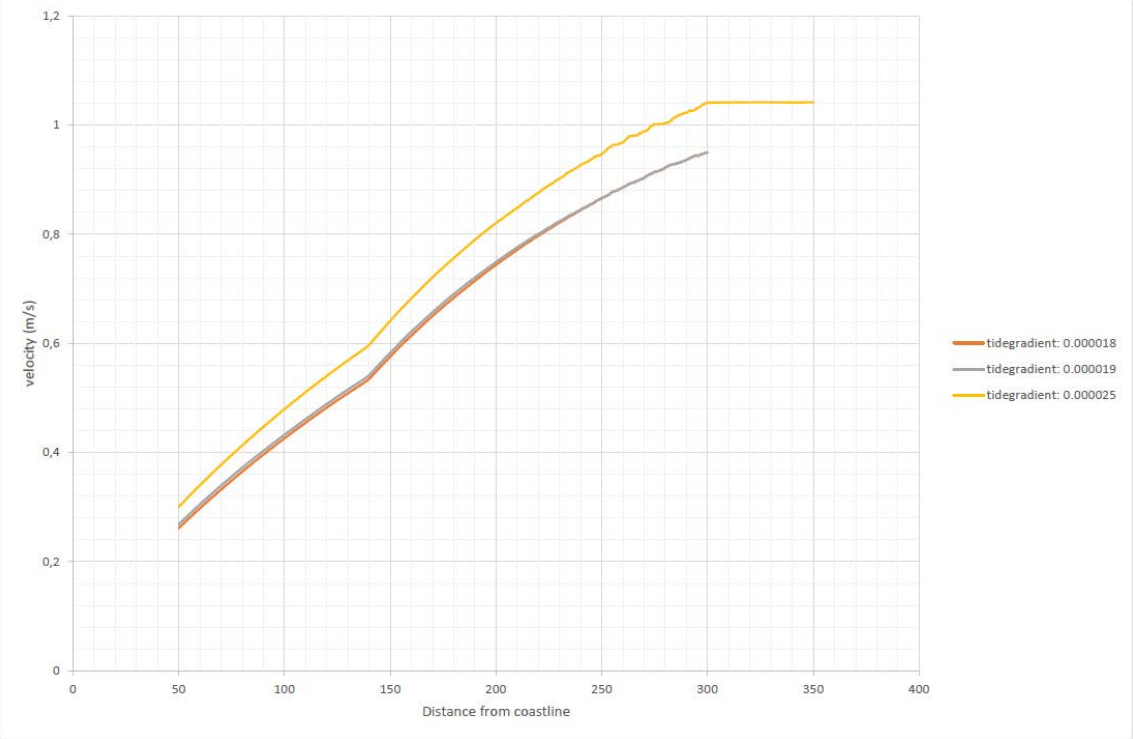

Figure 5.1 Tidal current velocity for different pseudo alongshore water level gradient

Specifically, as it is presented in Figure 5.1, the response of the coastal system to tide-gradients between $1.8*10^{-5}$ and $2.5*10^{-5}$ are considered. It is clearly observed that the velocity of the tidal current is strongly dependent on water depth. More precisely, at a distance of 140 m from the coastline the velocity profile is affected by the change in the bed slope and becomes constant after 300 m from the coastline where the bathymetry gradient changes to zero (horizontal bottom).Undoubtedly, bottom friction is the dominant factor that is hidden behind these variations.

Furthermore, with a pseudo alongshore water level gradient equal to $2.5* 10^{-5}$, the expected tidal current velocity of 1 m/s in the deep part of the domain is achieved. Consequently, the results of this simulation can be compared with those of Hulsbergen's report, since the represented domain is the same. The comparison is presented in Figure 5.2.

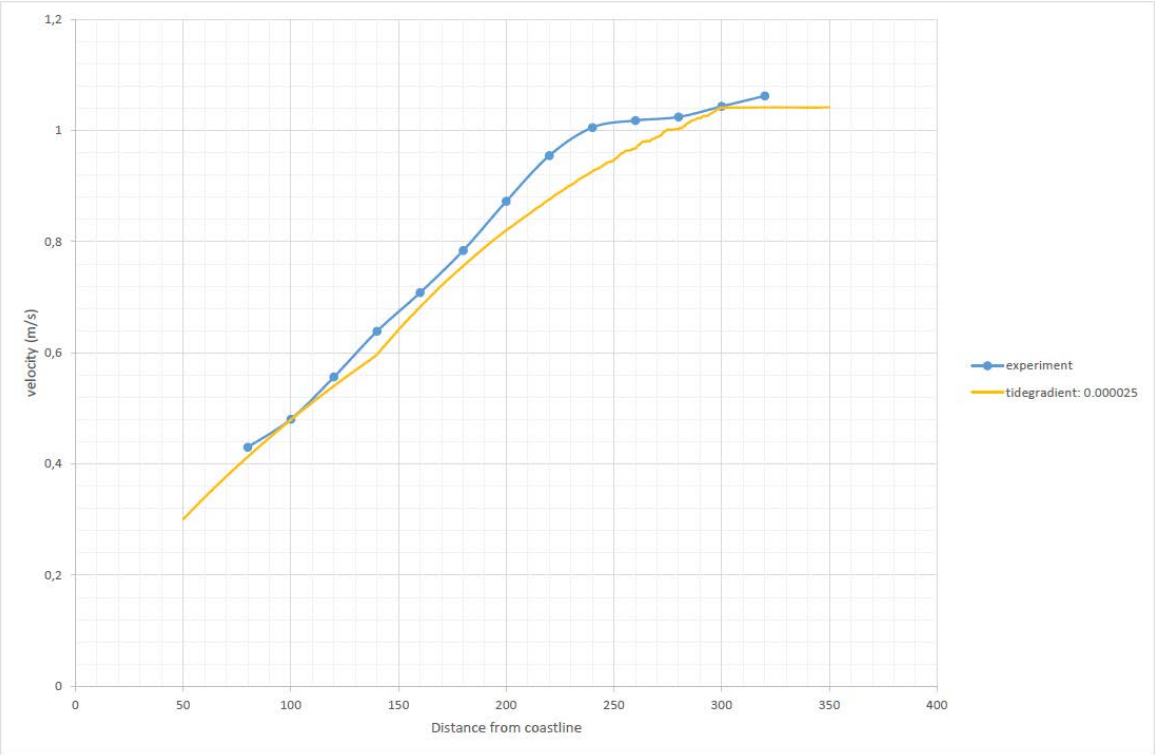

Figure 5.2 Comparison between measured and modeled tidal current

It is obvious that the new pressure gradient induced by the time averaged alongshore water level gradient is able to represent correctly the tide induced alongshore current. The measured current (blue line) is very close to the modeled one (yellow line). Additionally, the correlation coefficient between the two lines is 0.99.

From Figure 5.2, it is observed that although there is a change in the slope of the bed profile, the measurements cannot capture this alteration, in contrast with the SWASH model where the change of the water depth gradient affects the curve of the tidal current velocity. Moreover, according to the experiments, bottom friction stops influencing the velocity at 240 m from the coastline, while the respective distance resulting from the SWASH model is at 300 m from the coastline where the bottom becomes horizontal.

Finally, in Figure 5.3 the flow pattern obtained from SWASH output is illustrated.

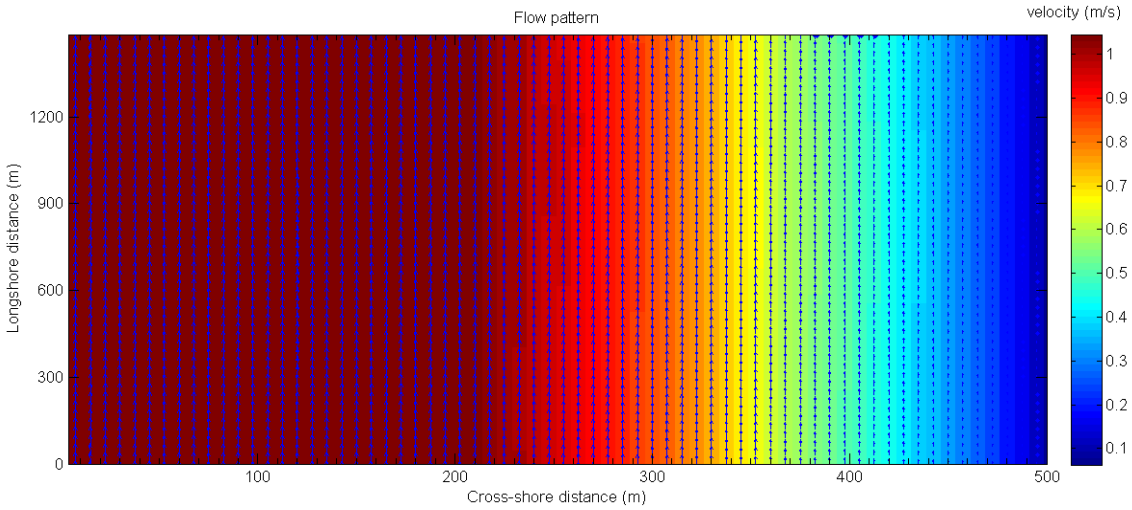

Figure 5.3Flow pattern obtained from SWASH for the tide only hydraulic condition

5.5 Conclusions

The main goal of this chapter was to simulate the tide induced alongshore current correctly. The main conclusions are summarized below:

- The pressure gradient induced by the time averaged alongshore water level gradient but without the presence of the water level gradient, based on the master thesis of Floris de Wit (2016), is able to represent correctly the tide induced alongshore current.

- Bottom friction has a dominant role in the final schematization of the flow pattern and thus tidal current velocity depends on the water depth.

- The model gives results very close to the ones observed from the experiments

- An initial flow field, based on the expected one, can be applied in order to reduce the spin up time.

6. Combination of tidal current and waves

6.1 Introduction

The most crucial hydraulic condition that erodes the Domburg coast consists of the superposition of strong tidal currents of 1 m/s occurring at 10 m water depth and wave induced current in the same direction. This situation is described in Hulsbergen's report as hydraulic condition 4. This hydraulic condition, the combination of tidal current and waves is going to be examined in the present chapter.

Firstly, the general set-up of SWASH model simulations is described in Section 6.2. Afterwards, figures containing model results and those of Hulsbergen's report are presented in Section 6.3. Finally, conclusions on this analysis are discussed in Section 6.4.

6.2 Model set-up

As it is already mentioned, the objective of this chapter is to study the combination of waves and tide. Therefore, the model set up of the two aforementioned situations (tide in section 4.2 and wave in section 5.3) are used together.

More precisely, the waves are entering the domain from the offshore boundary (west) with an angle of θ=15° with respect to the cross-shore axis. The waves, which are imposed in the model, are defined as regular waves with a wave height of 1.2 m and a period of 6.5 s. Moreover, different wave angles, θ=30° and θ=45°, are examined in order to investigate how this characteristic affects the longshore current. Furthermore, a tide-gradient of $2.5* 10^{-5}$ and an initial flow field are applied in order for tidal current to be realistically represented.

As far as the number of layers is concerned, two different number of vertical layers, two (2) and six (6), are applied. In the case of relatively coarse resolution in the vertical (2 layers), the amount of energy dissipation because of wave breaking is underestimated due to the inaccuracy with which the particle velocities near surface are approximated. In these situations, the BREAK command is used to control wave breaking.

As in Chapter 4, two different bottom friction models are considered, Manning and Logarithmic wall law and their effect on the longshore current is analyzed. In addition, model simulations with and without turbulence (vertical mixing) are implemented so that the extent up to which the nearshore hydraulics are affected by this factor to be examined.

Finally, all test-cases that are investigated in the present chapter and their model settings are summarized in Table 6.1. In addition, Figure 6.1 visualizes the general set-up of the SWASH model for the hydraulic condition where tide and waves are present.

Test-case	Number of layers	Bottom friction	Discretization	Break command	Vertical mixing
1	6	Loglaw	type 2	×	✓
2	6	Manning	type 1	×	✓
3	2	Manning	type 1	✓	×
4	2	Manning	type 1	✓	✓
5	2	Manning	type 2	✓	×

Table 6.1 Model set-up for different test-cases for the combination of waves and tide

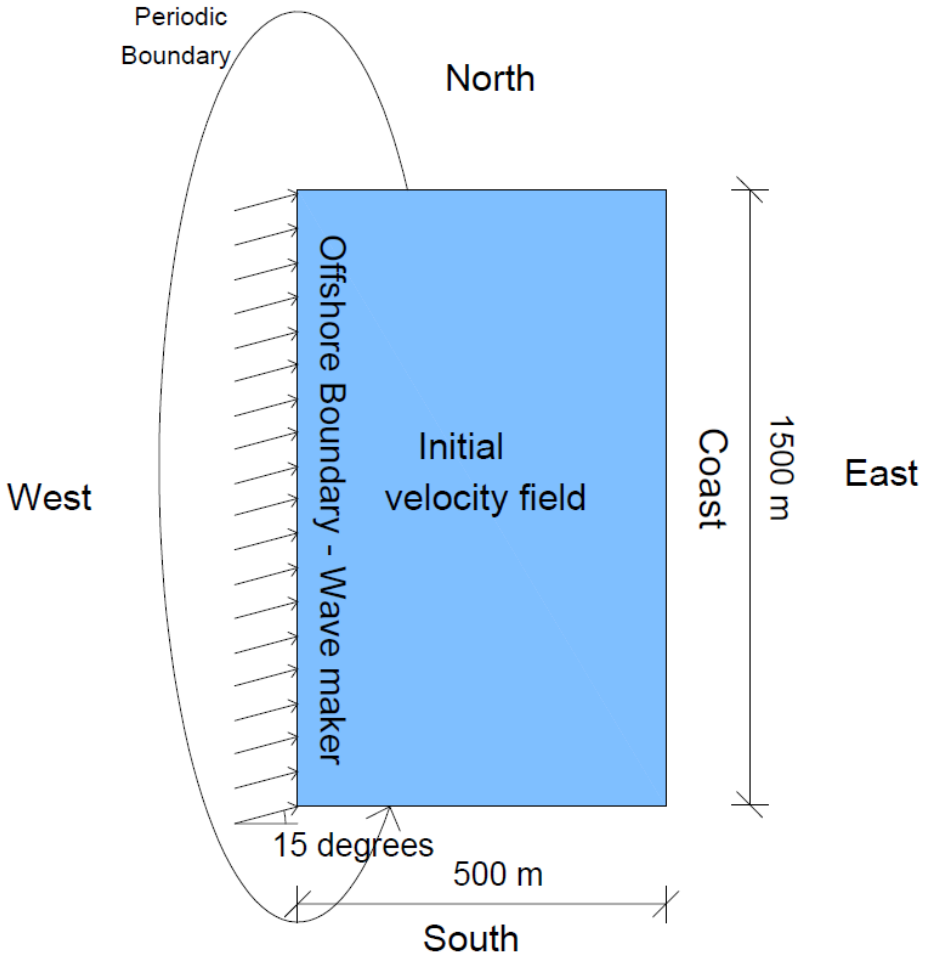

Figure 6.1 General set-up of the SWASH model for combination of waves and tide

6.3 Model results

To begin with, the transformation of the waves and how this is affected by the presence of the tidal current is examined. In Figure 6.2, the behavior of the significant wave height (H_s) for all the test-cases along the cross-shore is evaluated in respect with the observed breaking position.

According to Hulsbergen's observations, the tidal stream has only a slight influence on the transformation of the waves. From the comparison of Figure 4.4 and Figure 6.2, it can be witnessed that for the test-cases in which high vertical resolution (6-8 layers) has been applied, the transformation of the waves is not affected by the tidal stream. On the other hand, for the test cases where coarse vertical resolution (1-2 layers) is implemented, it is observed that there is a small influence of the tidal stream on the wave transformation, leading to higher wave heights.

Nevertheless, in all the test cases, tidal current does not sway the wave breaking position, since waves continue to break at the same point as in Chapter 4 where only waves were present. More precisely, in test-case 3, test-case 4 and test-case 5 in which 2 vertical layers have been applied, the waves break at a distance of 75 m from the coastline which is inside the marked area (Hulsbergen's observations). On the other hand, the waves of the high vertical resolution (6 layers) break closer to the shore at a distance of 60 m from the coastline. As it is already verified, the SWASH model captures with great accuracy the break position of the waves by means of the BREAK command.

Finally, the use of coarse resolution in the vertical direction leads to oscillations in the wave height as wave propagates from the offshore boundary to the shoreline. These oscillations were also present in Chapter 4 (where only waves were present), however it seems that tidal current aggravates these fluctuations. On the contrary, as it can be clarified from Figure 6.2, when 6 layers are applied, the wave height transformation follows a steadier pattern and the oscillations are diminished.

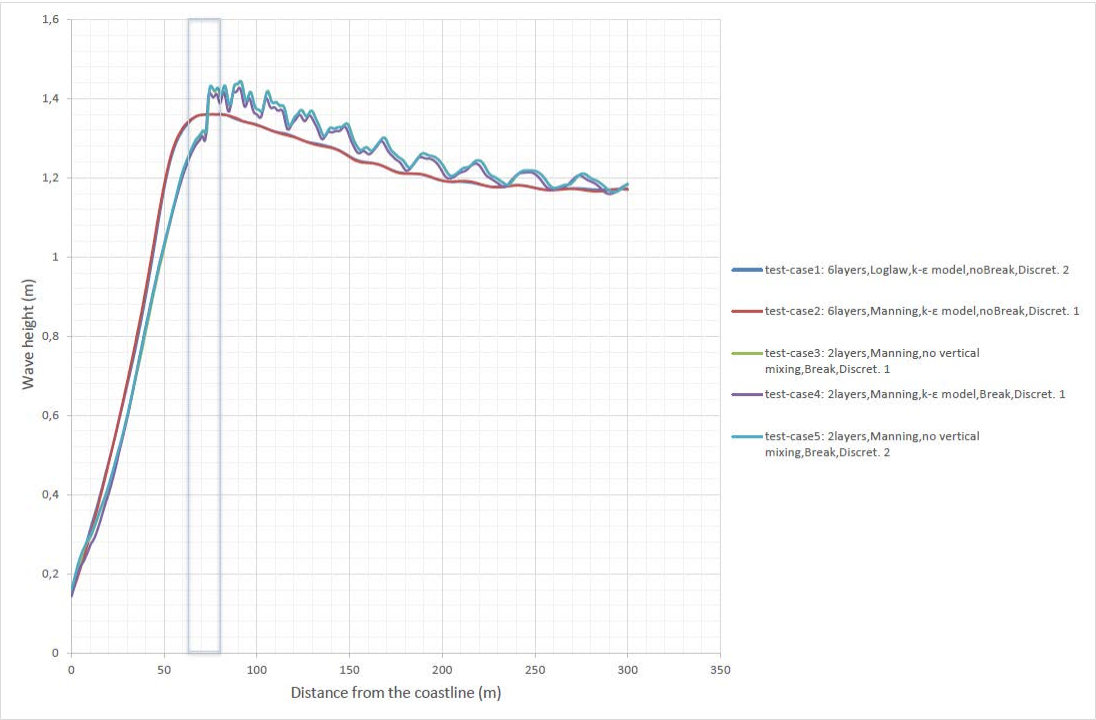

Figure 6.2 Significant wave height for different test-cases

Following, the results that came out for the combination of tide and wave induced current, meaning the velocity with respect to the distance from the coastline, are presented in Figures 6.3 to 6.7. In all the cases the resulting curve is compared to the 3 curves coming from the observations from Hulsbergen's experiment, where the blue line represents the average values of the velocity whereas the yellow and grey ones represent the maximum and minimum ones respectively.

In Figure 6.3 and Figure 6.4, the results for test-case 1 and test-case 2 are presented. In both model simulations, six (6) layers have been induced while their difference lies on the different bottom friction model and the different discretization type that have been used. The two different bottom friction models that are considered are Manning and Logarithmic wall law.

From the two figures, it can be observed that the logarithmic wall law (test case 1) leads to smaller values for the velocity in the area where the wave induced current is dominant. On the other hand, at the part of the curve in which the tide induced current is visualized, the two curves (test case 1 and test case 2) coincide.

As far as the comparison with Hulsbergen's report is concerned, the values of the velocities in both test cases are close to the average values of the experiment for the wave-induced-current part. In more detail, waves break more onshore than the experiment and that is the reason why the modeled curves are shifted to the left. Furthermore, as the distance from the coastline increases, starting from the breaking point where the tide-induced current becomes dominant, the modeled curves for both test cases are closer to the minimum values of the experiment. However, in general the model results are following the experimental curves both in shape and magnitude.

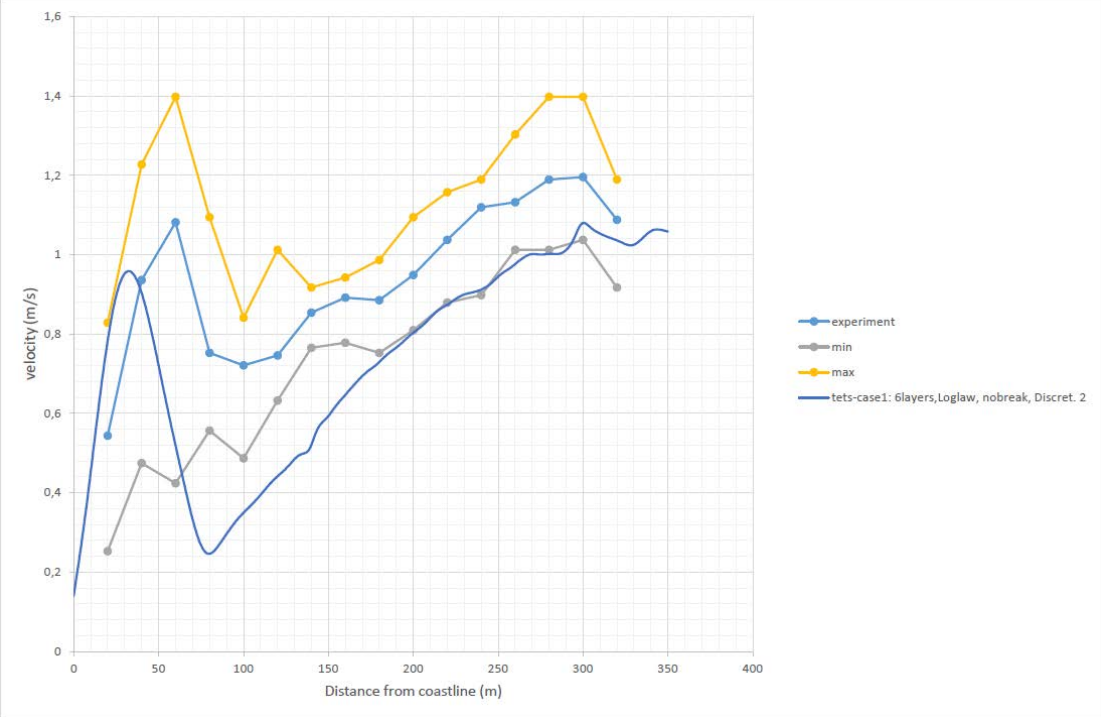

Figure 6.3 Combination of tide and wave induced current for test-case 1

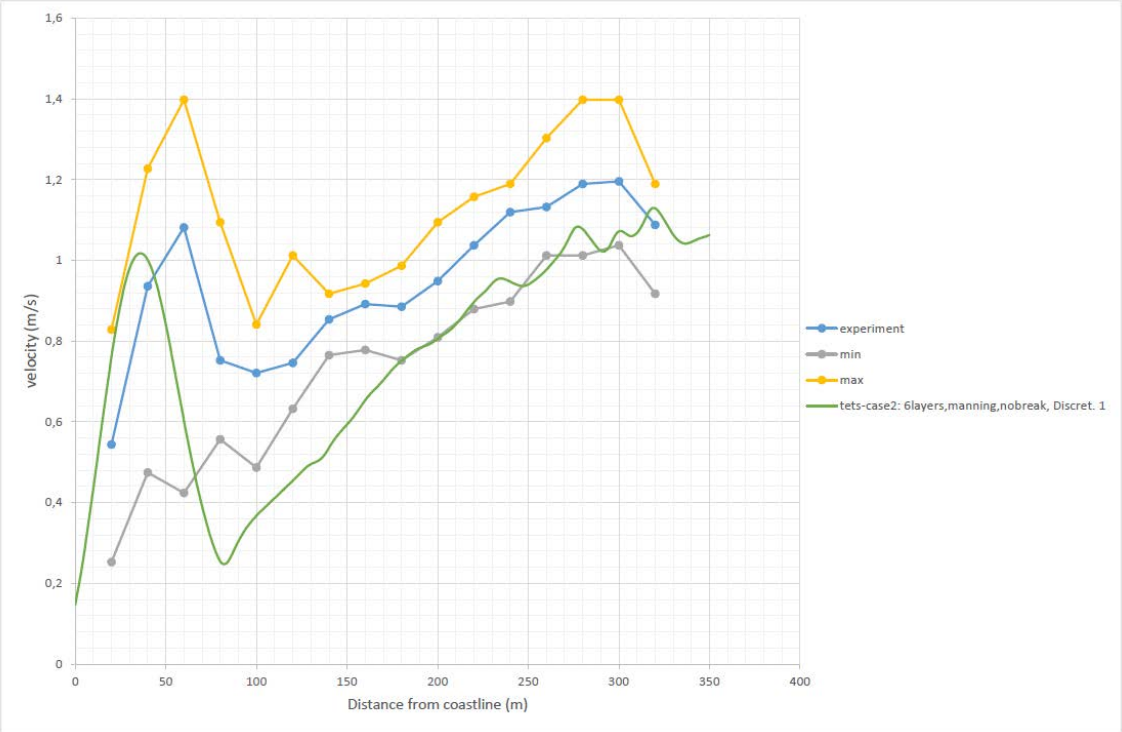

Figure 6.4 Combination of tide and wave induced current for test-case 2

In Figures 6.5 to 6.7, the results for test-case 3, test-case 4 and test-case 5 are presented. The common characteristic of these simulations is that two (2) layers are applied, while their difference lies on the vertical mixing model and the different discretization type that have been used.

In test-case 3 (Figure 6.5) and test-case 5 (Figure 6.7), different discretization schemes are used for the advective terms of momentum equations (Table 4.1). The first type represents the default settings of SWASH, while in the second one, the MUSCL limiter is implemented in order to avoid the generation of wiggles due to shocks, discontinuities or changes in the solution domain. As it can be witnessed from the comparison of the two figures, the different type of discretization does not lead to any difference since the two curves coincide in all over the domain.

Furthermore, the influence of the vertical mixing on the model simulation results is also examined in test-case 4. As it can be verified from Figure 6.6, where the standard k-ε model for the vertical mixing has been applied, the resulting curve shifts to the right while the magnitude of the velocities decrease in comparison with the other two test cases. This phenomenon is to be expected, since turbulent forces smooth the longshore current profile.

Finally, in all model tests, as the distance from the coastline increases, starting from the breaking point where the tide-induced current becomes dominant, fluctuations are observed. The origin of these fluctuations is the oscillations that were observed in the wave height as wave propagates from the offshore boundary to the shoreline (Figure 6.2). This, in combination with the fact that the ratio of wave height over the water depth is quite high, lead to these disturbances. However, the oscillations are around a mean value which follows the tidal current pattern as it was presented in Chapter 5 (Figure 5.2). On the other hand, when a high vertical

resolution is induced, from Figure 6.3 and Figure 6.4 can be concluded that this phenomenon is diminished.

When comparing these test cases to Hulsbergen's report, high correlation between the curve of average experimental values and the modeled ones is observed. More precisely, test case 4 in which the k-ε model has been implemented, coincides to a great extent with the experimental values in the whole domain, both in shape and magnitudes. Moreover, in the area where the tidal current is dominant, the model-simulation-resulting-curves are oscillated around the experimental one.

In addition, different wave angles, θ=30° and θ=45°, are examined in order to investigate how this characteristic affects the longshore current. In Figure 6.8, the alongshore velocity distribution with respect to the wave angle is presented. As it was expected, higher wave angles lead to stronger currents in the area near to breaking position where the wave induced current is dominant. On the contrary, different wave angles do not affect the alongshore current outside the surf zone.

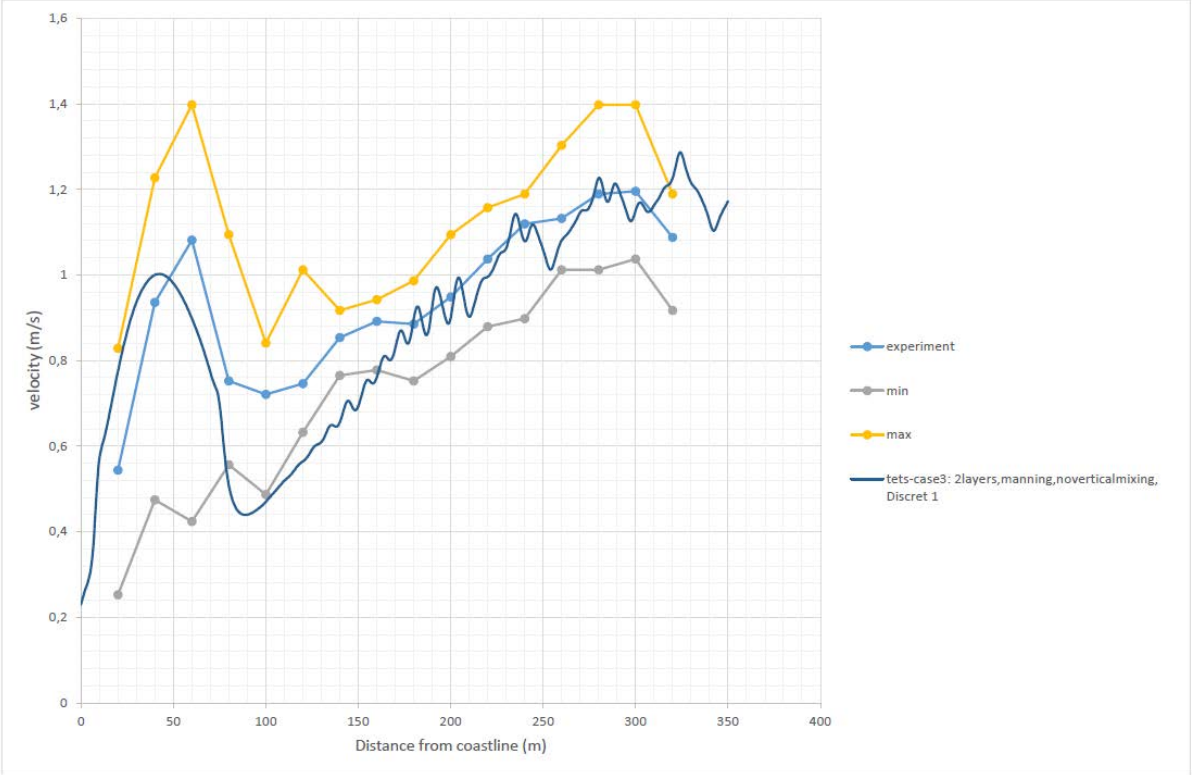

Figure 6.5 Combination of tide and wave induced current for test-case 3

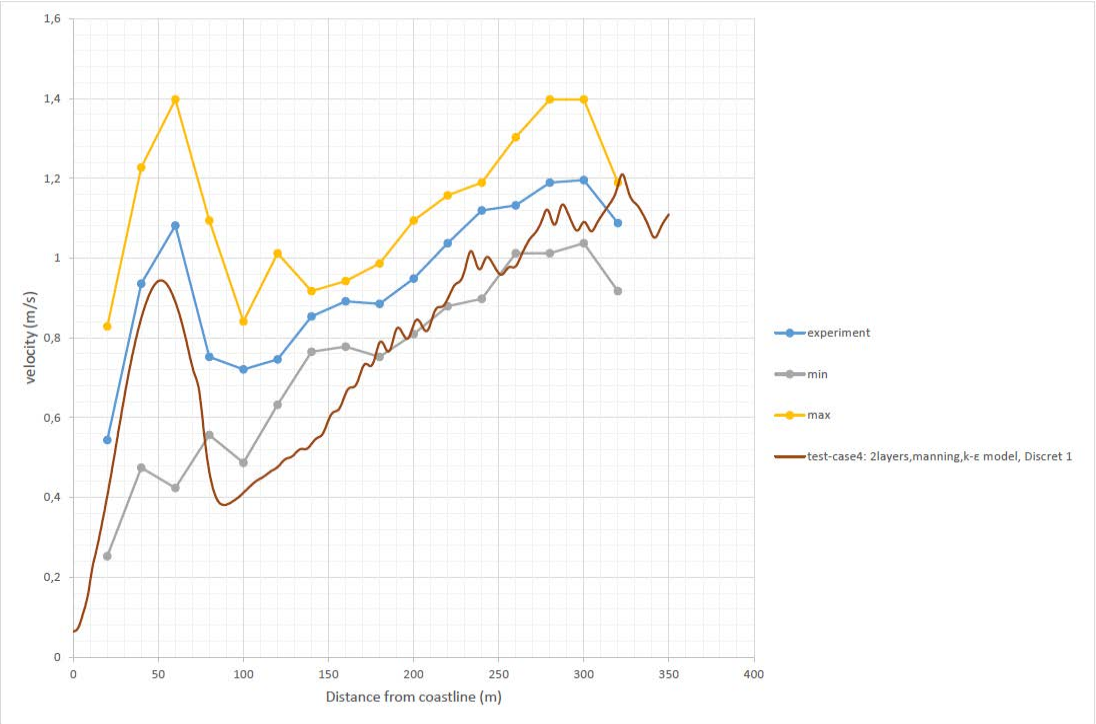

Figure 6.6 Combination of tide and wave induced current for test-case 4

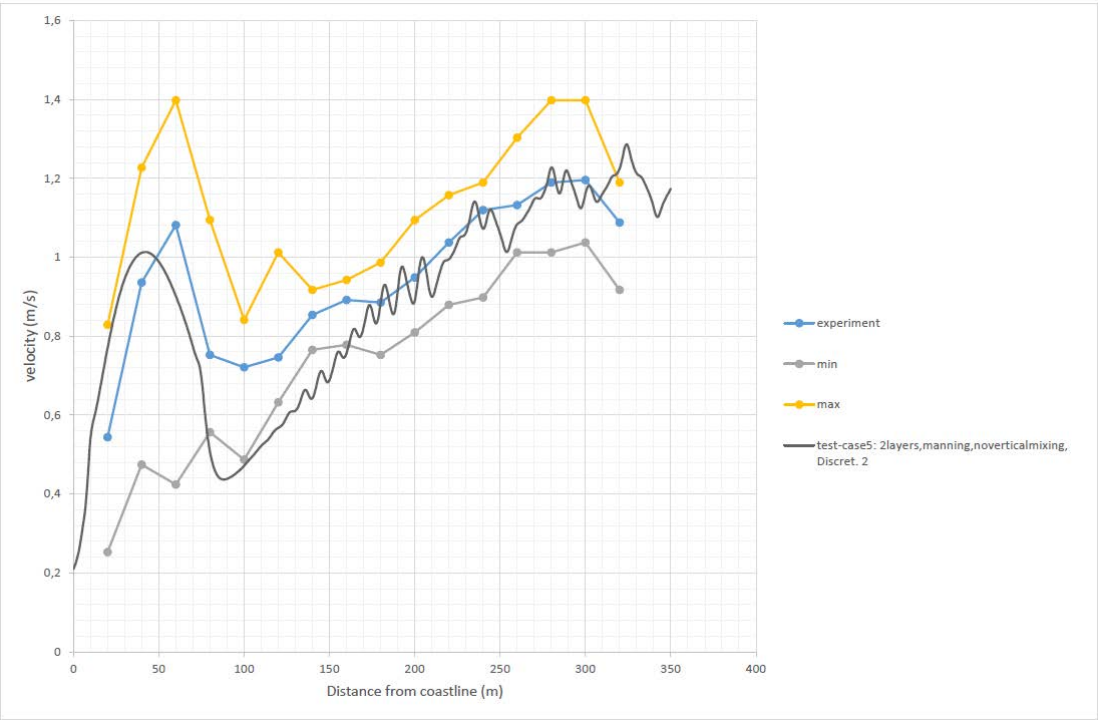

Figure 6.7 Combination of tide and wave induced current for test-case 5

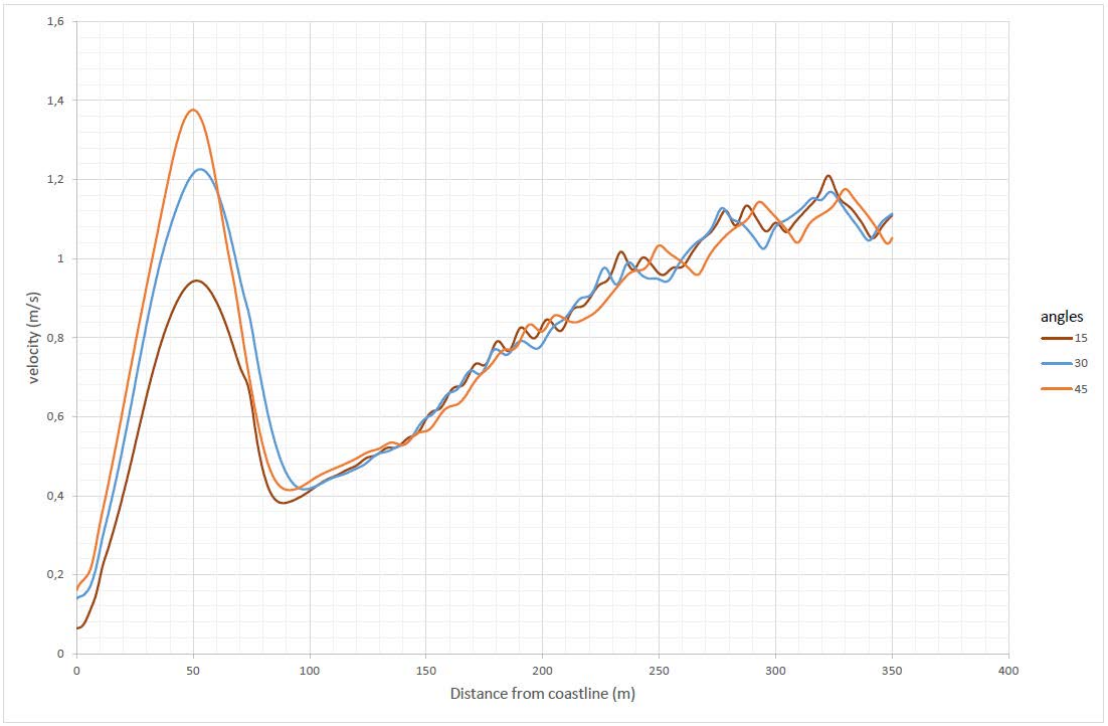

Figure 6.8 Current velocities for different wave angles

Finally, the flow patterns of the alongshore current for the combination of tide and waves obtained from SWASH and from Hulsbergen's observations are visualized in Figure 6.9 and Figure 6.10 respectively. It can be clearly observed that the two patterns are similar. Inside the surf zone the vectors represent the direction of the wave induced current while outside the surf zone the vector represents the tide induced current.

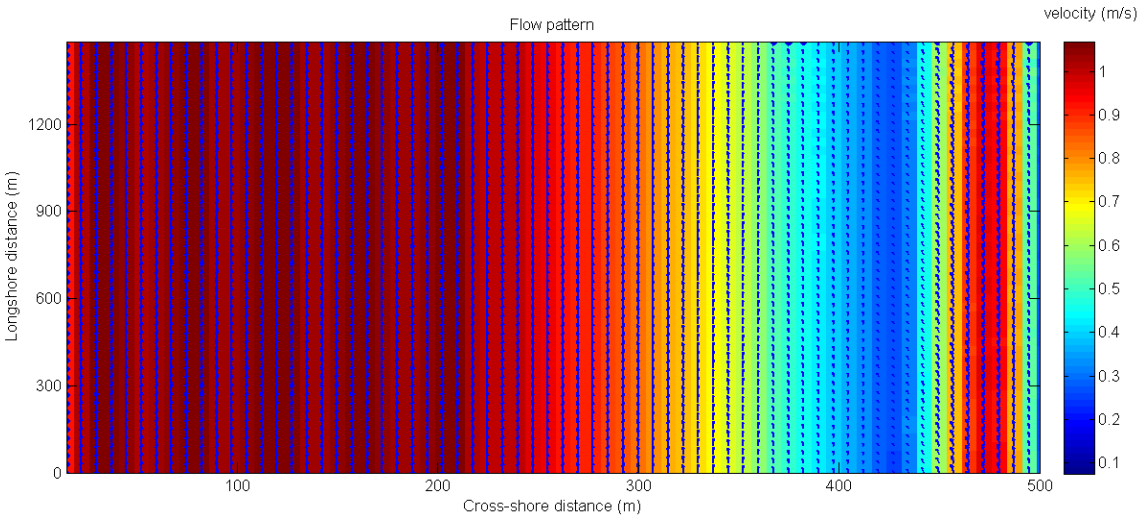

Figure 6.9 Flow pattern obtained from SWASH for the combination of tide and waves hydraulic condition

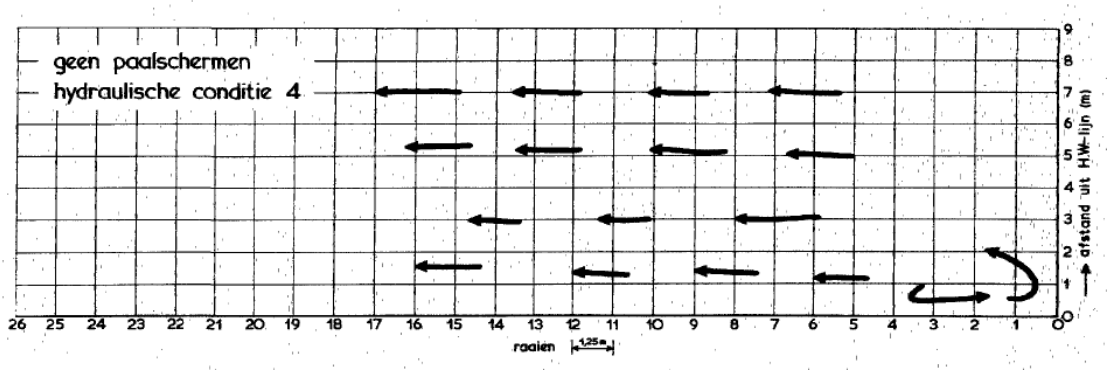

Figure 6.10 Flow pattern obtained from Hulsbergen's observations for the combination of tide and waves

6.4 Conclusions

In Figure 6.11, all the results for the combination of tide and waves are presented in comparison with the experimental results from Hulsbergen.

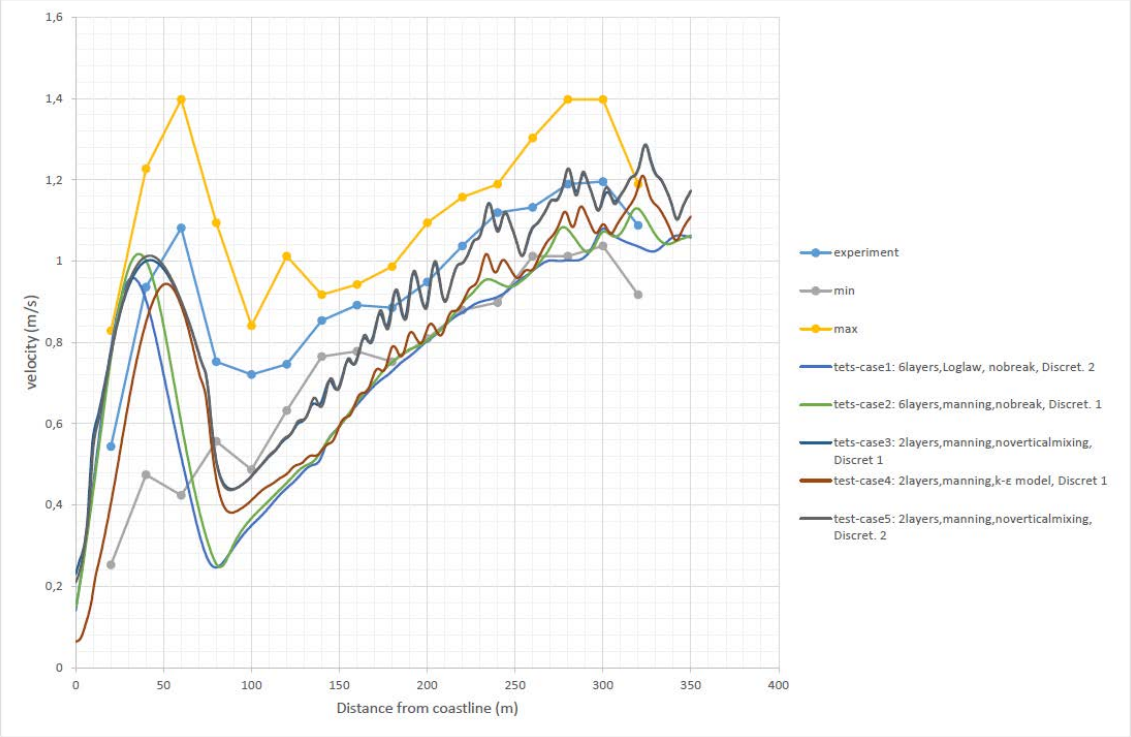

Figure 6.11 All examined test-cases for the tide and wave induced current

The main conclusions of this chapter are summarized below:

- For the test cases where coarse vertical resolution (1-2 layers) is implemented, it is observed that there is a small influence of the tidal stream on the wave transformation, leading to higher wave heights.

- Waves continue to break at the same point near to the marked area as in Chapter 4 where only waves were present. In conclusion, the tidal stream does not affect the breaking position.

- In general the results obtained from SWASH are following the experimental curves of Hulsbergen both in shape and magnitude.

- The oscillations, which are observed in the wave height as wave propagates from the offshore boundary to the shoreline, create fluctuations on the resulting current velocity values outside the surf zone.

- Higher wave angles lead to stronger currents in the area near to breaking position where the wave induced current is dominant.

- The flow pattern obtained from SWASH for the combination of tide and waves matches with the experimental one.

7. Influence of the permeable pile groin on the longshore current

7.1 Introduction

Despite the fact that the permeable groins have been constructed for several years along many world's coastlines, there is still limited research or study on their possible effects on the coastal system. The intention of this chapter is to examine how the permeable pile groins effect the longshore current under the combination of wave and tide forcing. Furthermore, the level of agreement between the results obtained from SWASH model and the experimental ones is investigated.

At first, in Section 7.2 the implementation of the piles is considered. Afterwards, the general set-up of the model and its results for the combination of waves and tide are presented in Section 7.3 and Section 7.4 respectively. These results are compared with those of Hulsbergen's report and finally conclusions on this analysis are discussed in Section 7.5.

7.2 Implementation of the piles

One of the most important aspects of the present master thesis is the implementation of the piles in the numerical model. A permeable pile groin can be applied in several ways which in turn will affect the model results. It is worth mentioning that because of the gravity of this choice, a software capable of simulating the behavior of these structures in high detail needs to be used. For the purpose of this study SWASH is considered the perfect tool to represent this behavior.

First of all, the piles can be described as stiff cylindrical plants which are characterized by their height, diameter and drag coefficient. In SWASH, this option can be applied by the VEGETATION command with which the user can activate wave damping induced by aquatic vegetation. In more detail, this optional command uses a Morison type equation (Morison, 1950) as it is already described in Section 2.6 to quantify the total force on pile in oscillatory flow. The drag coefficient (C_D) is very important in order to predict and estimate the damping effect of the piles. In this master thesis, a value of $C_D = 1.5$ is used according to RIZA (2003) for stem of trees. Furthermore, the diameter of the piles is $D = 0.25\ m$ and their height is larger than the water depth as it is visualized in Figure 3.1.

Another way for piles to be implemented is by using exception values. The user can exclude some cells from the computation and in this way these cells represent the piles which act as an obstacle to the flow. However, previous studies have concluded that this way leads to a lower effective permeability of the groin. As a consequence, the user should use larger values of permeability in order to achieve the desired equivalent one.

Finally, a permeable pile groin can be represented as a rubble mound groin. However, this option demands some characteristics of the structure such as the height of the structure, the characteristic grain size and the porosity. Considering the above, it is difficult to estimate and specify these parameters for a pile groin.

Having said this, for the purpose of the present master thesis, the VEGETATION command is considered as the most suitable option and according to this the permeable pile groin is implemented.

7.3 Model set-up

As it is already mentioned, the objective of this chapter is to study the influence of the permeable pile groins on the strong tidal current superposed by wave induced longshore current in the same direction. Therefore, the model set-up follows the same options of the previous Chapter (Chapter 6).

In more detail, the domain of the basin that is used has a size of $l_x = 570\ m$ in cross-shore direction and $l_y = 1500\ m$ in longshore direction. The size of the long-shore direction is chosen to be so large in order for the permeable pile groins not to affect the lateral boundaries. Due to the fact that periodic boundaries have been applied, disturbances leaving at one end of the domain should not enter at the opposite end. Thus, the distance of the lateral groins from the boundaries has been carefully chosen.

Moreover, the waves are entering the domain from the offshore boundary (west) with an angle of θ=15° with respect to the cross-shore axis, pointing towards the north direction. The waves, which are imposed in the model, are defined as regular waves with a wave height of 1.2 m and a period of 6.5 s. In addition, the implementation of the tide is according to chapter 5. The pressure gradient induced by the time averaged alongshore water level gradient but without the presence of the water level gradient (Floris de Wit, 2016) should be defined.

Hulsbergen examined different permeable pile groin schematizations for different hydraulic conditions. For the combination of waves and tide, Hulsbergen investigated three different groin forms (B, C and E, Figure 3.4) from which groin-scheme B (Figure 7.1) and groin-scheme E (Figure 7.2) have many common characteristics with the permeable pile groins at Domburg coast. Groins consisting of two rows of piles are more widely used at the southwest Zeeland coast in the Netherlands. Thus, these two groin fields are considered in the present master thesis and the results obtained from SWASH model are compared with those of Hulsbergen's report.

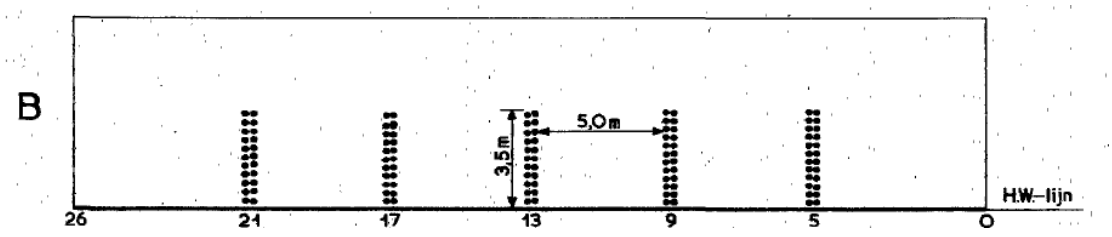

Figure 7.1 Permeable pile groins scheme B

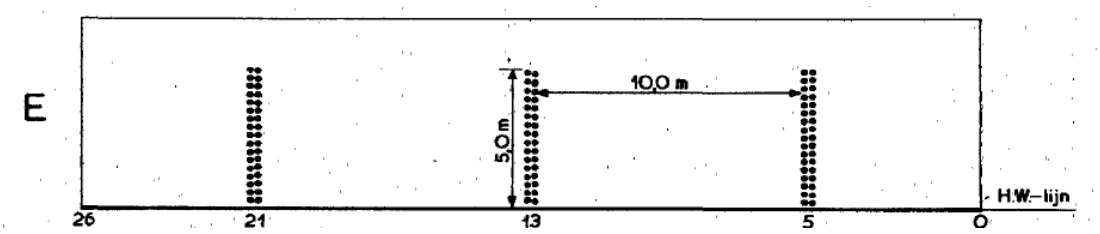

Figure 7.2 Permeable pile groins scheme E

In more detail, groin system B is consisted of five double rows of permeable pile groins. The longshore distance between the groins is 200 m and their length is 140 m. On the other hand, groin system E is consisted of three double rows of permeable pile groins. However, the distance between the groins is twice of that of system B and their length is 200 m. Finally, the angle between the piles and the coastline was 90° for all cases. Figure 7.3 and Figure 7.4 visualize the general set-up of the SWASH model for the hydraulic condition where tide and waves are present for groin system B and E respectively.

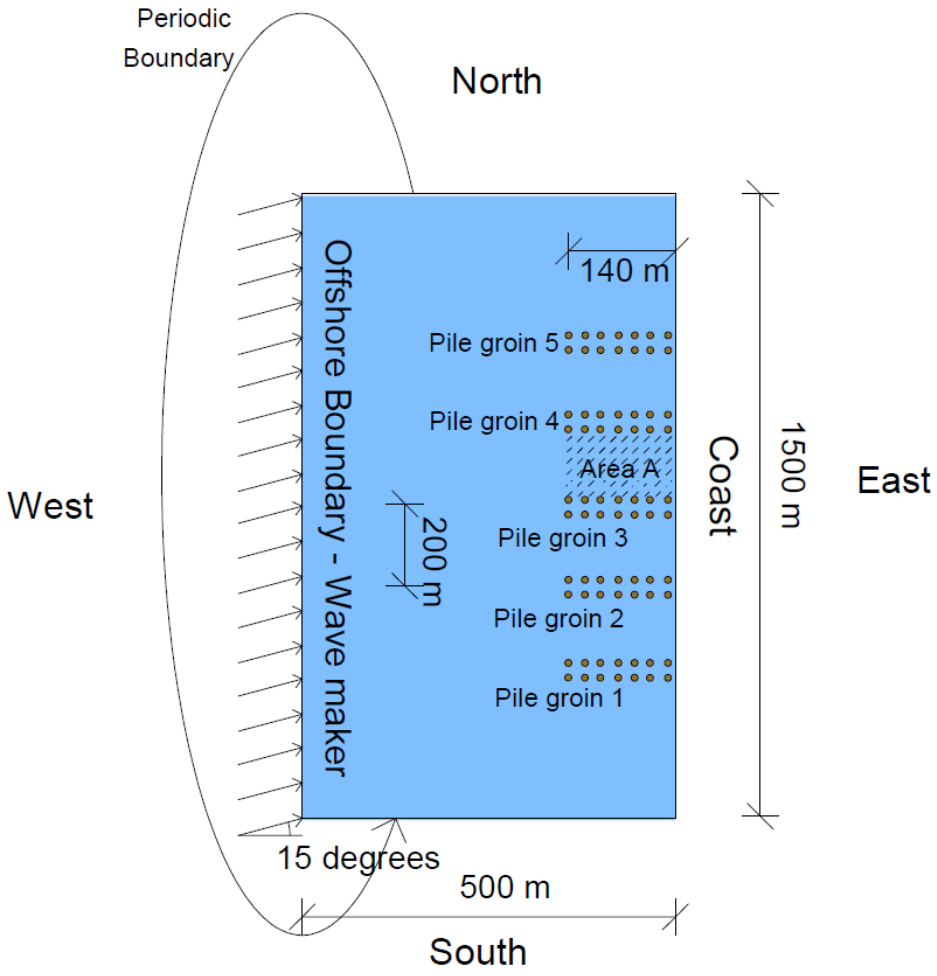

Figure 7.3 General set-up of the SWASH model for pile groin scheme B

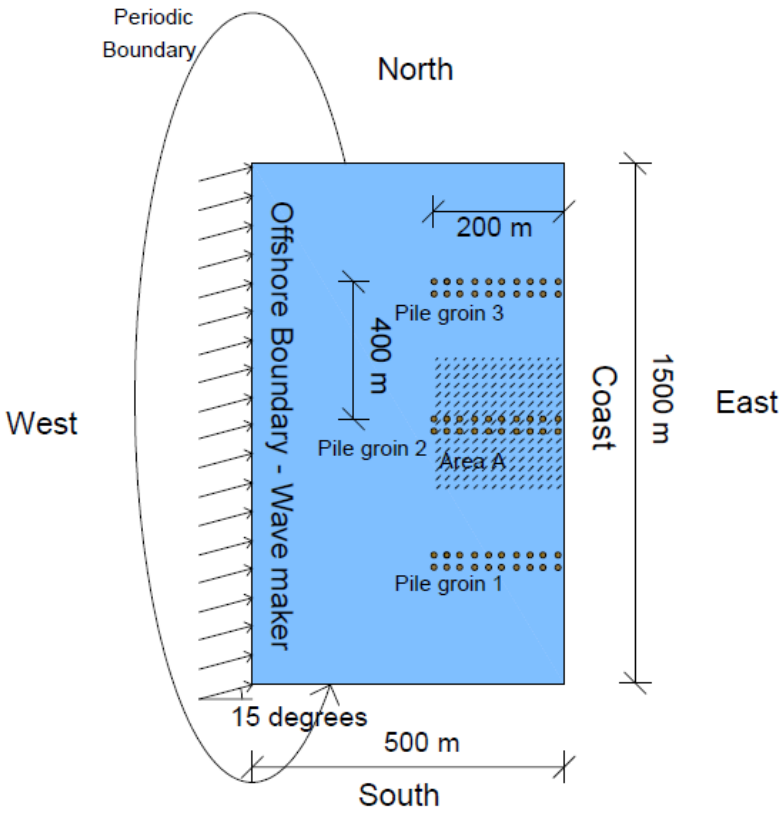

Figure 7.4 General set-up of the SWASH model for pile groin scheme E

Finally, all test-cases that are investigated in the present chapter and their model settings are summarized in Table 7.1 and Table 7.2. It is worth mentioning that in the present chapter only Manning type formulation is considered, since Logarithmic wall law with a roughness height of 0.01 m has turned out to be conservative for the under consideration wave induced current (Chapter 4). Additionally, in a coastal application, preference is given to the approach by Manning. According to SWASH manual, numerical experiments have indicated that the Manning formula provides a good representation of wave dynamics in the surf zone, and even better to that returned by other friction formulations.

Test-case	Number of layers	Bottom friction	Discretization	Break command	Vertical mixing
1	2	Manning	type 1	✓	×
2	2	Manning	type 1	✓	✓
3	6	Manning	type 1	×	✓

Table 7.1 Model set-up for different test-cases for the influence of groin-field B on longshore current

Test-case	Number of layers	Bottom friction	Discretization	Break command	Vertical mixing
1	2	Manning	type 1	✓	×
2	2	Manning	type 1	✓	✓

Table 7.2 Model set-up for different test-cases for the influence of groin-field E on longshore current

7.4 Model results

7.4.1 Groin system B

To begin with, the influence of the permeable pile groin system B on the longshore current is examined. The results that came out for the combination of tide and wave induced current, meaning the velocity with respect to the distance from the coastline, are presented in Figures 7.5 to 7.8. In all the cases the resulting curve is compared to the curve coming from the observations from Hulsbergen's experiment. In more detail, Hulsbergen measured the current velocities between pile groin 3 and pile groin 4 (marked area A in Figure 7.3). The average values of the velocity obtained from Hulsbergen's observations are visualized with the blue line in the following figures.

In Figure 7.5 and Figure 7.6, the results for test-case 1 and test-case 2 are presented. In both model simulations, two (2) layers have been induced while their difference lies on the vertical mixing model. More precisely, in test-case 2 the standard k-ε model has been implemented while in test case 1 the vertical mixing is not considered. According to the manual of SWASH, within the vegetation canopy, it is assumed that all energy of the mean flow is converted to turbulent energy due to the plant drag. In SWASH this process is modelled by means of the vegetation-induced turbulence production terms in the k-ε model (The SWASH team, 2016).

As it can be verified from Figure 7.6, where the standard k-ε model for the vertical mixing has been applied, the resulting curve shifts to the right in comparison with Figure 7.5. This phenomenon is to be expected, since turbulent forces smooth the longshore current profile earlier. Furthermore, the curve resulting from test case 2 seems to be almost coinciding with the experimental curve at the area of the surf zone, in contrast with the curve resulting from test case 1, for which the difference from the experimental values is bigger. This means that vertical mixing plays an important role in the present study, especially near to the pile groins where vertical eddy viscosities are expected. However, outside the surf zone, test-case 1 can estimate more accurate the tidal current.

In Figure 7.7, the results of test-case 3, in which six (6) vertical layers have been applied, are observed. In this case, waves break more onshore than the experiment due to the fact that the BREAK command is not applied for high vertical resolution as it is already mentioned in Chapter 6. As a consequence, the modeled curve is shifted to the left.

In all model tests, as the distance outside the surf zone increases, starting from the wave breaking point where the tide-induced current becomes dominant, fluctuations are observed as those witnessed in Chapter 6. The origin of these fluctuations is the oscillations that were observed in the wave height as wave propagates from the offshore boundary to the shoreline. These oscillations are around a mean value which follows the experimental curve. However, a more stable pattern can be achieved when a high vertical resolution is induced (test-case 3), where these oscillations are diminished.

To sum up, when comparing these test cases to Hulsbergen's report (Figure 7.8), high correlation between the curve of average experimental values and the modeled ones is observed (Table 7.3). The results obtained from SWASH are following the experimental curves of Hulsbergen both in shape and magnitude all over the domain.

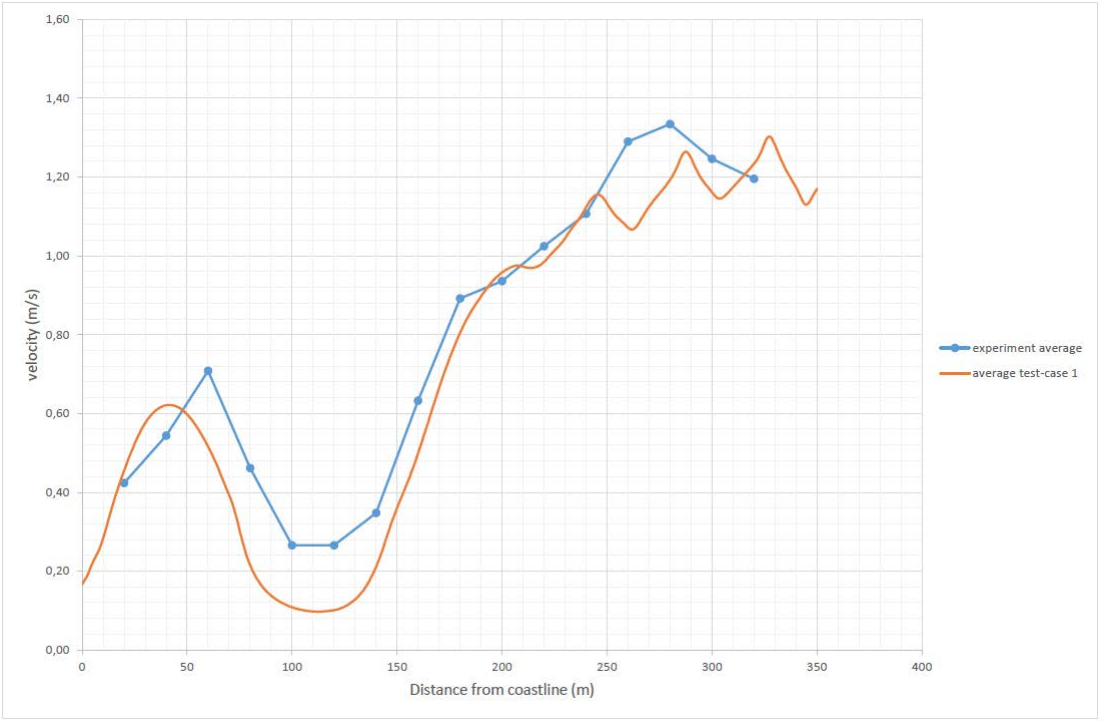

Figure 7.5 Influence of pile groin system B on the longshore current velocity for test-case 1

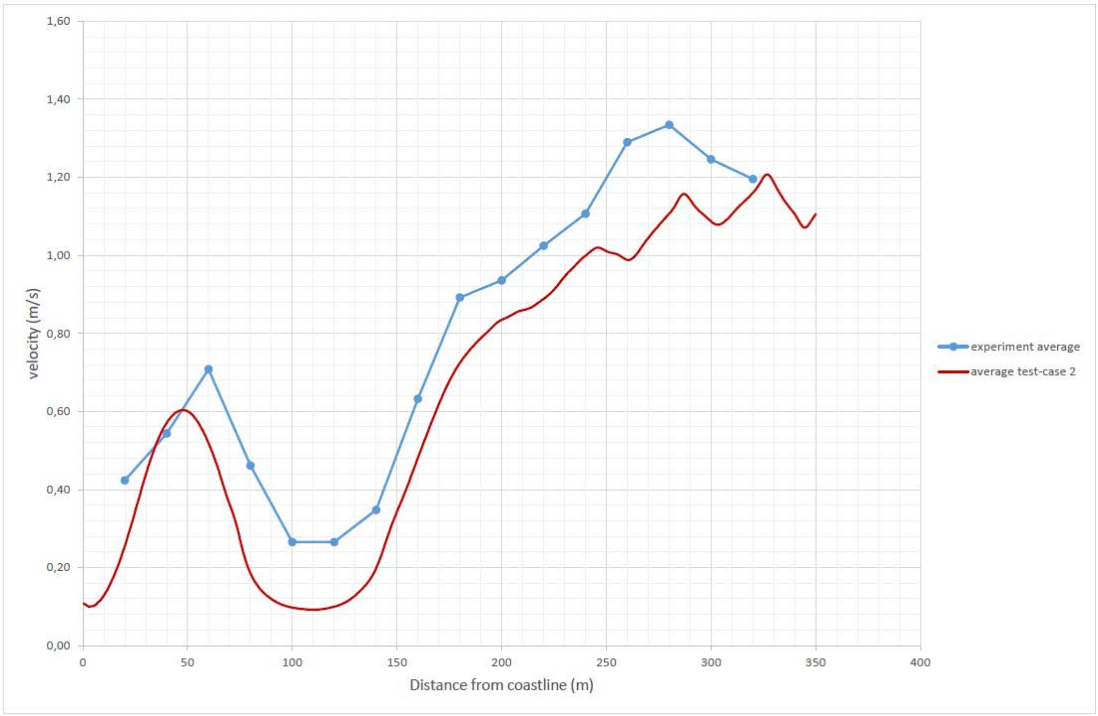

Figure 7.6 Influence of pile groin system B on the longshore current velocity for test-case 2

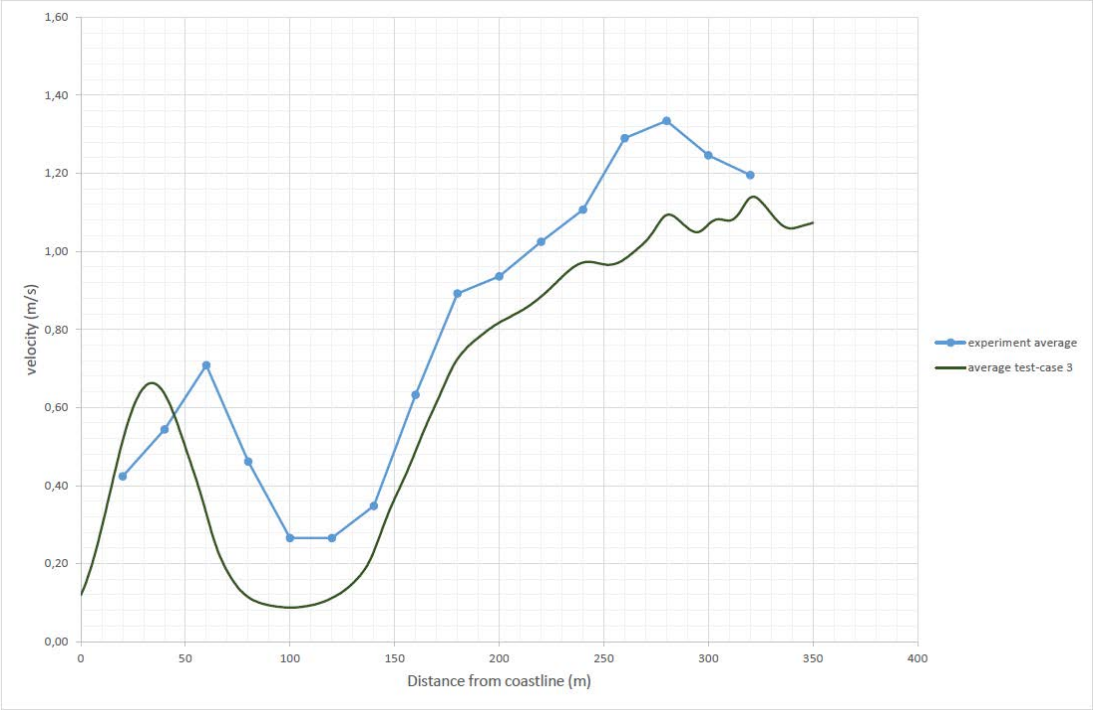

Figure 7.7 Influence of pile groin system B on the longshore current velocity for test-case 3

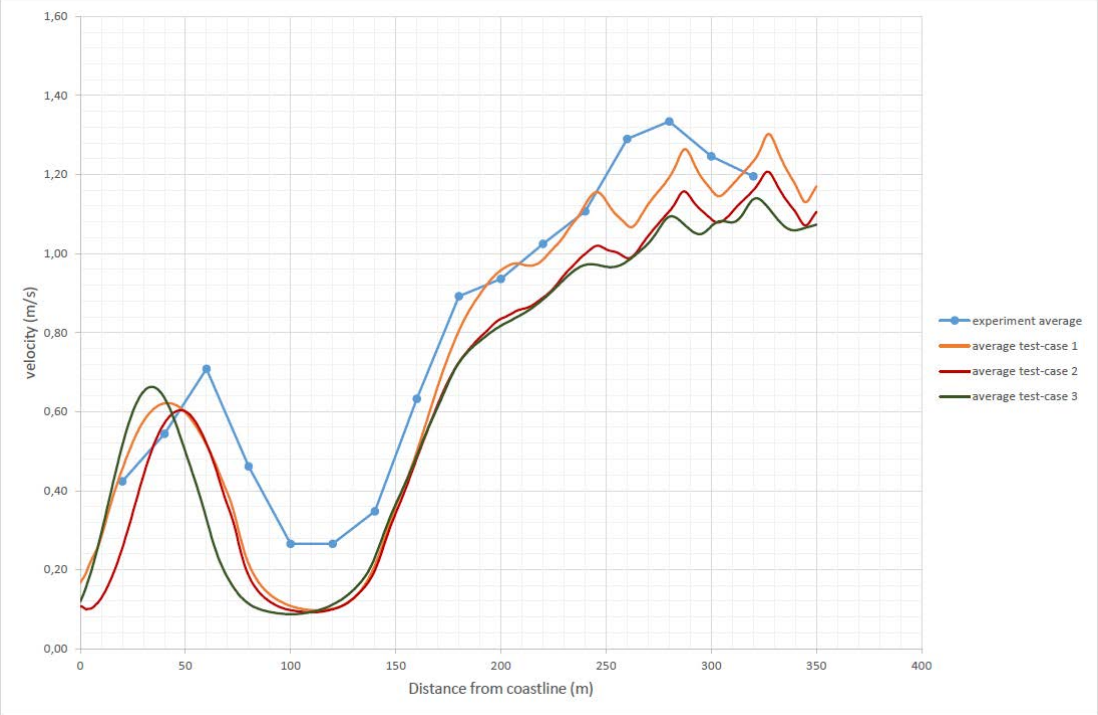

Figure 7.8 All examined test-cases for pile groin system B

test-cases	correlation
1	0.96
2	0.97
3	0.95

Table 7.3 Correlation coefficient between the modeled curves and the experimental one

In Figure 7.9, the longshore current profile is visualized, as the current propagates from pile groin 3 to pile groin 4. It can be noted that the rate of the increase of the velocity is decreasing as the distance from pile groin gets larger. Furthermore, from Figure 7.10 where the longshore current velocity in the entire domain is presented, it can be clearly observed that current tries to progressively gain the same characteristics as before reaching the pile groin but this is not achieved due to the small distance between the pile groins. In this way, permeable pile groins manage to retard the longshore current in their vicinity.

In addition, in Figure 7.11 the cross-shore current velocity in the whole domain is indicated. According to Hulsbergen's observations, in the position of the groins a seaward velocity of 0.3 m/s is occurring. In the results obtained from SWASH model (Figure 7.11), rip currents with exactly the same magnitude of velocity (0.3 m/s) are present at the groin spots. The agreement between these two values is a good indication that the SWASH model is capable of simulating the real phenomenon.

Following, the flow patterns for pile groin system B obtained from SWASH and from Hulsbergen's observations are visualized in Figure 7.12 and Figure 7.13 respectively. It can be clearly observed that the two patterns are similar. First of all, in the position of the pile groins, offshore vectors that represent the rip currents are distinguished in both figures. Secondly, there are no large-scale eddies inside the groin system as it is noticed in cases of impermeable groins. The reason behind this phenomenon is that the water level induced currents (gravity currents) are not predominant. In addition, gravity currents have opposite direction leading to a further reduction of the longshore current velocity. This can be verified by the fact that there are areas with water at rest between the pile groins. Finally, some offshore components exactly after the pile groins in the velocity pattern are showed in Figure 7.12.

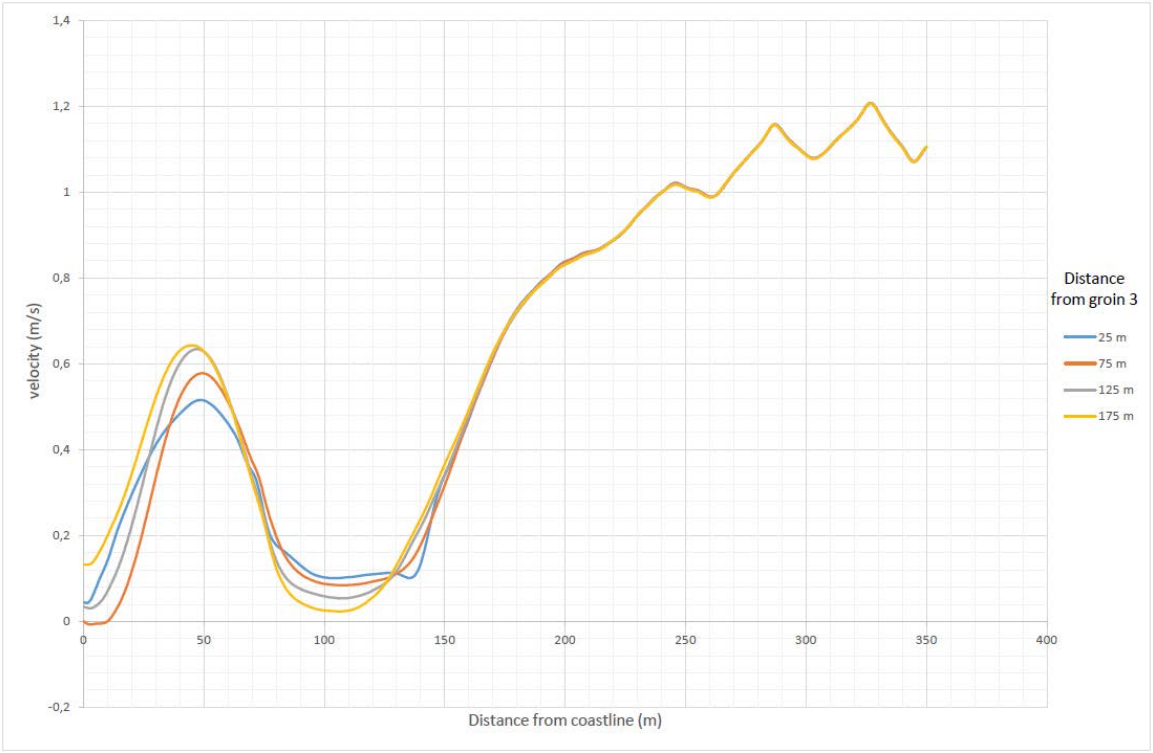

Figure 7.9 Longshore current profile with increasing distance from the pile groin 3

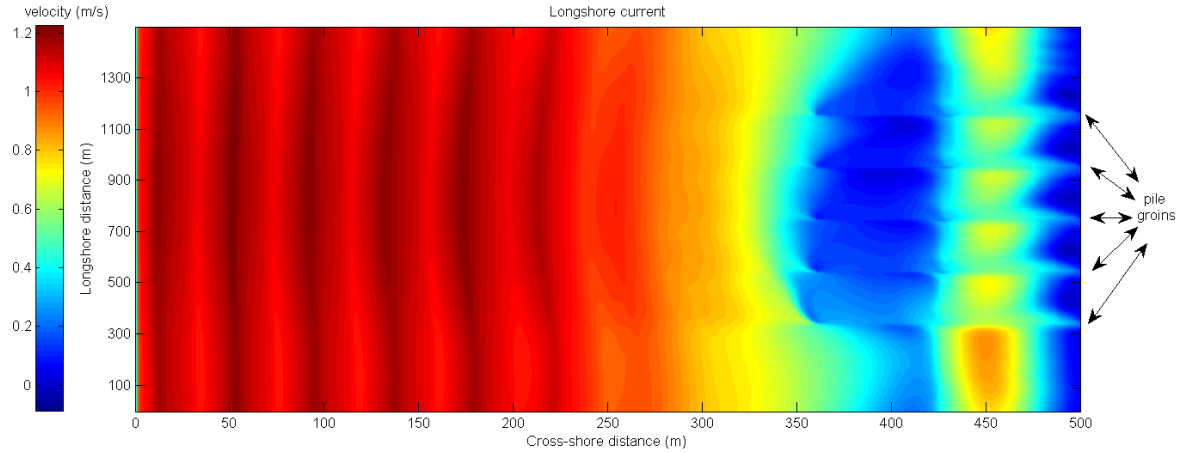

Figure 7.10 Longshore current velocity for pile groin system B

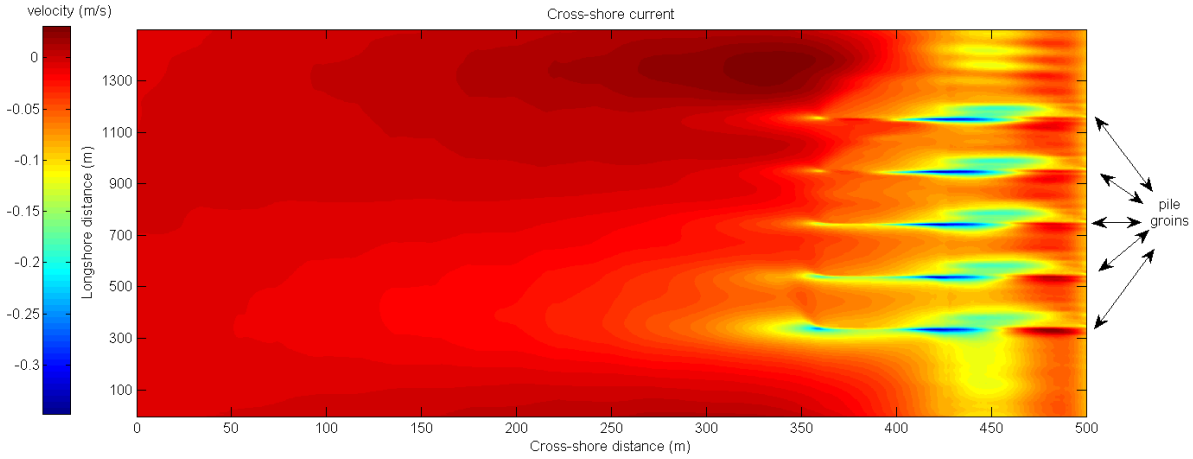

Figure 7.11 Cross-shore current velocity for pile groin system B

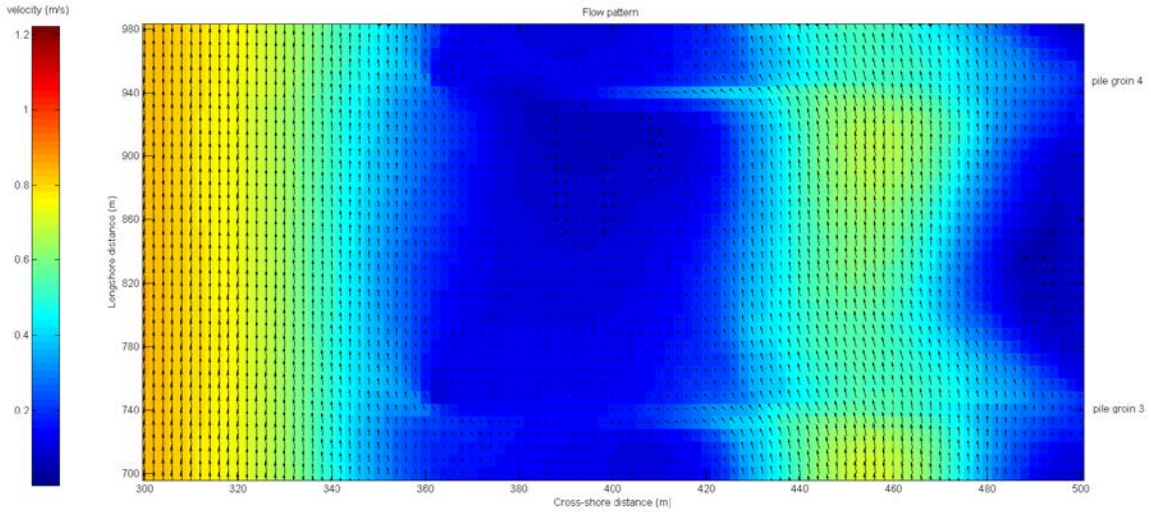

Figure 7.12 Flow pattern for pile groin system B obtained from SWASH

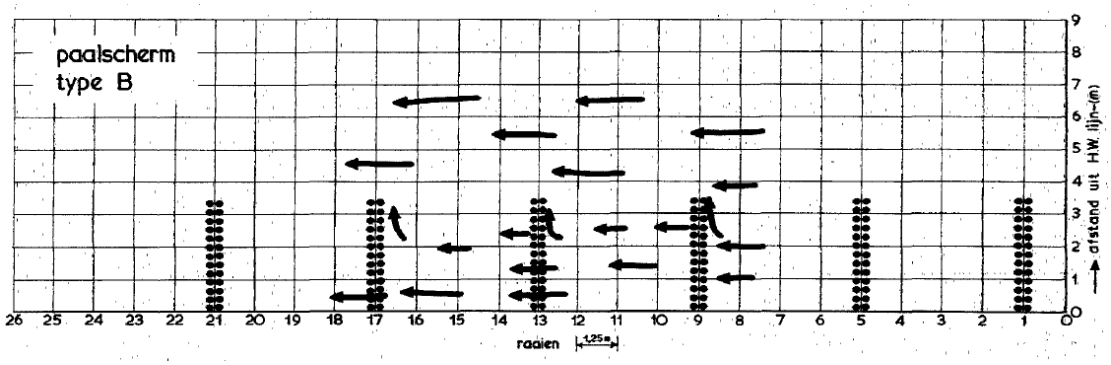

Figure 7.13 Flow pattern for pile groin system B obtained from Hulsbergen's observations

7.4.2 Groin system E

At this second part of the results, the influence of the permeable pile groin system E on the longshore current is examined. More precisely, the longshore current profile under wave and tide forcing inside the groin field E is presented in Figure 7.14 to 7.16. In all the cases the resulting curve is compared to the curve coming from the observations from Hulsbergen's experiment. Hulsbergen examined the current velocities around pile groin 2 and this area of measurements is marked in Figure 7.4 (Area A). The average values of the velocity obtained from Hulsbergen's observations are visualized with the blue line in the following figures.

For the present pile groin scheme, only coarse vertical resolution (2 layers) has been examined since this option has been proven more accurate, judging from the results for groin scheme B. However, as in Section 7.4.1, the influence of the vertical mixing (vertical eddy viscosities) is investigated. Therefore, in test-case 2 the standard k-ε model has been implemented while in test case 1 the vertical mixing is not considered.

As it can be verified from Figure 7.15, where the standard k-ε model for the vertical mixing has been applied, the resulting curve shifts to the right in comparison with Figure 7.14 where vertical mixing is not included. In more detail, test-case 1 can estimate more accurately the magnitude of the current velocities inside the surf zone, while test-case 2 can predict the position where the maximum velocities occur. In addition, as far as the tidal current part is concerned, the two modeled curves are very close to the experimental one. These observations can also be verified by the Table 7.4 where the correlation coefficients between the modeled curves and the experimental one are indicated. The correlation coefficient is 0.97 for test-case1 and 0.98 for test-case 2.

In general, the obtained results for groin system E match with the experimental values to a greater extent than those of groin system B. Furthermore, in this case the previously observed oscillations are not so dominant since they appear after 250 m from the coastline and their amplitude is smaller.

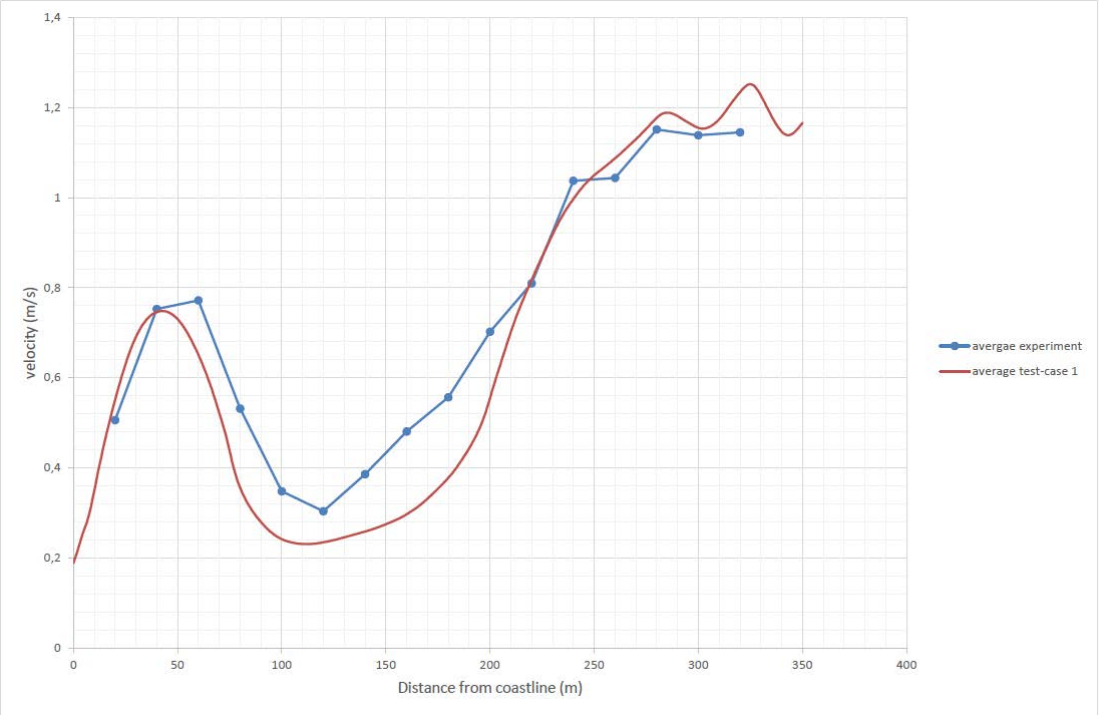

Figure 7.14 Influence of pile groin system E on the longshore current velocity for test-case 1

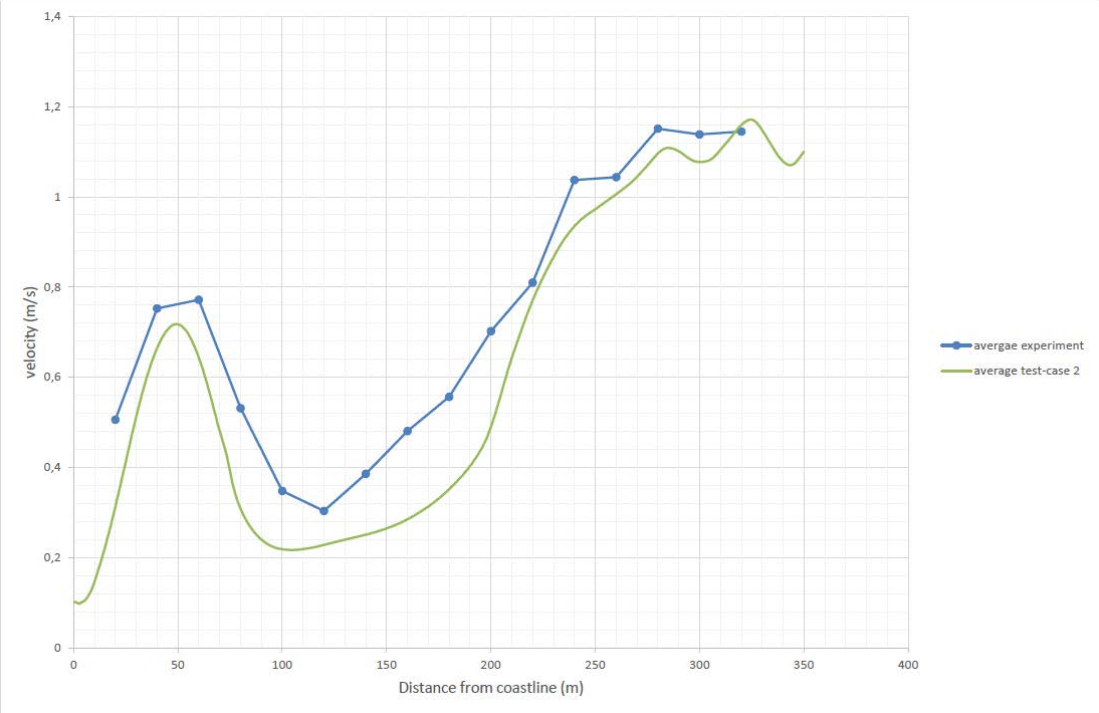

Figure 7.15 Influence of pile groin system E on the longshore current velocity for test-case 2

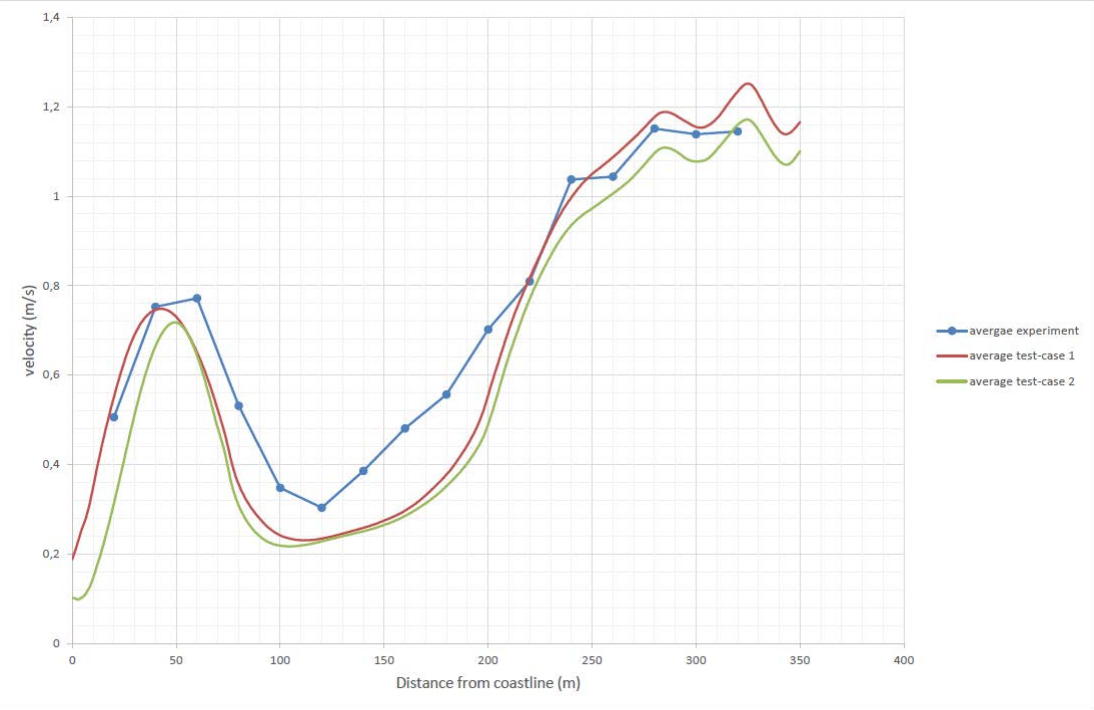

Figure 7.16 All examined test-cases for pile groin system E

test-cases	correlation
1	0.97
2	0.98

Table 7.4 Correlation coefficient between the modeled curves and the experimental one

In Figure 7.18 and Figure 7.17, the longshore current profile is visualized, as the current propagates from pile groin 1 to pile groin 2 and from pile groin 2 to pile groin 3 respectively. This represents the area that Hulsbergen examined during his experiment. It can be noted that the rate of the increase of the velocity is decreasing as the distance from pile groin gets larger. This remark can be verified by the fact that in Figure 7.18 the curves are very close with each other in comparison with the curves in Figure 7.17.

Furthermore, from Figure 7.19 where the longshore current velocity in the whole domain is presented, it can be clearly observed that current tries to progressively gain the same characteristics as before reaching the pile groin but this is not achieved due to the small distance between the pile groins. Nevertheless, it is worth noticing that current can get larger velocities than in case of groin system B due to the distance between the pile groins being double. In this way, permeable pile groins manage to retard the longshore current in their vicinity. Moreover, in Figure 7.20 the cross-shore current velocity in the entire domain is indicated. As in previous Section, rip-currents in the position of the groins with a magnitude of 0.3 m/s are observed. These results are in accordance with Hulsbergen's experimental values.

Following, the flow patterns for pile groin system E obtained from SWASH and from Hulsbergen's observations are visualized in Figure 7.21 and Figure 7.22 respectively. It can be clearly observed that the flow pattern for pile groin system E is similar to the one for pile groin system B (Figure 7.12) while the only difference is the magnitude of the velocities inside the groin field.

Compared to Hulsbergen's experiment, offshore vectors that represent the rip currents are distinguished in both figures. As in the case of Section 7.4.1, there are no large-scale eddies inside the groin system as it is noticed in cases of impermeable groins. Moreover, areas with water at rest near the coastline can be found between the pile groins. These areas are created due to the fact that the water level induced currents have opposite direction from the longshore current. Finally, once more, some offshore components exactly after the pile groins in the velocity pattern are showed in Figure 7.21. These results can be verified by the experimental observations where the same components exist (Figure 7.22). An explanation behind this phenomenon may be the collision of the longshore current with the areas of water being at rest inside the groin field.

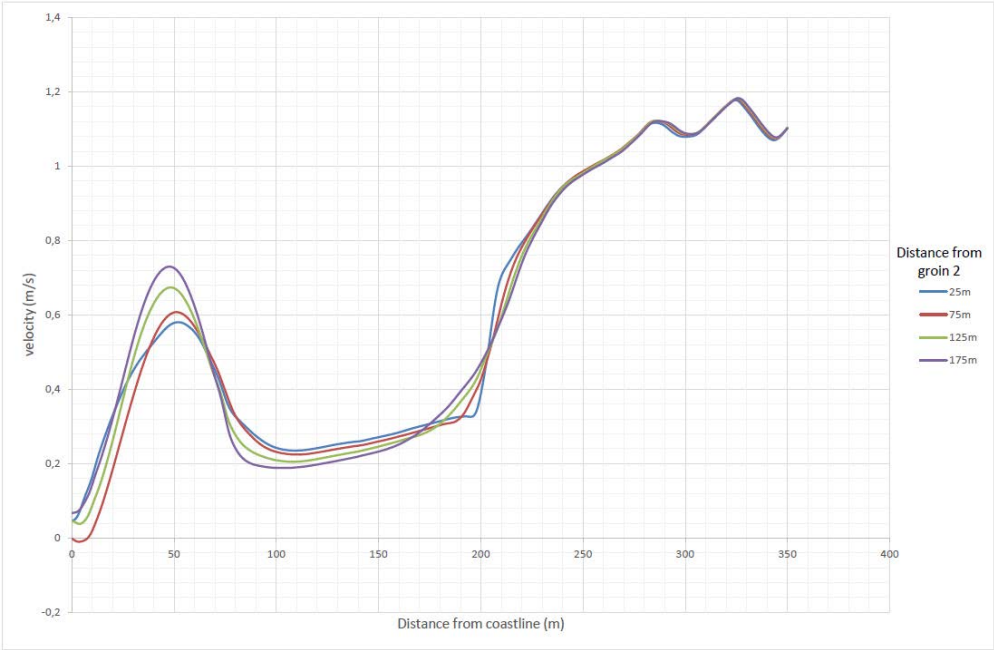

Figure 7.17 Longshore current profile with increasing distance from the pile groin 2

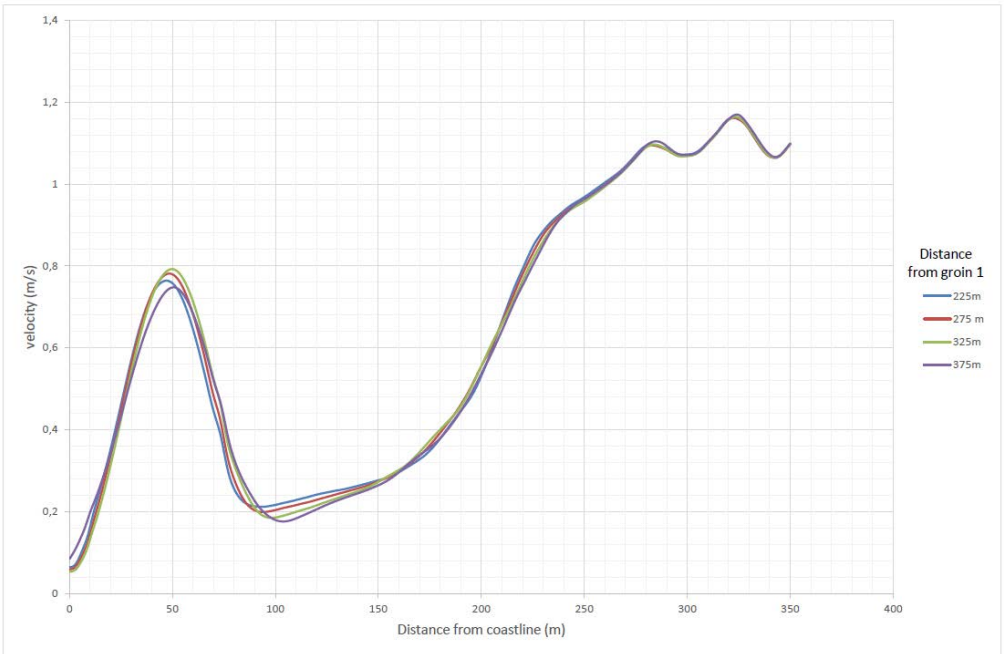

Figure 7.18 Longshore current profile with increasing distance from the pile groin 1

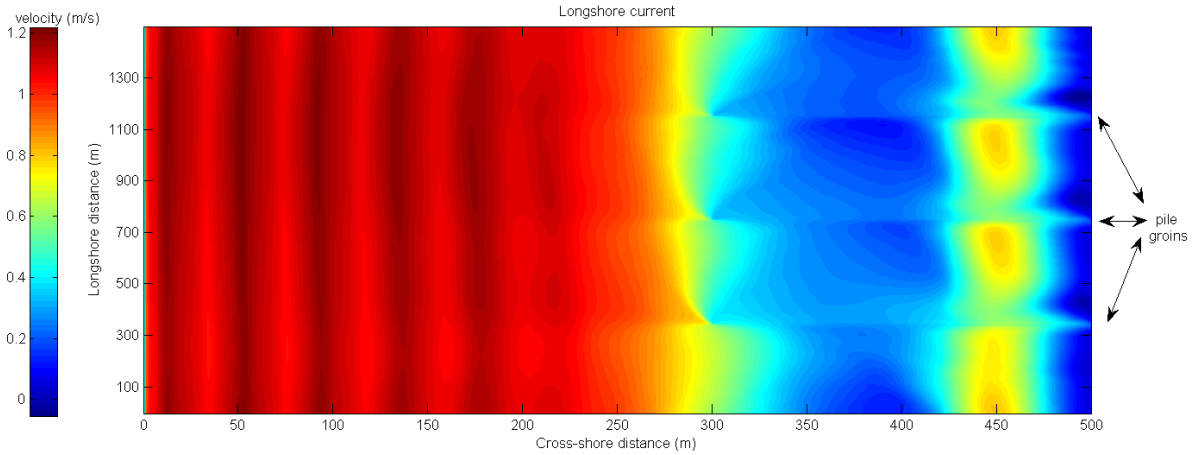

Figure 7.19 Longshore current velocity for pile groin system E

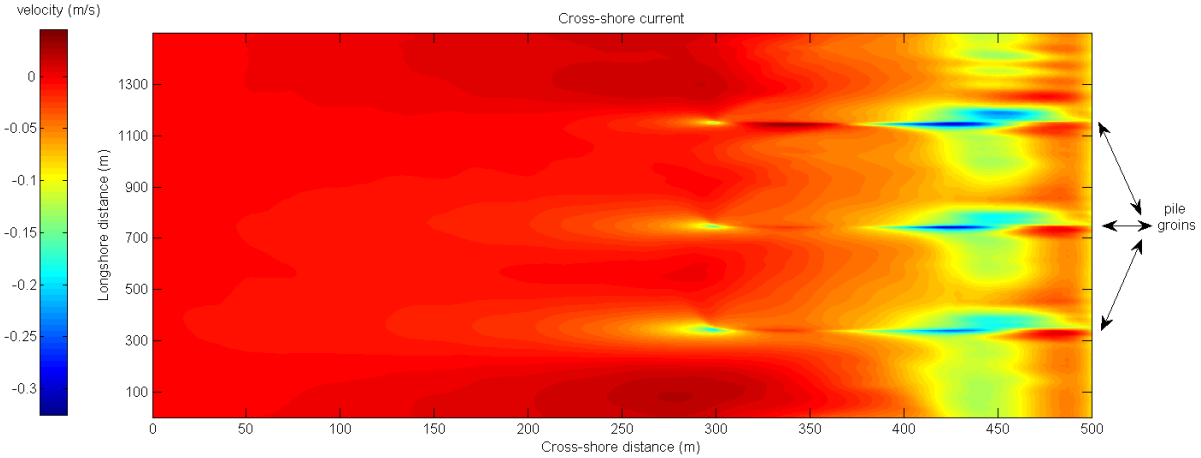

Figure 7.20 Cross-shore current velocity for pile groin system E

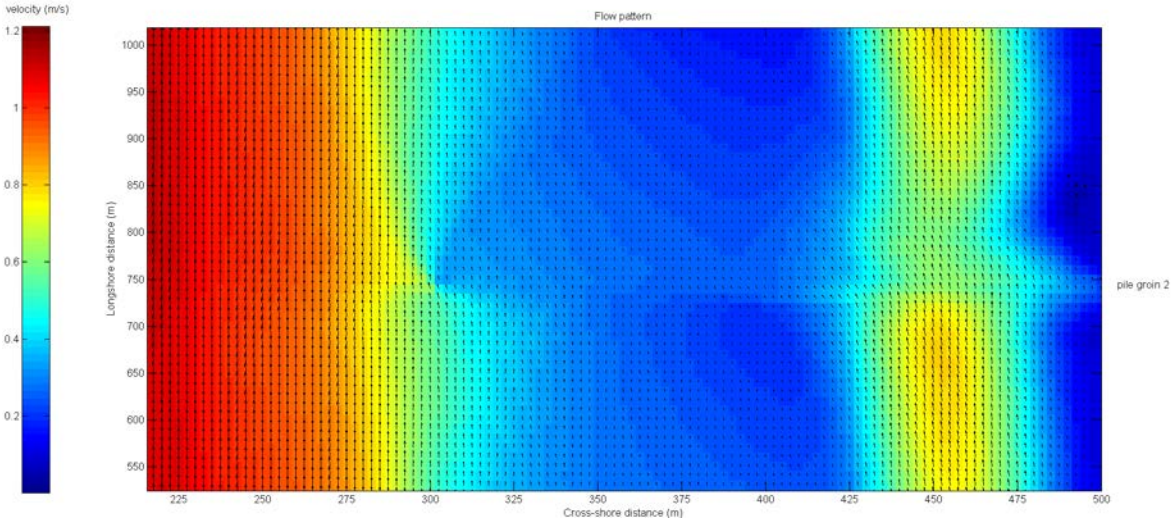

Figure 7.21 Flow pattern for pile groin system E obtained from SWASH

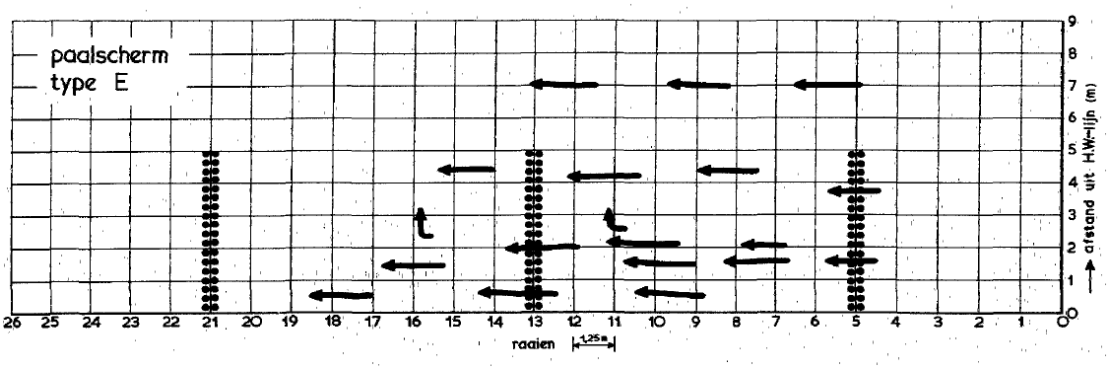

Figure 7.22 Flow pattern for pile groin system E obtained from Hulsbergen's observations

7.4.3 Comparison between results for groin system B and groin system E

A comparison between the two pile groin forms is visualized in Figure 7.23. As it can be witnessed, there is a clear retardation of the longshore current inside the vicinity of the groins. More precisely, a more quantitative indication of the retardation gives a reduction of 36% of the longshore current in the groin system B and 25% in the case of groin system E. Furthermore, the fact that the velocities are larger inside the surf zone for groin system E, can be explained from the larger distance between the double rows of permeable pile groins. Additionally, it has to be taken into account that in case of groin scheme B, the current has met three groins before reaching the measurement area while in the case of groin system E only one. Finally, the two curves (blue and red) are crossing each other at a distance of 140 m from the coastline due to the different groin lengths. In more detail, pile groin B stops influencing the longshore current at a distance 140 m from the coastline while pile groin E continues influencing the current up to 200 m from the coastline. These distances represent the lengths of each groin respectively (Figure 7.3, Figure 7.4).

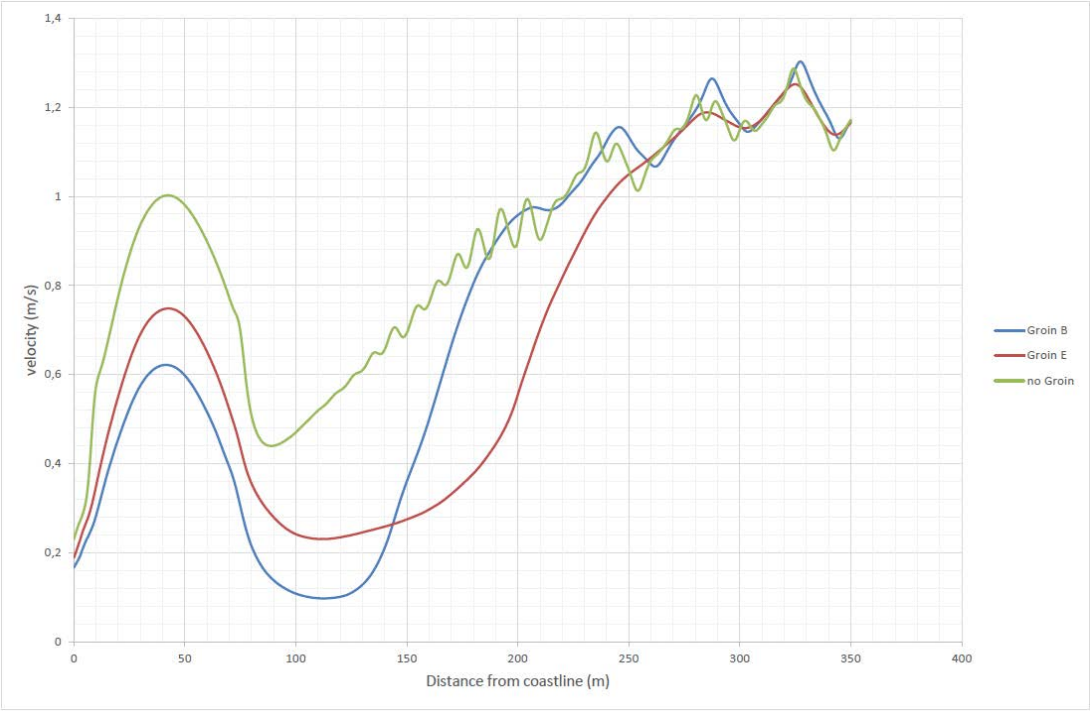

Figure 7.23 Comparison between results for groin system B and groin system E

7.5 Conclusions

The main conclusions of this chapter are summarized below:

- Vertical mixing plays an important role in the present study, especially near to the pile groins where vertical eddy viscosities are expected since the test results obtained from SWASH, which include this parameter, predict with more accuracy the longshore current profile.

- The rate of the increase of the velocity is decreasing as the distance from pile groin gets larger.

- Permeable pile groins manage to retard the longshore current in their vicinity.

- Cross-shore current obtained from SWASH model for both pile groin systems, show rip currents with exactly the same magnitude of velocity (0.3 m/s) at the groin position as those that Hulsbergen observed.

- There are no large-scale eddies inside the groin system.

- Water level differences in the groin fields and the subsequent gravity current reduce further the longshore current.

- Areas with water at rest near the coastline can be found between the pile groins. These areas lead to offshore velocity components when longshore current collides with them.

- From comparison of groin system B and groin system E, it can be verified that longer groins affect the current profile for larger distances from the coastline.

8. Conclusions and Recommendations

8.1 Conclusions

The main objective of this Master Thesis Project was to assess the influence of permeable pile groins on nearshore hydraulics at Domburg coast by means of numerical model (SWASH). After dividing the aforementioned objective in several sub-objectives the following conclusions have been derived:

- The SWASH model can capture with great accuracy the break position of the waves by means of the BREAK command.

- SWASH model is capable to estimate the wave induced current with relative accuracy as it can be witnessed by the correlation of the experimental (Hulsbergen's report) and the modeled values.

- The pressure gradient in SWASH model induced by the time averaged alongshore water level gradient but without the presence of the water level gradient, based on the master thesis of Floris de Wit (2016), is able to represent correctly the tide induced alongshore current.

- The tidal stream does not have an important influence on the breaking position of the waves.

As far as the influence of the pile groins on the nearshore hydraulics is concerned the following conclusions have come out.

- Permeable pile groins manage to retard the longshore current in their vicinity. Thus, it can also be expected that they decrease the capacity of the current to transport sediment leading to sedimentation inside the groin field.

- Vertical mixing plays an important role, especially near to the pile groins where vertical eddy viscosities are expected since the test results obtained from SWASH, which include this parameter, predict with more accuracy the longshore current profile.

- There are no large-scale eddies inside the groin system and the water level differences in the groin field and the subsequent gravity current reduce further the longshore current.

Having said this, SWASH is very well capable of modeling a coastal area with permeable pile groins under the combination of wave and tide forcing, since the SWASH model results are verified with the observations of Hulsbergen.

8.2 Recommendations

In this section recommendations for further research-studies that arose during the present master thesis are presented:

- As it is already mentioned, because permeable pile groins permit both water and sediment to pass through them, they retard the longshore current in their vicinity and decrease the capacity of the current to transport sediment. The reduction of the strength of the current has been verified by the present study. Nevertheless, it is strongly recommended that a research that includes the sediment transport should be carried out. In this way the influence of permeable pile groins on the coastal underwater profile will be evaluated.

- In test-cases where high vertical resolution has been applied, the waves break closer to the shoreline compared to test-cases where BREAK command of SWASH is used. The calibration of α and β values of the BREAK command in respect with the number of layers has to be examined in order to achieve more accurate results.

- The implementation of the pile groins has been done by the VEGETATION command of SWASH with which user can activate wave damping induced by aquatic vegetation. In this way the piles can be described as stiff cylindrical plants which are characterized by their height, diameter and drag coefficient. The drag coefficient (C_D) is very important in order to predict and estimate the damping effect of the piles. In this master thesis, a value of $C_D = 1.5$ is used according to RIZA (2003) for stem of trees. Other values for drag coefficient can be examined in order to assess the influence of this parameter on the results.

- The Hulsbergen's experiments that are used to validate the SWASH model where executed from 1971 to 1972. Due to the limited means existing during that period, experimental results may contain some errors and inaccuracies. Thus, new experiments in real dimensions or using a scale model have to be executed in order to have a more clear view of the phenomenon.

- A parametric study including permeability, length and space of the pile groins can be performed in order to examine how these parameters affect hydraulic features such as rip currents, longshore current and eddies inside the groin field. Based on this parametric study, design standards, which are not available at the moment, for this type of construction can be proposed.

- Especially, a more detailed study on the rip currents needs to be done because a blocking effect of the flow through the permeable groins may be caused by high velocity currents along the groins, thus making the groins impermeable (Trampenau, 2004).

- Although pile groins reduce the longshore current velocity, the flow accelerates when passing through the piles and deaccelerates exactly after the groin. Due to this change of the behavior of the current a lot of turbulence is created which can produce

significant scour around the base of the piles. As a consequence the study of the turbulence is considered vital.

- From previous studies it has been proposed that pile groin systems not only act as a structure to trap sediment inside their vicinity, but also can provide a reservoir of sand and act as an erosion control structure during severe wave conditions. SWASH model can be used to verify this claim.

A. Additional figures for wave induced current

Figures A.1 to A.8 visualize the wave induced current under wave conditions. The waves, which are imposed in the model, are defined as regular waves with a wave height of 1.7 m and a period of 6.5s. In addition, the waves are entering the domain from the offshore boundary (west) with an angle of θ=15° with respect to the cross-shore axis. Finally, all test-cases that are investigated in the present chapter and their model settings are summarized in Table A.1. However, the aforementioned simulations do not represent the real wave conditions of Domburg coast that need to be examined (Chapter 4). That are some first trials in order to investigate the influence of each model set-up in the results.

Test-case	wave height (m)	wave period (s)	wave angle	Number of layers	Bottom friction	Discretization	Break command
1	1.7	6.5	15 °	1	Manning	type 2	✓
2	1.7	6.5	15 °	1	Manning	type 1	✓
3	1.7	6.5	15 °	1	Loglaw	type 2	✓
4	1.7	6.5	15 °	1	Manning	type 1	×
5	1.7	6.5	15 °	8	Manning	type 1	×
6	1.7	6.5	15 °	8	Loglaw	type 2	×
7	1.7	6.5	15 °	10	Loglaw	type 2	×

Table A.1 Model set-up for different test-cases

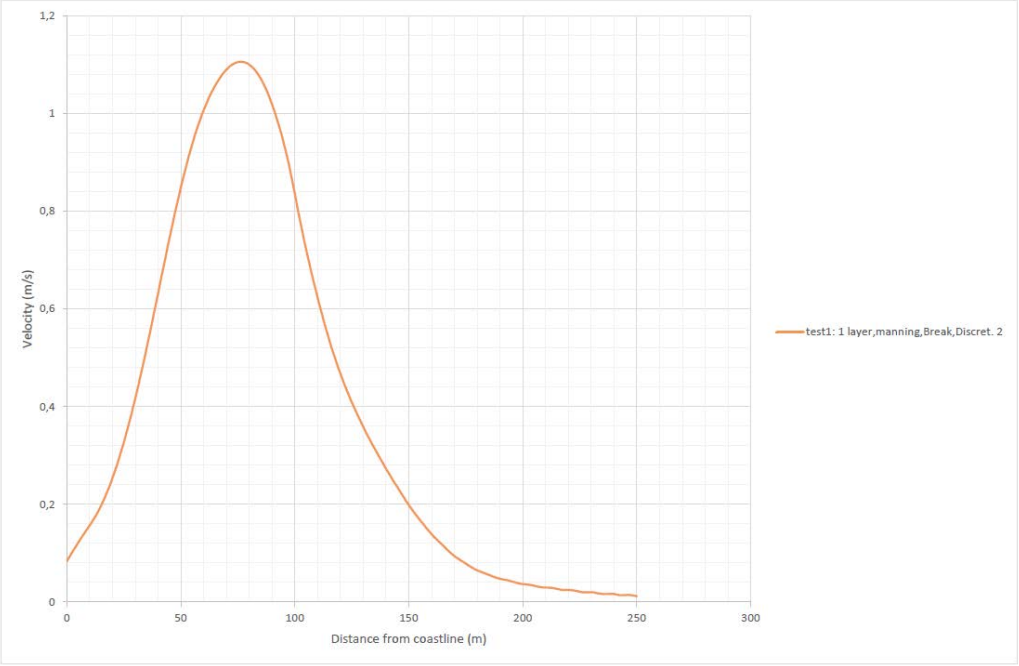

Figure A.1 Wave induced current for test-case 1

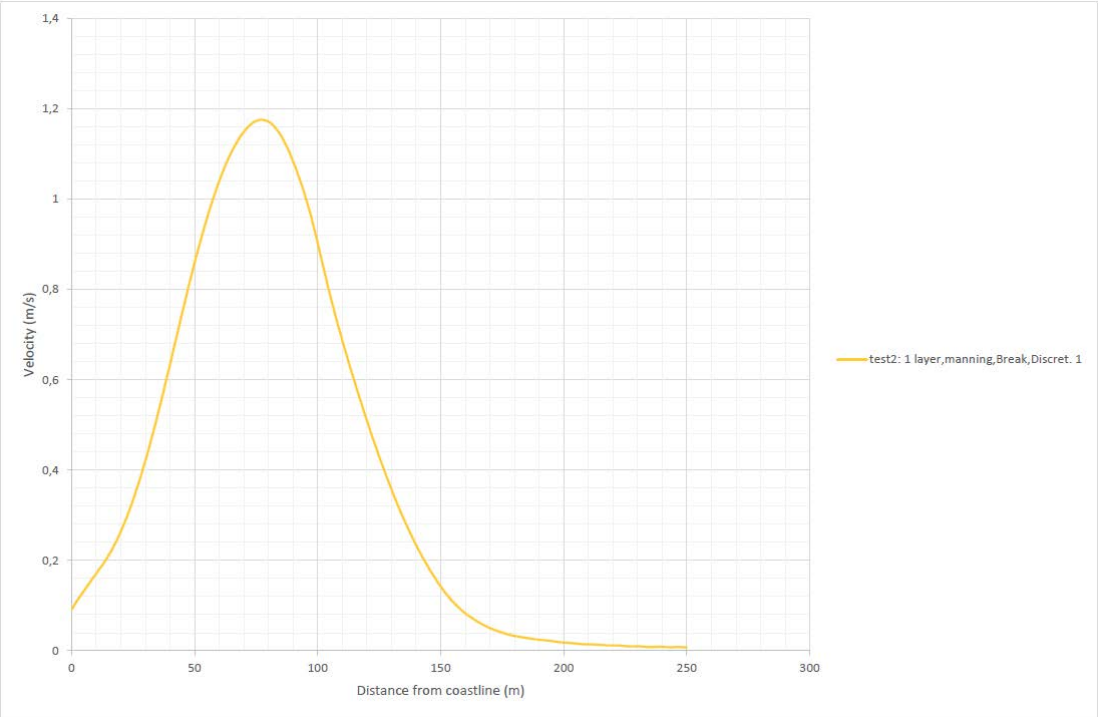

Figure A.2 Wave induced current for test-case 2

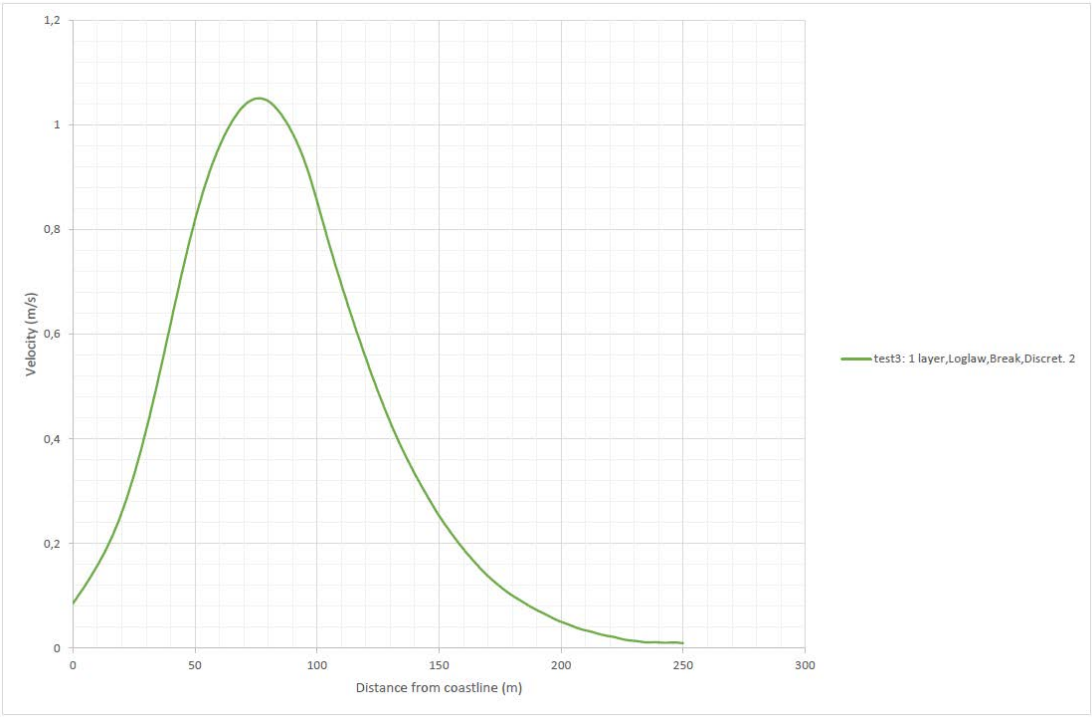

Figure A.3 Wave induced current for test-case 3

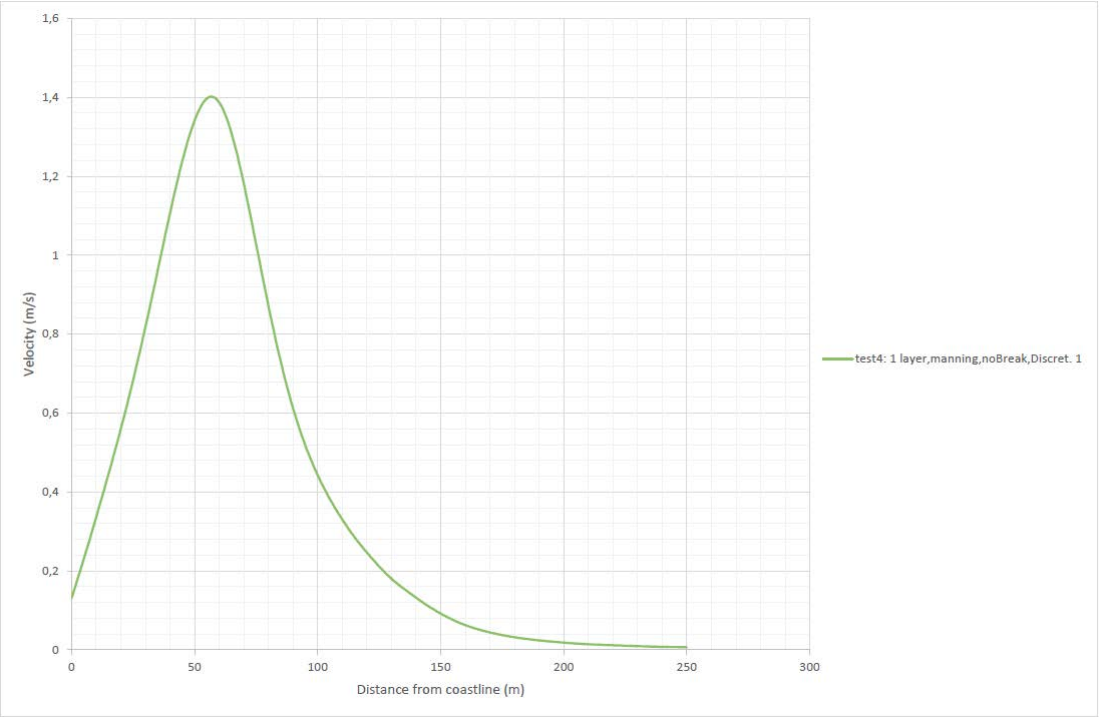

Figure A.4 Wave induced current for test-case 4

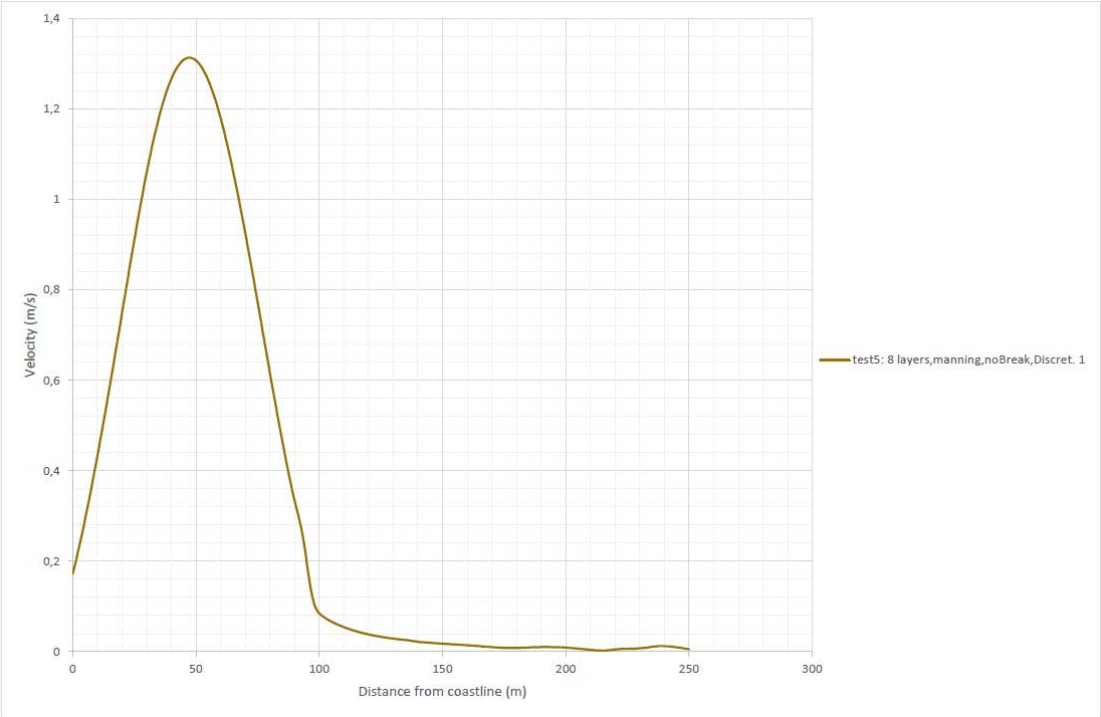

Figure A.5 Wave induced current for test-case 5

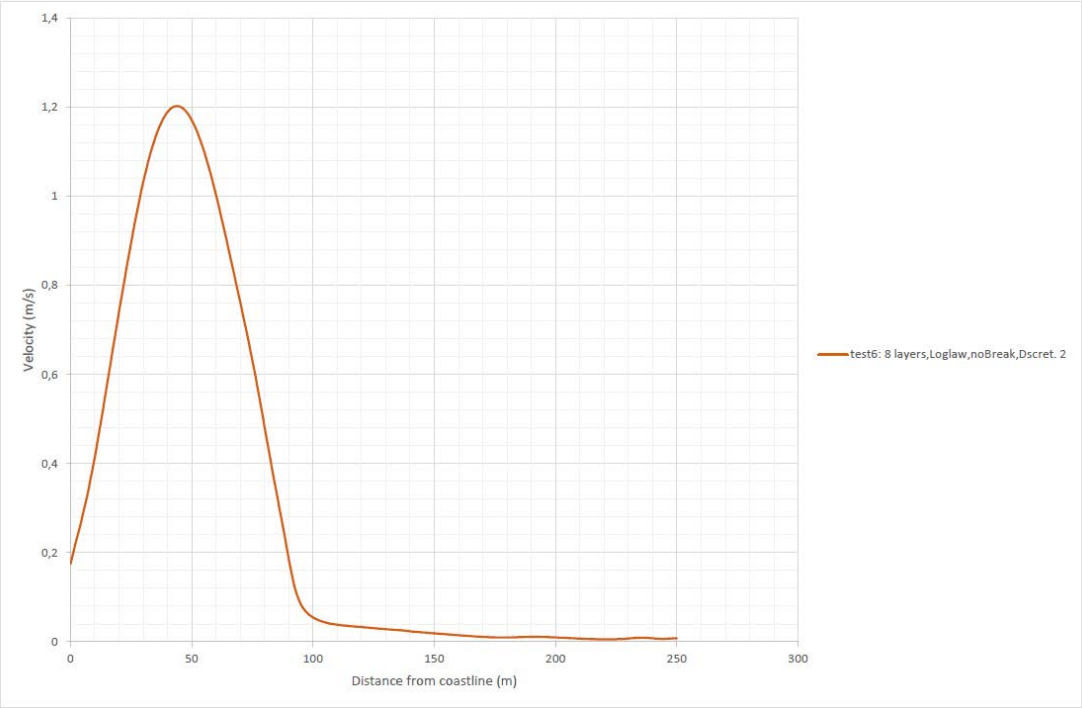

Figure A.6 Wave induced current for test-case 6

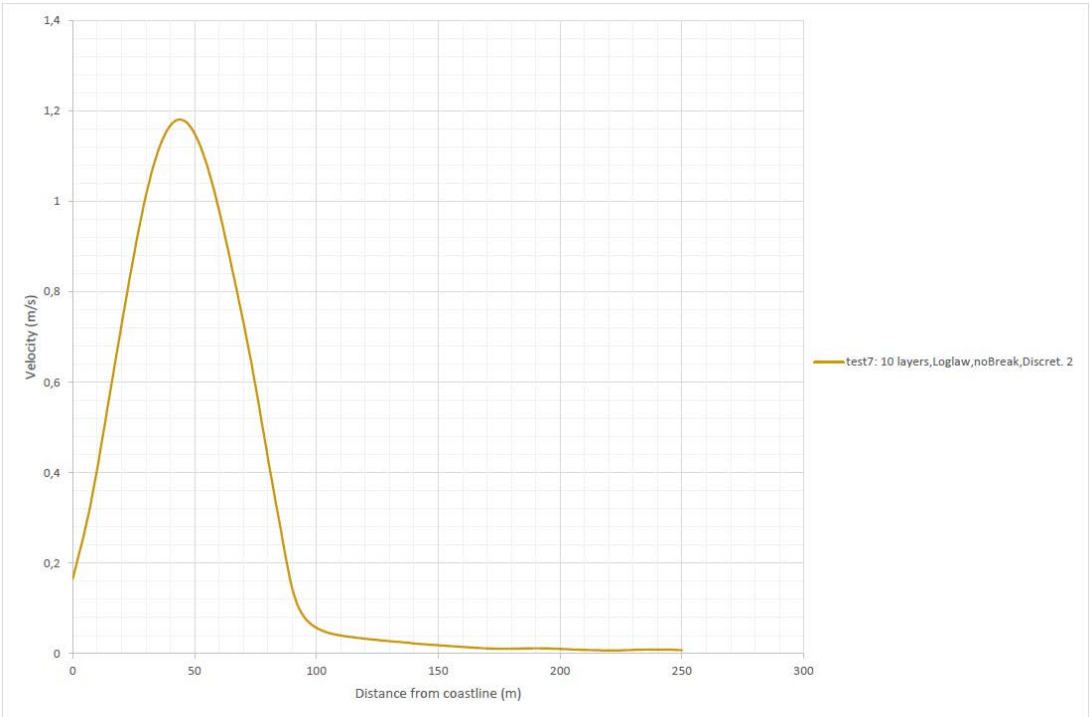

Figure A.7 Wave induced current for test-case 7

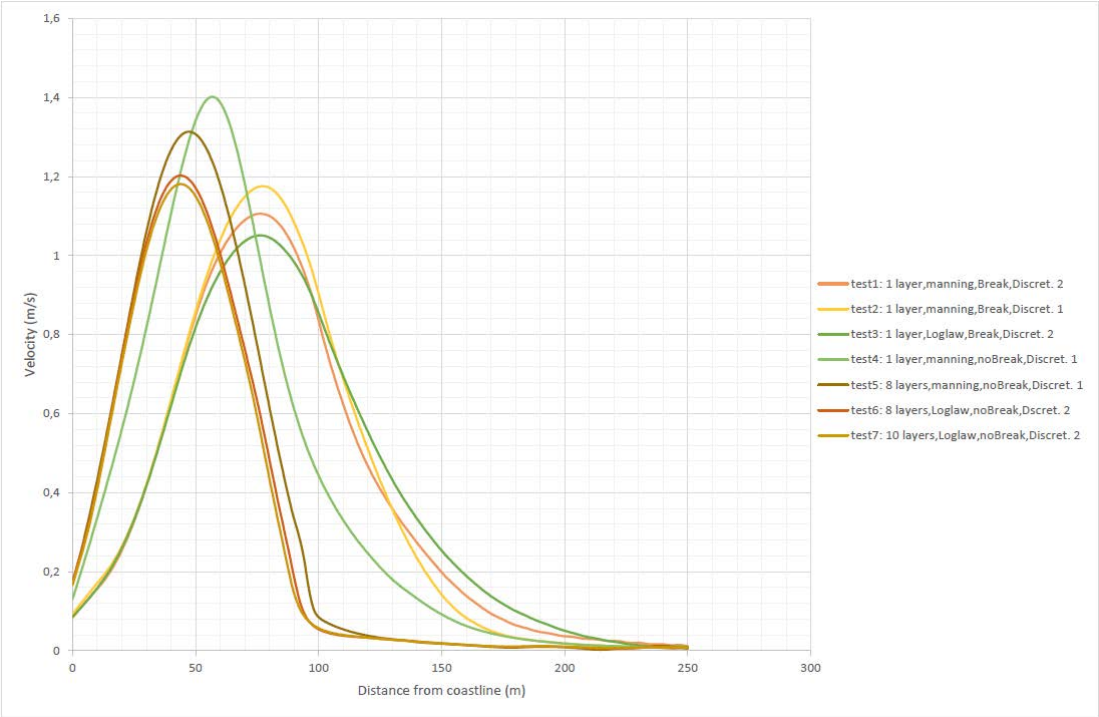

Figure A.8 All examined test-cases for the wave induced current

B. Additional figures for longshore current and permeable groins

In Chapter 7 the influence of the permeable pile groins on the longshore current is considered. More precisely, the average longshore current profile inside the measurement areas were presented. On the other hand, in the present appendix, the longshore current profiles in specific spots inside the measurement areas are showed. In Figures B.1 to B.12, the modelled curves of the SWASH are compared with the experimental curves of Hulsbergen.

Groin system B

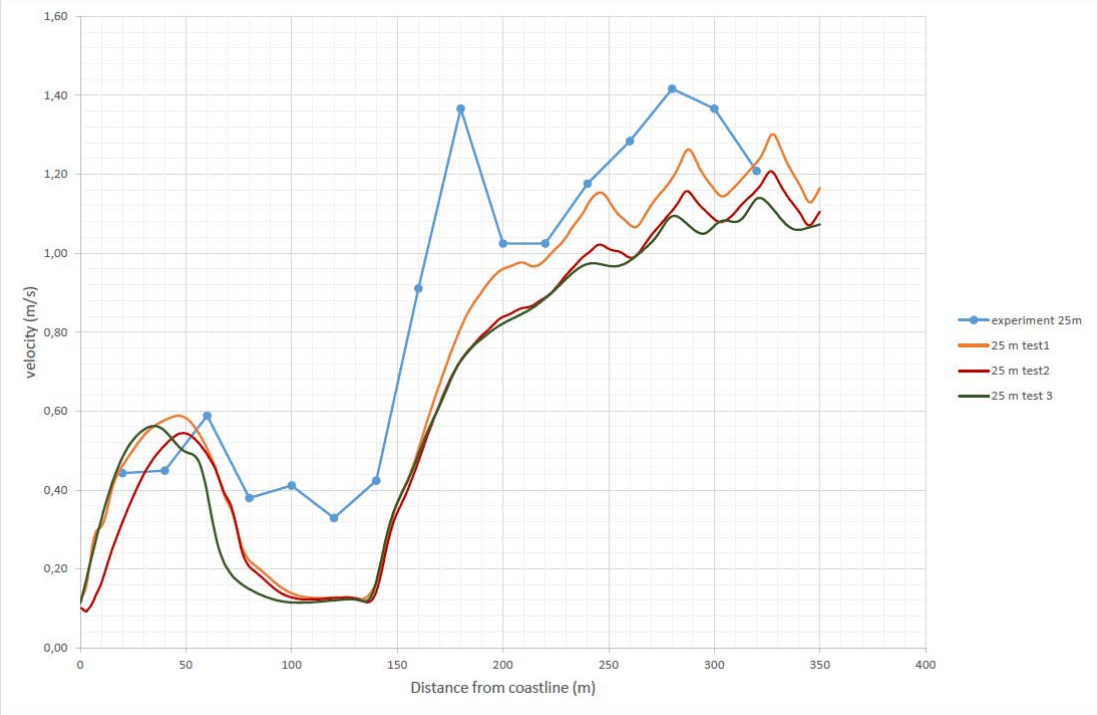

Figure B.1 Longshore current profile at a distance of 25 m from the pile groin 3.

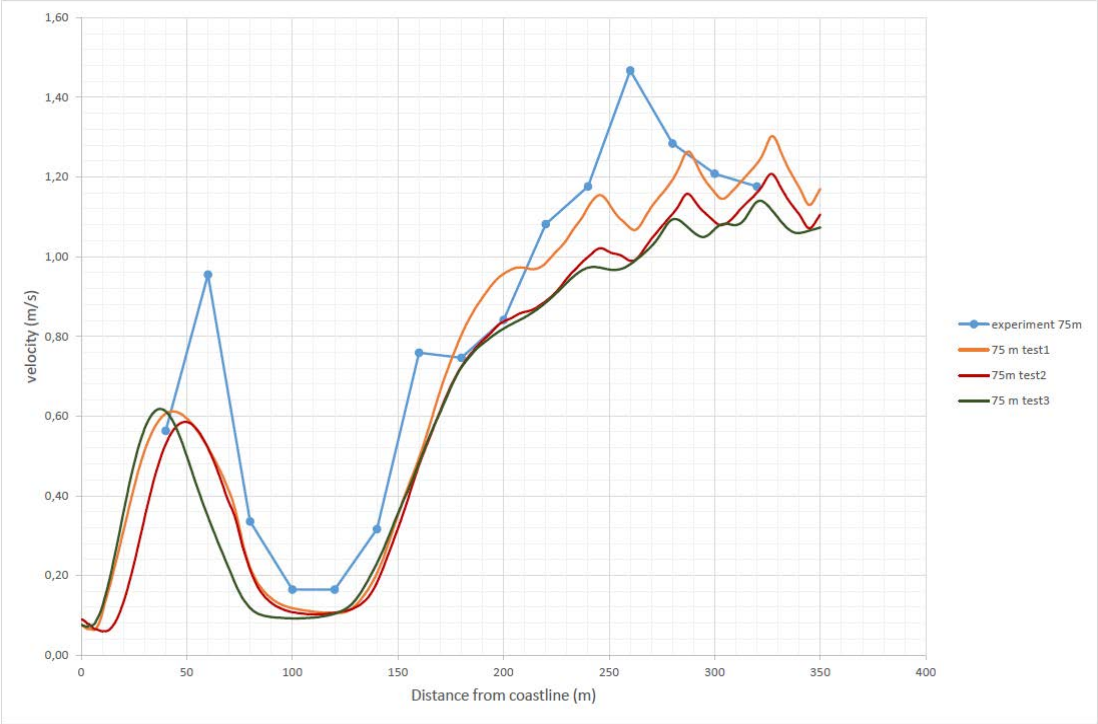

Figure B.2 Longshore current profile at a distance of 75 m from the pile groin 3

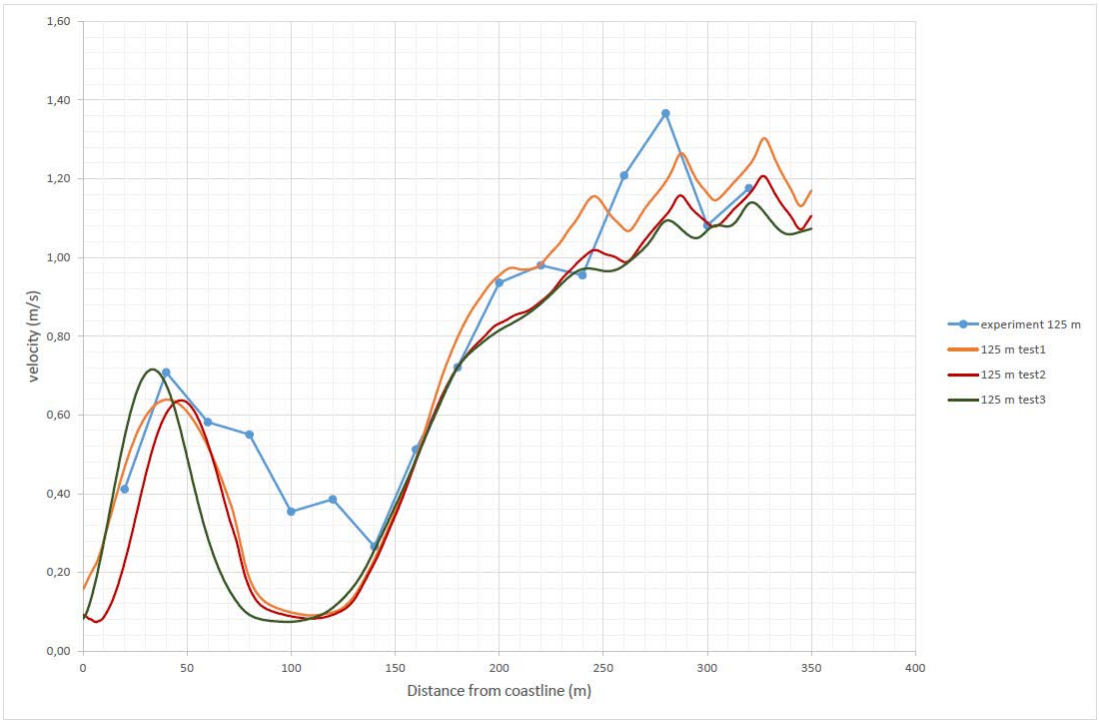

Figure B.3 Longshore current profile at a distance of 125 m from the pile groin 3

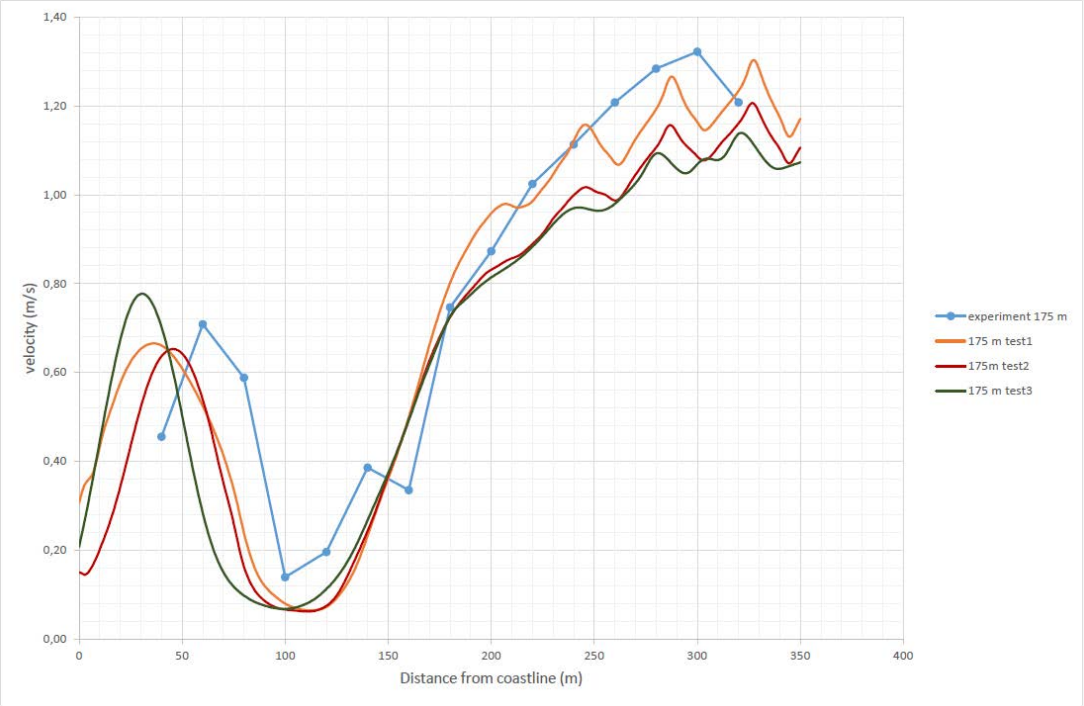

Figure B.4 Longshore current profile at a distance of 175 m from the pile groin 3

Groin system E

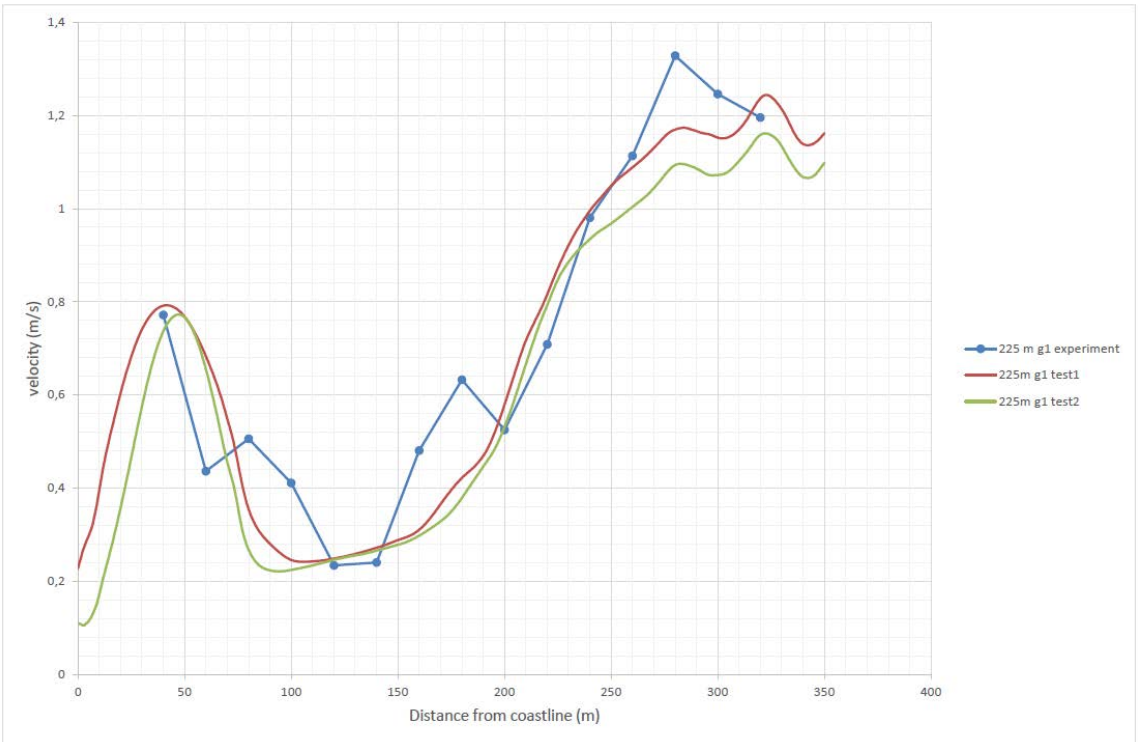

Figure B.5 Longshore current profile at a distance of 225 m from the pile groin 1

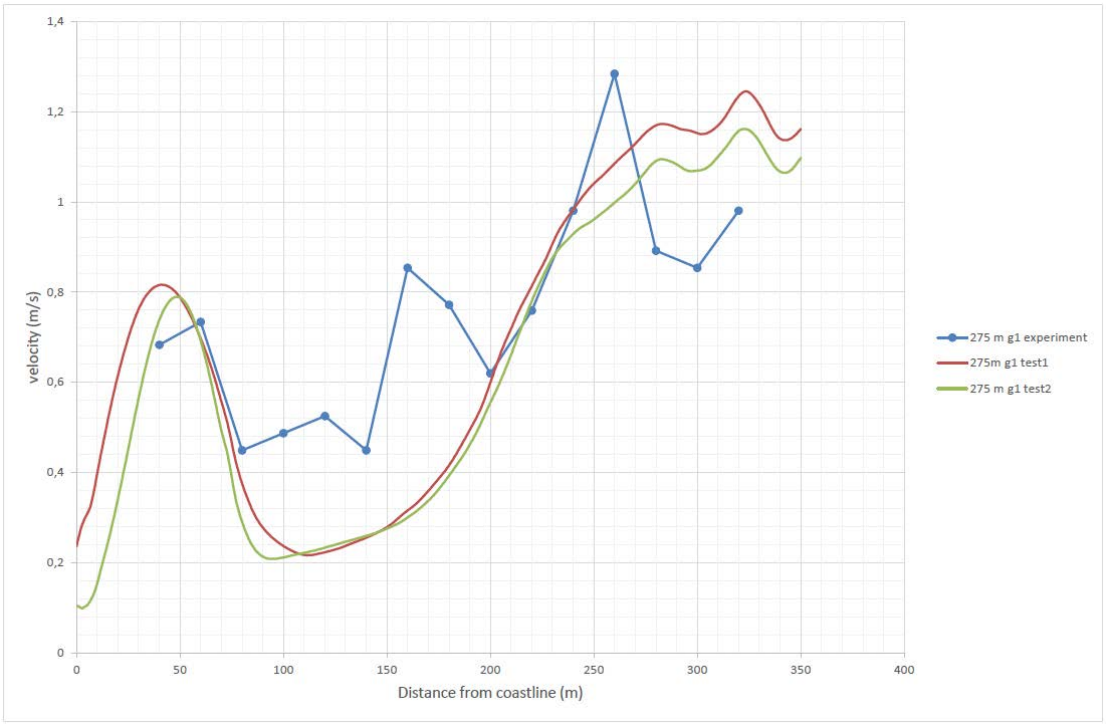

Figure B.6 Longshore current profile at a distance of 275 m from the pile groin 1

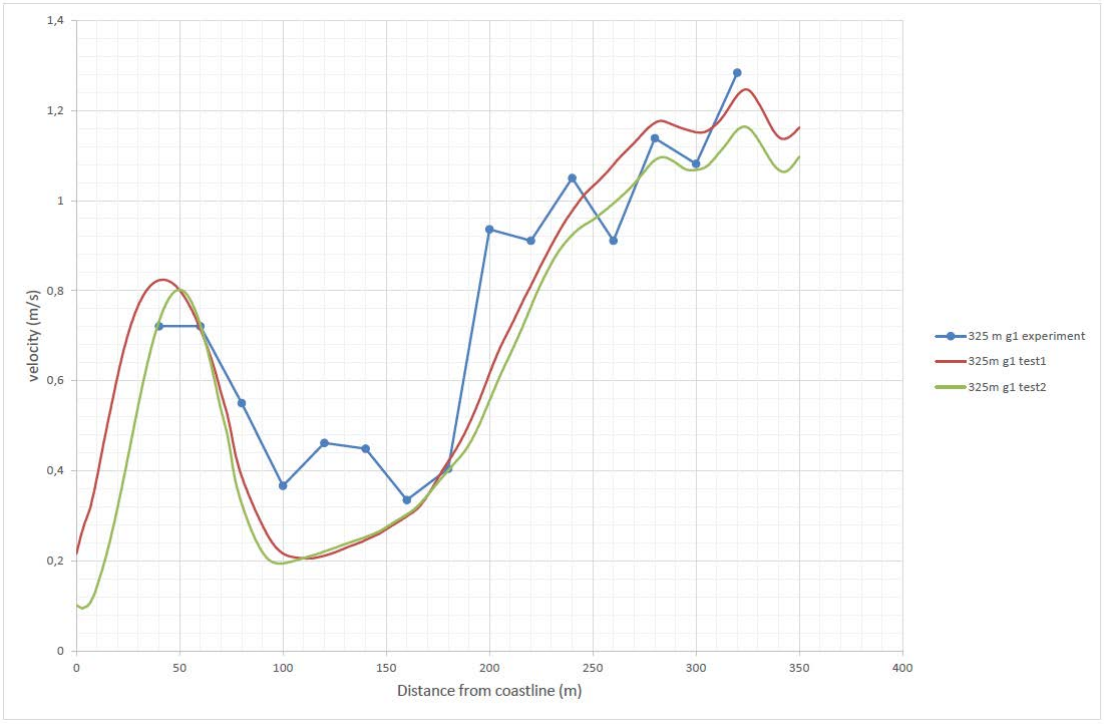

Figure B.7 Longshore current profile at a distance of 325 m from the pile groin 1

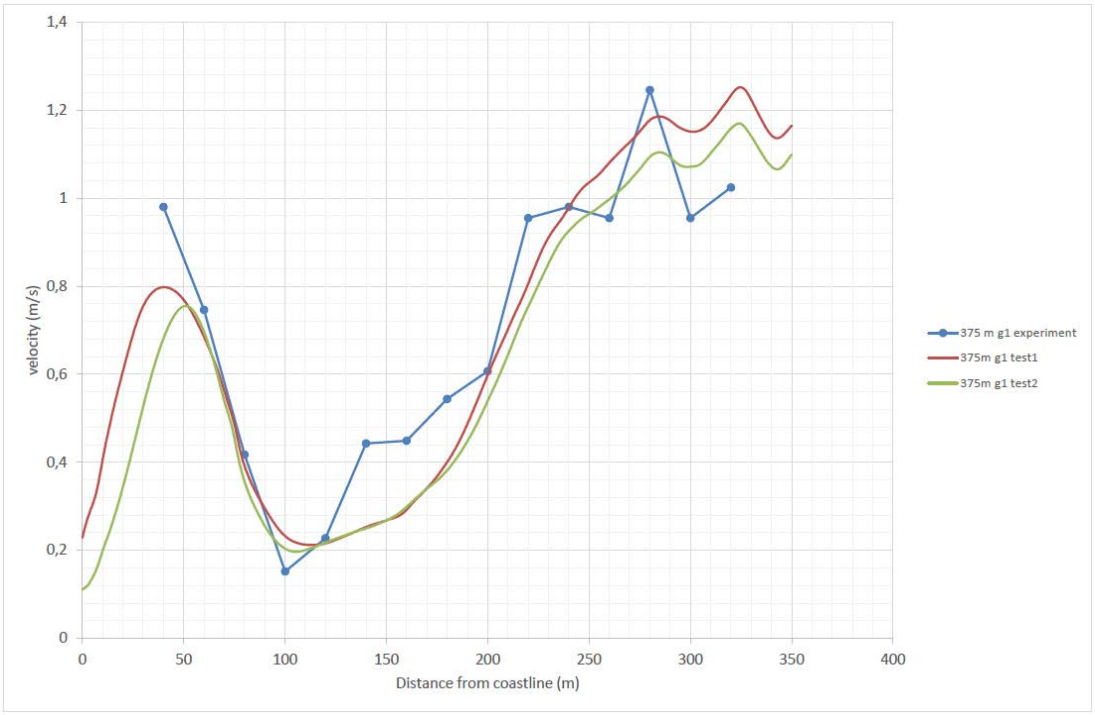

Figure B.8 Longshore current profile at a distance of 375 m from the pile groin 1

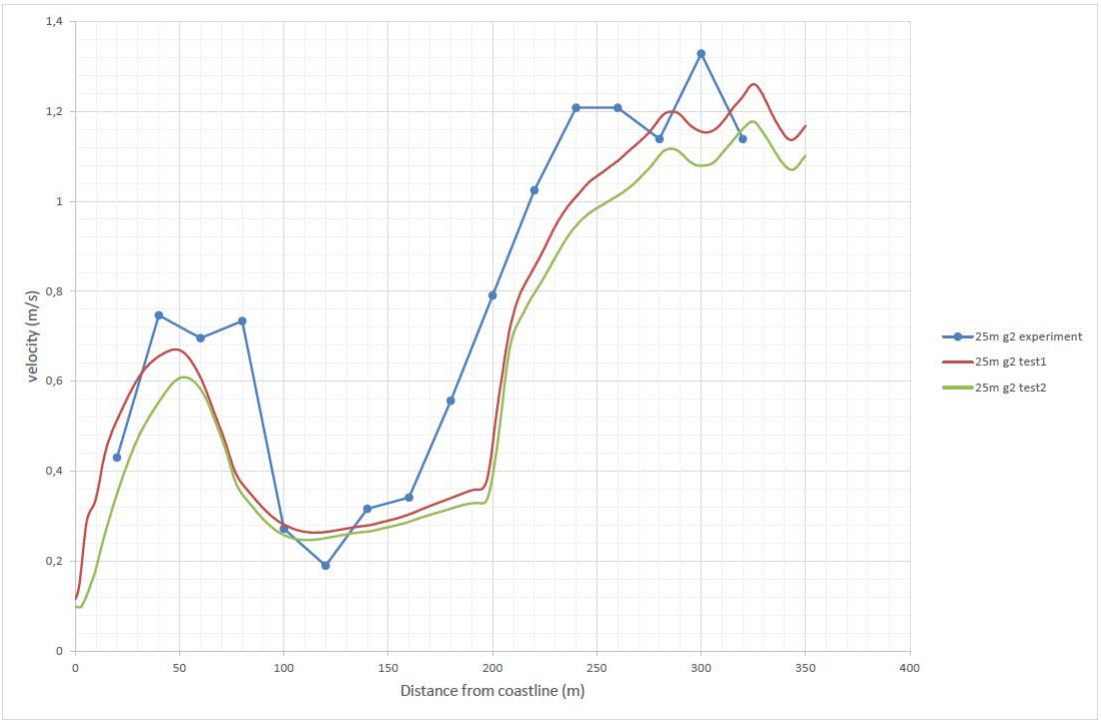

Figure B.9 Longshore current profile at a distance of 25 m from the pile groin 2

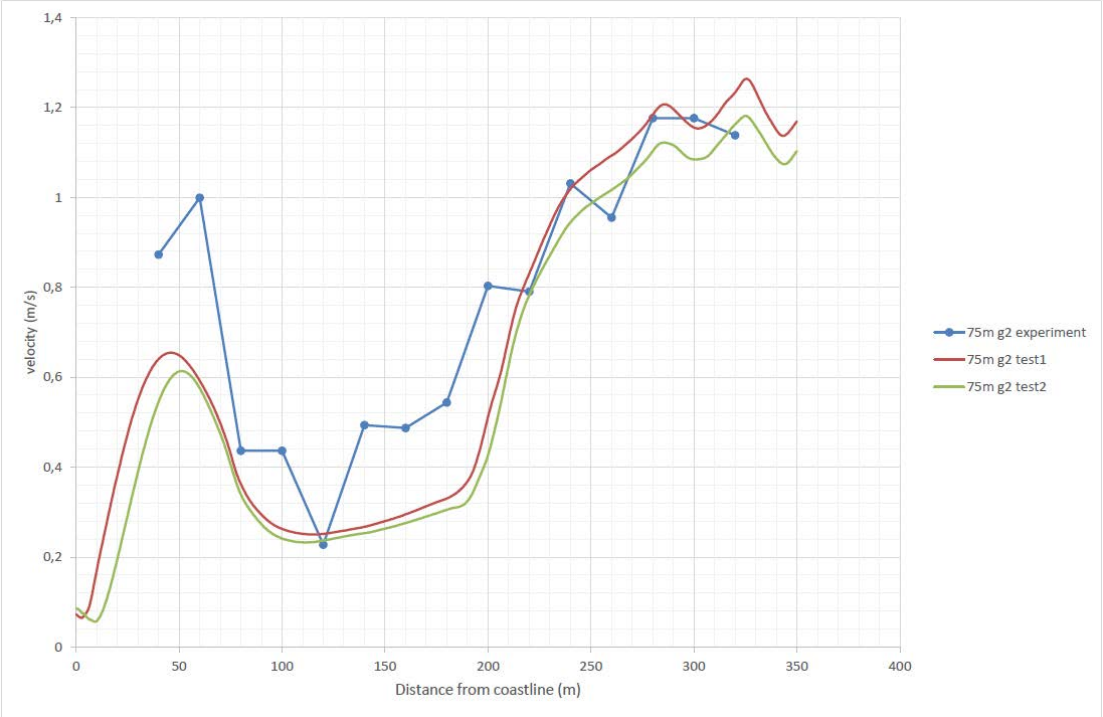

Figure B.10 Longshore current profile at a distance of 75 m from the pile groin 2

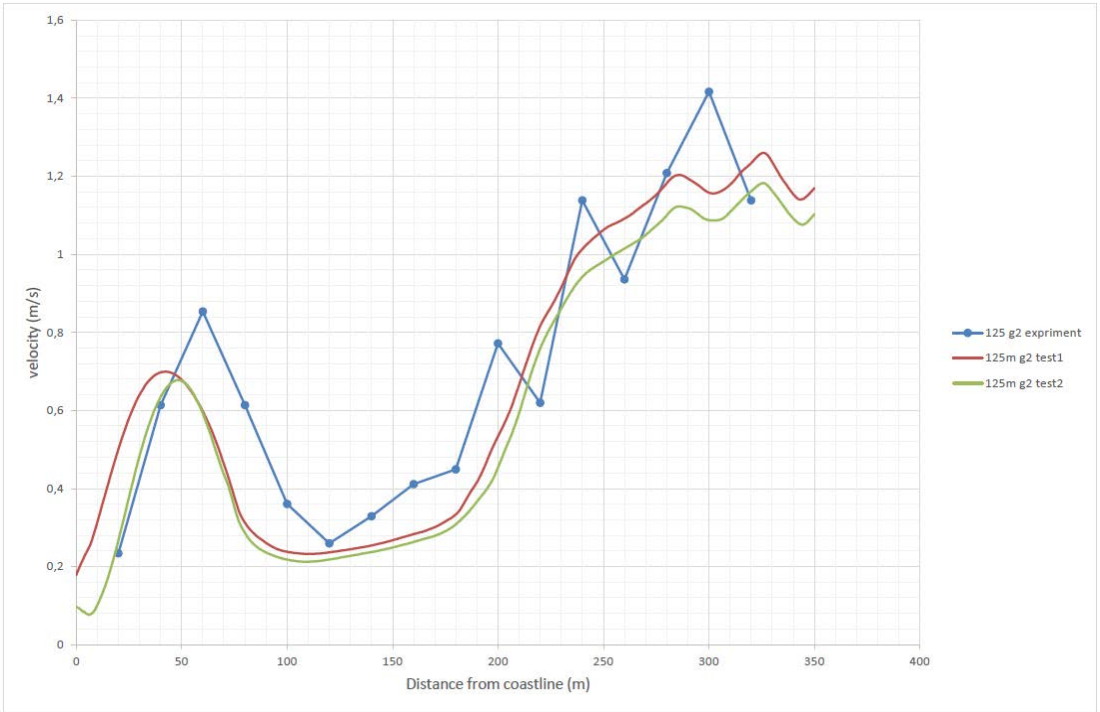

Figure B.11 Longshore current profile at a distance of 125 m from the pile groin 2

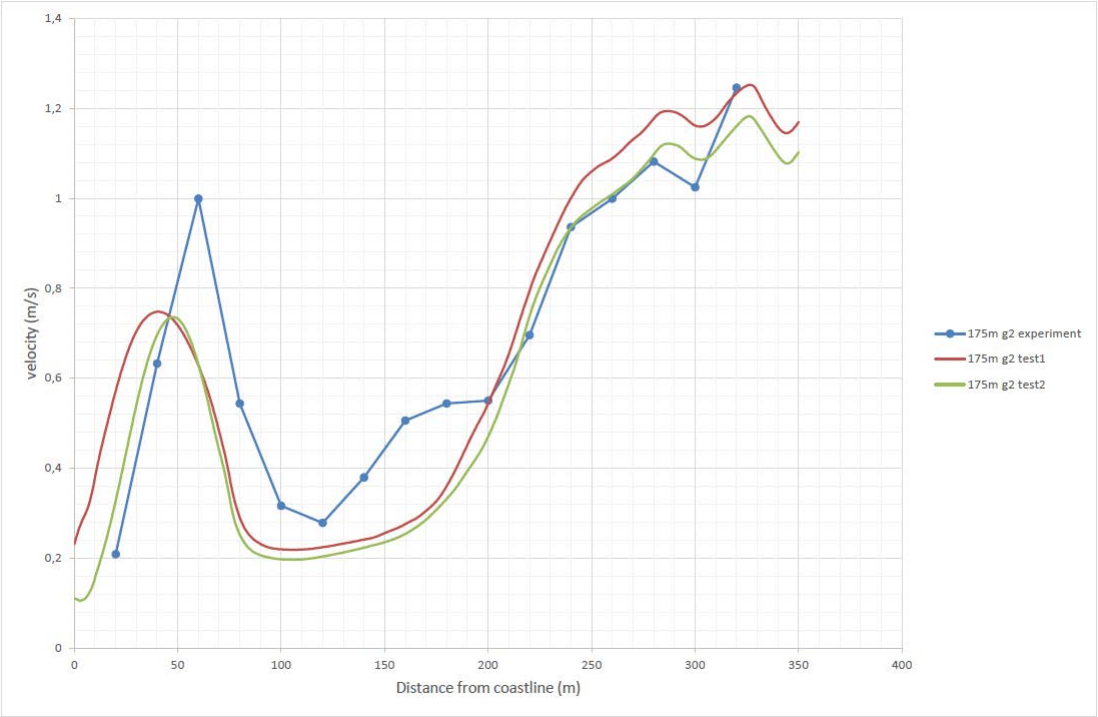

Figure B.12 Longshore current profile at a distance of 175 m from the pile groin 2

Bibliography

Abdel-Mawla, S. and Khaled, M. (2002). Application of Permeable Groins on Tourist Shore Protection. *Ocean Wave Measurement and Analysis* , pp. 1735-1744.

Bakker, W.T., Hulsbergen, C.H., Roelse, P., de Smit, C., and Svasek, J.N. (1984). Permeable Groynes: Experiments and Practice in the Netherlands. *Proceedings of the 19th Conference on Coastal Engineering*, pp. 2026-2041.

Bodge, K.R. (1989). A Literature Review of the Distribution of Longshore Sediment Transport across the Surf Zone. *Journal of Coastal Research 5*, pp. 307-328.

Bosboom, J. and Stive, M. J. (2015). *Coastal Dynamics I: Lectures Notes CIE4305.* Delft Academic Press.

Briele, A. (2014). *Assessment of the application of permeable pile groins as coastal protection.* Master thesis, Delft University of Technology.

Chen, F.Y., and Ikeda, S. (1997). Horizontal separation in shallow open channels wirh spur dikes. *JOURNAL OF HYDROSCIENCE AND HYDRAULIC ENGINEERING*, pp. 15-30.

Dette, H.H., Raudkivi, A.J., and Oumeraci, H. (2004). Permeable Pile Groin Fields. *Journal of Coastal Research*, pp. 145-159.

Ettema, R., and Muste, M. (2004). Scale effects in Flume Experiments on flow around a Spur Dike in Flatbed Channel. *Journal of Hydraulic Engineering 130*, pp. 635-646.

Floris de Wit. (2016). *Tide-induced currents in a phase-resolving wave model.* Master Thesis, Delft University of Technology.

Gangfeng Ma, Kirby, J., Shih-Feng Su, Fengyan Shi. (2013). Numerical study of turbulence and wave damping induced by vegetation canopies. *Coastal Engineering 80*, pp. 68-78.

Hanson, H., and Larson, M. (2004). Wave directional characteristics as a design parameter for groin performance. *Journal of Coastal Research*, pp. 188-197.

Hayashi, T., Hattori, M., Kano, T., and Shirai, M. (1967). Hydraulic Research on the Closely Spaced Pile Breakwater. *Coastal Engineering*, pp. 873-884.

Hulsbergen, C.H. (1973). *Effect of permeable pile groins on coastal currents.* Delft Hydraulics.

Kraus, N., Hanson, H., and Blomgren, S. (1995). Modern Functional Design of Groin Systems. *Coastal Engineering*, pp. 1327-1342.

Kraus, N.C., and Rankin, K.L. (2004). Foreword; Functioning and design of coastal groins: The interaction of groins and the beach: Processes and Planning. *Journal of Coastal Research*, pp. 1-2.

Mani, J. and Jayakumar, S. (1995). Wave Transmission by Suspended Pipe Breakwater. *Journal of Waterway, Port, Coastal, and Ocean Engineering 121*, pp. 335-338.

Mulcahy, S.E. (2000). *Laboratory and numerical studies of a pile cluster groin.* Master Thesis. University of Florida.

Otay, E., Güngördü, Ö., and Börekçi, O. (1997). Shoreline Changes in the Vicinity of a Permeable Groin .

Ouillon, S., and Dartus, D. (1997). Three-dimensional computation of flow around groyne. *Journal of Hydraulic Engineering*, pp. 962-970.

Perdok, U., Crossman, M., Verhagen, H., Howard, S., and Simm, J. (2004). Design of timber groynes. *Coastal Structures*, pp. 962-974.

Poff, M.T., Stephen, M.F., Dean, R.G., Mulcahy, S. (2004). Permeable Wood Groins: Case Study on their impact on the coastal system. *Journal of Coastal Research*, pp. 131-144.

Price, W.A., Tomlinson, K.W., and Willis, D.H. (1972). Filed tests on two permeable groins. *Coastal Engineering Proceedings*, pp. 1312-1325.

Rankin, K.L., Bruno, M.S. and Herrington, T.O. (2004). Nearshore currents and sediment transport measured at noched groins. *Journal of Coastal Research*, pp. 237-254.

Raudkivi, A.J. (1996). Permeable Pile Groins. *Journal of Waterway, Port, Coastal, and Ocean Engineering 122*, pp. 267-272.

Raudkivi, A.J., and Dette, H.H. (2002). Reduction of sand demand for shore protection. *Coastal Engineering 45*, pp. 239-259.

RIZA. (2003). *Stromingsweerstand vegetatie in uiterwaarden.*

Rodi, W. (2000). *Turbulence Models and Their Application in Hydraulics.* A.A. Balkema.

Schiereck, G.S. updated by Verhagen, H. (2012). *Introduction to Bed, bank and shore protection.* VSSD.

Smit, P., Zijlema, M., and Stelling, G. (2013). Depth-induced wave breaking in a non-hydrostatic, near-shore wave model. *Coastal Engineering 76*, pp. 1-16.

Stelling, G. and Zijlema, M. (2003). An accurate and efficient finite-difference algorithm for non-hydrostatic free-surface flow with application to wave propagation. *International Journal for Numerical Methods in Fluids*, pp. 1-23.

Stelling, G. and Zijlema, M. (2010). Numerical Modeling of Wave Propagation, Breaking and Run-Up on a Beach. *Advanced Computational Methods in Science and Engineering*, pp. 373-401.

SWASH-User-Manual. (2016). *Swash user manual version 3.14A.*

Teraguchi, H., Nakagawa, H., Muto, Y., and Zhang H. . (2008). FLOW AND SEDIMENT TRANSPORT AROUND IMPERMEABLE OR PERMEABLE GROINS. *PROCEEDINGS OF HYDRAULIC ENGINEERING 52*, pp. 175-180.

Tingsanchali, T., and Maheswaran, S. (1990). 2D Depth averaged flow computation near groyne. *Journal of Hydraulic Engineering 116*, pp. 71-86.

Trampenau, T., Goricke, F., and Raudkivi, A.J. (1996). Permeable pile groins. *Coastal Engineering Proceedings*, pp. 2142-2151.

Trampenau, T., Oumeraci, H., and Dette, H.H. (2004). Hydraulic functioning of permeable pile groins. *Journal of Coastal Research*, pp. 160-187.

Uijttewaal , W.S. (2005). Effects of groyne layout on the flow in groyne fields: Laboratory experiments. *Journal of Hydraulic Engineering 131*, pp. 782-791.

Uijttewaal, W.S. (1999). Groyne field velocity patterns determined with particle tracking velocimetry . *28th IAHR Congress.*

Van Lynden, P. and Everts, V. (2007). *A Resistible Force: When Man Meets the Sea.* Stichting Visual Legacy.

Van Schijndel, S.H., and Jagers, H.R. (2003). Complex flow around groynes, computations with Delft3D in combination with HLES. *Research Presented at the International Symposium on Shallow Flows, Delft, Netherlands*, pp. 645-650.

Verhagen, H.J. (1985). *Groin height determination with an empirical parametric method.* Rijkswaterstaat, DWW.

Weitbrecht, V. (2004). *Influence of dead-water zones on the dispersive mass transport in rivers.* Doctoral Thesis, Universitat Karlsruhe.

Yossef, M.F.M. (2002). *Literature review The Effect of Groynes on Rivers.* Delft University of Technology.

Zijlema, M. (2014). MODELLING VERTICAL VARIATION OF TURBULENT FLOW ACROSS A SURF ZONE USING SWASH. *Coastal Engineering Proceedings*.

Zijlema, M., Stelling, G., and Smit, P. (2011). SWASH: An operational public domain code for simulating wave fields and rapidly varied flows in coastal waters. *Coastal Engineering*, pp. 992-1012.